Self-Organization in Catalytically Active Mixtures

SUBMITTED BY
VINCENT OUAZAN–REBOUL
FROM PARIS, FRANCE
GÖTTINGEN, MAY 2023

THESIS ADVISORY COMMITTEE

Prof. Dr. Ramin Golestanian
Living Matter Physics Department
Max Planck Institute for Dynamics and Self Organization, Göttingen

Prof. Dr. Jörg Enderlein
III. Institute of Physics – Biophysics
Georg August University, Göttingen

Prof. Dr. Marcus Müller
Institute for Theoretical Physics
Georg August University, Göttingen

MEMBERS OF THE EXAMINATION BOARD

Referree: Prof. Dr. Ramin Golestanian
Living Matter Physics Department
Max Planck Institute for Dynamics and Self Organization, Göttingen

Second referree: Prof. Dr. Jörg Enderlein
III. Institute of Physics – Biophysics
Georg August University, Göttingen

Prof. Dr. Marcus Müller
Institute for Theoretical Physics
Georg August University, Göttingen

Dr. Aljaz Godec
Research Group Mathematical Biophysics
Max Planck Institute for Multidisciplinary Sciences, Götingen

Prof. Dr. Peter Sollich
Institute for Theoretical Physics
Georg August University, Göttingen

Dr. David Zwicker
Max Planck Research Group Theory of Biological Fluids
Max Planck Institute for Dynamics and Self Organization, Göttingen

Date of examination: June 26, 2023

Self-Organization in Catalytically Active Mixtures

Abstract

Living systems are intrinsically out of equilibrium, which makes their physical description challenging. This has led to the emergence, over the past thirty years, of a new field of physics, active matter, which studies collectives whose components dissipate energy to perform work.

Two common features of biological and artificial active matter systems are their ability to respond to environmental stimuli through gradient-following behavior, and to affect the fields whose gradients they respond to. The interplay between these two phenomena lead to the emergence of intrinsically out-of-equilibrium field-mediated interactions, which are long-ranged and potentially non-reciprocal, and can lead to spectacular self-organization behavior. Field-mediated interactions are relevant to many biological systems, for instance populations of bacteria and mixtures of catalytic enzymes, and are likely to be involved in intracellular organization processes.

Previous studies on the collective behavior of non-reciprocally interacting agents have focused on short-range interactions. The effect of long-range, intrinsically out-of-equilibrium interactions at the collective level is meanwhile still not fully understood. In this thesis, we thus study the self-organization of catalytic systems which exhibit field-mediated non-reciprocal interactions using analytical and numerical tools.

We begin with an overview of the concepts approached in this thesis. We describe the mechanisms through which active particles can interact with, create and respond to field gradients, explain how these two abilities lead to effective interactions between active particles and their relevance to intracellular behavior. Throughout this introduction, we introduce minimal models describing the self-organization of catalytic particles, which serve as a starting point for the rest of the thesis.

We then characterize the consequences of using a detailed description of the catalytically active particles under study. We do so by adding a Michaelis-Menten-like substrate concentration dependence to the catalytic activity, and by taking into account the effect of size dispersity. Our analytical calculations show that these two ingredients strongly enrich the phenomenology of catalytic phase separation.

In the second part, we switch our focus to the study of catalytically active particles involved in model metabolic cycles, in which the product of a given catalytic species is the substrate of the next. We analytically and numerically characterize the behavior of a metabolic cycle

involving an arbitrary number of catalytically active and chemotactic particles with identical parameters. We find that cycles with an even number and an odd number of catalytic species show a qualitatively different behavior, with the latter being able to develop oscillatory steady states.

We then study metabolic cycles of three species with arbitrary parameters. We discover that the resulting network effects can give rise to clustering of active species which are all self-repelling, the conditions for which we calculate analytically and confirm numerically.

Going beyond this result, we perform a classification of all the three-species metabolic networks depending on their ability to self-organize. Coarse-graining the interactions between the active species leads to the identification of the inter-species interaction motifs which tend to stabilize or destabilize a metabolic cycle. Generic cycles can be mapped to a small subset of elementary cycles, whose stability is obtained based on the decomposition into single-species and pair interaction motifs.

Finally, we summarize in detail the results obtained in this thesis, and propose some directions for future research.

Contents

Acknowledgments

When I decided to come to Göttingen for my PhD, I had no idea what to expect: it was a city I had never visited, much smaller than Paris in which I'd spent the first 23 years of my life, in a country I didn't know all that well and whose language I didn't speak. Reflecting on my experience over these 3 years and 9 months, I can safely say my choice was the right one, in large part thanks to the amazing people I met here and the support of my friends and family back in France.

I would first and most importantly like to thank my advisor, Ramin Golestanian, for his constant guidance and support during my PhD. Under Ramin's supervision, I have grown a lot as a physicist and a researcher, and thanks to all he taught me during my time in his department, I feel like I couldn't be better prepared for the next challenges I will be facing.

I would then like to thank my group leader, Jaime Agudo-Canalejo, without whom I would never have managed to produce the work presented in this thesis. Working closely with Jaime was the occasion to discover his approach to physics and research, which has been a constant inspiration to my work. I am particularly grateful for his constant help, infinite patience with my questions and typos, and eagle eye for detail in calculations and manuscripts.

Dealing with German bureaucracy is a notoriously tricky affair, especially when one doesn't speak the language. This is why I would like to thank Ayse Bolik and Vika Novak from the LMP department, and Frauke Bergmann and Antje Erdmann from the IMPRS for Physics of Biological and Complex Systems, for their essential help with all things administrative, and for answering my questions about living in Germany.

I would like to thank the members of my Thesis Advisory Committee, Jörg Enderlein and Marcus Müller, for accepting to follow my progress and for their valuable advice and suggestions during our meetings. I am also grateful to the members of my thesis evaluation board, Aljaz Godec, Peter Sollich, and David Zwicker, for their interest in my work and for accepting to attend my defence.

I would like to give my thanks to Luca Cocconni, Mike Chatzittofi, and especially Navdeep Rana, for sacrificing part of their weekend to proofread this manuscript, and for the very useful suggestions they gave me.

As a part of the first wave of PhD students to join the LMP department, I had the privilege to watch the community of LMP students and postdocs grow into a group of colleagues and close friends, with whom I've spent an incredible PhD adventure. I also had the chance to make amazing friends outside of the Institute, in particular the roommates I've had the pleasure of sharing a flat with over the years. I do not have space here to thank everyone

individually and to list all the fun times we've had, so I will just say that I am very grateful to all my friends in Göttingen for making it a city worth living in.

Special thanks go to Lorenzo Piro, who from day one has been the best friend and PhD buddy I could ever had hoped for. It was always a pleasure to come by his office for a chat and to hang out with him outside work for a beer or a board game. Whenever I had anything on my mind, no matter the issue, I knew I could always rely on him for help and advice.

I must of course thank my family for accompanying me through this journey, especially my parents Anne and Bruno and my brother Rémi, without whom I would never had made it this far. Doing a PhD, especially during a worldwide pandemic, involves some difficult periods, and their support during these has been invaluable to me. This is also the occasion to thank all of my friends in France, in particular the members of the Garderie, who always welcomed me back home as if I had left yesterday, no matter how little I kept in touch.

Leaving the best for last, I would like to thank Sara, for everything. Meeting her was by far the best thing to happen to me in Göttingen.

1

Introduction

1.1 Phoretic and chemotactic active matter

Biological systems self-organize at all scales, from flocks of birds[1] and fish[2] to ordered structures within cells[3]. Starting from the seminal work of Vicsek *et al.*[4], a physical framework has emerged to describe such behavior: active matter[5–7], a rapidly expanding field concerned with the study of collectives which dissipate energy at the component level in order to perform work[6]. In the most common subclass of active matter models, this work is used to drive self-propelled motion, as described by the famous active Brownian particle model and its declinations[8]. Two broad approaches can be distinguished in active matter theory. First,

the use of minimal agents-based descriptions, of which the Vicsek model[4] is an example, as it analyzes the collective behavior of self-propelled particles which attempt to align with their neighbours. The second approach is the formulation of continuum field theories which capture the essential features of the system under study. For instance, Toner and Tu[9] wrote a hydrodynamic description of the Vicsek model, which obeys the same symmetries, features a similar phase transition, and can be derived by coarse-graining a Vicsek-like microscopic model[10].

One of the defining features of biological organisms, which extends to active systems, is the sensing and processing of, as well as the subsequent adaptation to, stimuli[11]. A particularly biologically relevant example of this is *chemotaxis*, a gradient-sensing behavior used by organisms to forage for nutrients, initiate social behavior, or escape harmful environments[12].

1.1.1 Chemotaxis of microorganisms

The ability of organisms to move in response to environmental cues is essential to their survival, which has led to the emergence of a variety of mechanisms to perform these functions. For instance, macroscopic animals forage for food by following olfactory trails, which involves intermittent signal acquisition by a complex sensory apparatus and information processing by the brain[13]. Microorganisms share similar concerns: they need to find nutrient sources and avoid toxins, which entails directed motion as a response to chemical gradients using simpler tools than the ones available to more complex organisms.

One issue faced by microorganisms is that they live in a world dominated by viscous effects[14], which creates challenges that larger organisms do not encounter in their locomotion. Purcell elegantly formulated this idea in his celebrated Scallop theorem[15], which states that
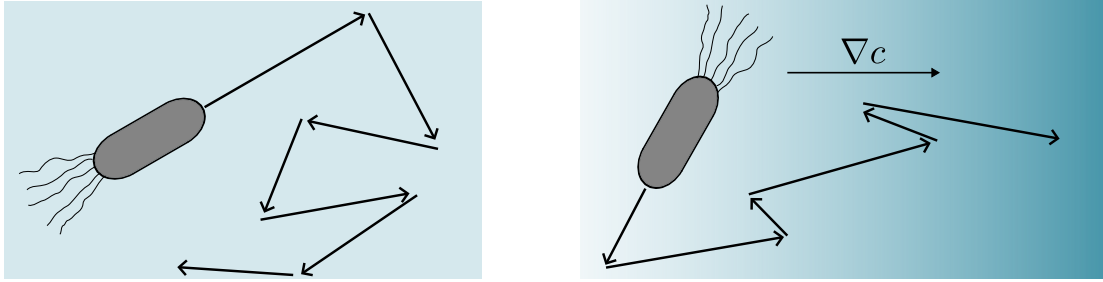
Figure 1.1: Bacterial swimming and chemotaxis. **Left**: In an uniform concentration profile, a bacterium swims through a series of linear runs, interrupted by tumbling periods during which it randomly reorients. The net effect is a random walk. **Right**: In the presence of a chemoattractant concentration gradient ∇c, the bacterium biases its random walk, going towards the higher attractant concentrations.

swimming at low Reynolds number is impossible with a single degree of freedom. Evolution has nonetheless provided microorganisms with elegant solutions to solve this problem, by actuating an organelle or a group of organelles in a time-asymmetric stroke[16]. For example, many species of bacteria (most famously *E. Coli*[17]) swim using flagella driven by a rotary motor embedded in their cell wall[18].

Many species of bacteria swim according to a "run and tumble" pattern[17]: they move straight for some period of time, then stop and reorient before starting to swim again, performing a random walk in the absence of stimuli[19,20]. In the presence of a concentration gradient of a food chemical or secreted attractant, these bacteria change their running time to move towards higher food concentrations, biasing their random walk in a manner which results in chemotaxis[17,21]. Many other stimuli can trigger directed motion, for instance light[22] (phototaxis) or temperature gradients[23] (thermotaxis). Chemotaxis allows microorganisms to efficiently manage the amount of resources at their disposal[24], or to assemble into multicellular structures[25], among other functions[26]. Its usefulness naturally makes chemotaxis a common behavior in different kinds of cells: lymphocites chemotax as a part of immune response[27–29], cancer cells use chemotaxis to direct their migration[30], and eukaryotic amoebae

move in response to chemical signals left by their kin[31], among many other examples.

The chemotaxis of unicellular organisms results from the operation of intricate sensing and locomotion mechanisms. For instance, in *E. Coli*, the activation of membrane-embedded sensors modulate the activation of the flagella[32,33], biasing the random walk these bacteria perform towards sources of nutrients. Describing the action of this machinery in detail is a complex task, for which several timescales must be taken into account, from the stochastic activation of the chemotactic receptors to the resulting motion[34]. Phenomenologically, its effect can be described as follows[35]: at long enough time and length scales, a biological system undergoing chemotaxis in an external concentration gradient ∇c can be described with a chemotactic drift velocity $\boldsymbol{V}$ along the gradient

$$\boldsymbol{V} = -\mu \nabla c. \tag{1.1}$$

The drift velocity given by Eq. (1.1) is proportional to a mobility μ. If negative, it leads to motion towards higher concentrations of the chemical, and if positive, it makes the cell swim away from the chemical source [*].

The term chemotaxis is used in literature to describe different behaviors. In some cases, it designates the ability of agents to move along a concentration gradient, irrespective of the mechanisms through which this movement occurs[37–40]. Some other sources have a more restrictive definition, and make the difference between chemotaxis, which is the reorientation of a swimmer's swimming direction to follow concentration gradients, and "chemokinesis", a concentration-dependent modulation of the velocity magnitude which also results in a drift

---

[*]In general, the chemotactic mobility is concentration-dependent[35] $\mu(c)$, which reflects the change in receptor sensitivity with chemoattractant/repellent concentration[36]. Here, for simplicity, we do not include that dependence.

in gradients [41,42]. In this thesis, we will use a more permissive definition, and designate as chemotactic any object which develops a net drift velocity in concentration gradients.

1.1.2 PHORETIC MICROSWIMMERS

Artificial swimmers able to propel themselves and follow concentrations gradients are useful model systems for swimming microorganisms and have a staggering wealth of potential applications, from the removal of environmental contaminants [43,44] to biomedical applications such as targeted drug delivery [45] or sensing of biomarkers [46]. While some artificial swimmers have successfully been designed to move using the same principles as motile cells [47,48], another entirely different – and more easily implemented – swimming method has also been successful: the use of phoretic effects to drive motions in self-induced gradients.
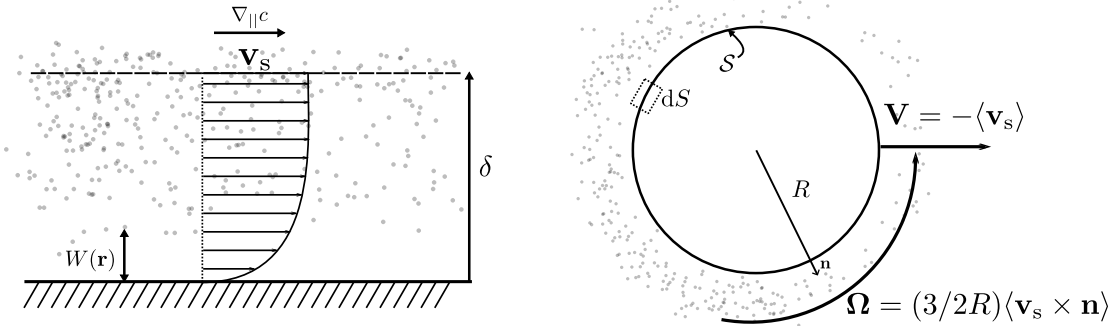
Figure 1.2: Diffusiophoretic drift of a spherical colloid. Left: the interaction potential $W(\mathbf{r})$ between an interface and a solute diluted in a fluid (gray spheres) creates a flow over a slip layer of thickness δ. At the boundary between the slip layer and the rest of the medium, the fluid has a velocity $\mathbf{v}_s$ given by Eq. (1.2). Right: The surface $\mathcal{S}$ of a spherical colloid of radius R can be decomposed into surface elements $\mathrm{d}S$ which have the behavior shown in the left panel. Due to these phoretic effects, in a solute gradient, the colloid develops a translational velocity $\mathbf{V}$ given by Eq. (1.3) and a rotational velocity Ω given by Eq. (1.4).

Phoresis is the motion of a body through interfacial effects driven by the gradient of a scalar field Φ [49–51], which can for instance represent temperature [52,53] (thermophoresis), electric potential [54–56] (electrophoresis), or concentration of a solute [57–61] (diffusiophoresis). Consider an

interface immersed in a fluid and in the presence of a field gradient $\nabla\Phi$. The interface perturbs the field Φ, which applies a body force to the fluid in the vicinity of the interface, resulting in a fluid flow whose expression depends on the nature of Φ[51]. If Φ is the concentration $c(\boldsymbol{r}, t)$ of a solute diluted in the fluid medium, the interface has a short-range interaction with the solute particles over a characteristic distance δ which locally changes their concentration, giving rise to a pressure gradient which causes a flow over a layer of thickness δ (Fig. 1.2, left)[49]. Electrophoresis, on the other hand, relies on the existence of a thin layer of ions around the interface[51], which experiences a force when an electric field is applied leading to the development of a flow over the Debye screening length $\delta = \kappa^{-1}$.

Different kinds of phoretic effects then result in the apparition of a *slip velocity* over the distance δ (Fig. 1.2, left), which in its general form can be written as[51],

$$\boldsymbol{v}_{\text{s}} = m\nabla_{||}\Phi_{\text{int}}, \tag{1.2}$$

where Φ_{int} is the value of the field at the interface between the slip layer and the outer fluid, $\nabla_{||}$ represents the spatial gradient parallel to the interface, and m is the local phoretic mobility, which can be derived using a hydrodynamic[49-51] or a stochastic many-body approach[49,62].

In the case of a spherical colloid of radius $R \gg \delta$ and surface $\mathcal{S}$ with a position-dependent mobility $m(\boldsymbol{r}_s \in \mathcal{S})$ (Fig. 1.2, right), we can obtain the drift velocity of the colloid by using the slip velocity $\boldsymbol{v}_{\text{s}}$ as a boundary condition and the Lorentz reciprocal theorem[63]:

$$\boldsymbol{V} = -\langle\boldsymbol{v}_{\text{s}}\rangle_{\mathcal{S}} = -\frac{1}{4\pi R^2}\iint_S m(\boldsymbol{r}_{\text{s}})\nabla_{||}\Phi(\boldsymbol{r}_s)\,\mathrm{d}S, \tag{1.3}$$

where $\langle\cdot\rangle_{\mathcal{S}}$ is the averaging operator over the colloid surface, and $\mathrm{d}S$ is a surface element. If

the colloid has an asymmetric coating, it also experiences a rotational velocity[49,51]:

$$\boldsymbol{\Omega} = \frac{3}{2R}\langle \boldsymbol{v}_\text{s} \times \boldsymbol{n}\rangle_\mathcal{S} = \frac{3}{8\pi R^3} \iint_\mathcal{S} m(\boldsymbol{r}_\text{s})\left(\nabla_{||}\Phi(\boldsymbol{r}_s) \times \boldsymbol{n}\right) \text{d}S. \qquad (1.4)$$

with $\boldsymbol{n}$ the normal unit vector to the surface element $\text{d}S$. For an isotropically coated colloid, and in the limit of a system size large compared to R, Eq. (1.3) reduces to Eq. (1.1)[38], where μ takes the role of the local phoretic mobility averaged over the colloid surface.

The phoretic phenomena we described here are driven but passive, allowing diffusiophoretic colloids to follow external concentration gradients and accumulate in regions of higher or lower concentrations of some chemicals[57,64]. Biological systems, meanwhile, are active: they consume energy to locomote, and respond to gradients by adjusting their propulsion direction or speed[17]. To accurately model biological systems, phoretic colloids must then be made active.

Phoretic transport phenomena are force-free[65], i.e. no net force is applied on the system composed of the colloid and its slip boundary layer. This makes them a good candidate for self-propelled swimmers, provided that they can create and sustain a gradient which puts them in motion[66–68]. In order for a phoretic particle to swim, this gradient must be anisotropic, which is typically achieved through an asymmetric particle structure[67,69,70]. However, isotropically coated spherical colloids can also self-propel using alternate mechanisms which include symmetry-breaking of the field gradients through advection[71] and the formation of motile assemblies[72–76]. The first described self-propelled phoretic swimmers consisted of micrometer-long cylinders composed of a gold-coated half and a platinum-coated half[70], which develop motion along their central axis in the presence of hydrogen peroxide. This motion is fueled by the catalyzed decomposition of hydrogen peroxide at the platinum end of the rod and the
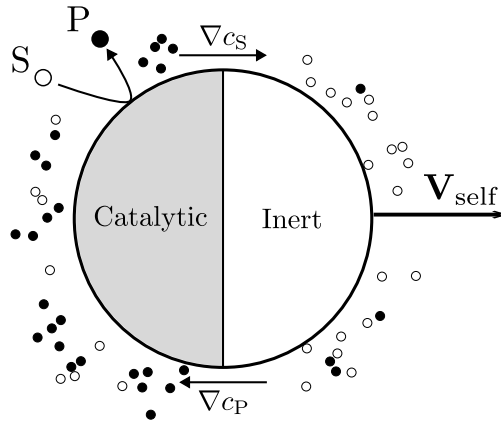
Figure 1.3: Self-diffusiophoretic Janus swimmer, composed of an inert half (right) and a catalytic half (left). The catalytic hemisphere catalyzes the conversion of a substrate S into a product P, creating a gradient of their respective concentrations ∇c_S and ∇c_P. The concentration gradients, according to Eq. (1.3), result in a swimming speed V_{self}.

recombination of the resulting hydrogen ions at the gold end[77], which generates an electric field around the rod and leads to its motion *via* self-electrophoresis[78]. Another extensively studied class of phoretic swimmers are spherical diffusiophoretic Janus colloids, composed of one inert hemisphere (for instance polystyrene[79]) and one active hemisphere (for instance platinum[79]) which catalyzes a chemical reaction[67,69] (Fig. 1.3).

Diffusiophoretic Janus swimmers exhibit greatly enhanced diffusive motion at long times in an homogeneous fuel concentration[79], and couple their translational (Eq. (1.3)) and rotational (Eq. (1.4)) degrees of freedom to fuel gradients, resulting in a drift velocity and rotation speed whose directions are determined by the material properties and the pattern of the colloid coating[80,81]. Self-phoretic particles have indeed been shown to align their swimming direction with external fuel gradients,[38,81–83], offering a good analogue to cellular chemotaxis without the complex biochemical machinery cells use. Similar mechanisms have been exploited to design thermophoretic light-activated Janus swimmers[84].

Catalytic enzymes are proteins which accelerate chemical reactions by lowering the corresponding energy barrier, leading to an exponential increase in reaction rate[85], and have been conceptualized as nanomotors and an example of active matter[86–88].
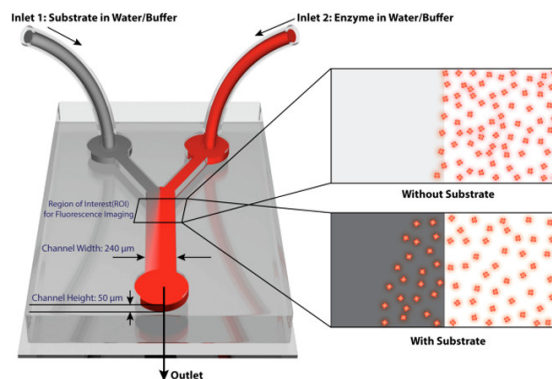
Figure 1.4: Microfluidic measurement of enzyme chemotaxis. An enzyme is introduced in the right input and its substrate or a buffer in the left input. The introduction of substrate induces an increased enzyme concentration in the left of the microfluidic channel compared to the buffer. Reprinted with permission from "Enzyme Molecules as Nanomotors ", Samudra Sengupta, Krishna K. Dey,Hari S. Muddana, Tristan Tabouillot, Michael E. Ibele, Peter J. Butler, and Ayusman Sen, J. Am. Chem. Soc. 2013, 135, 4, 1406–1414[89]. Copyright 2013 American Chemical Society.

Microfluidics assays (Fig. 1.4) have shown that enzymes perform collective directed motion in concentration gradients of their substrate, both towards higher[86,90–92] and lower[87,93] concentrations. This constitutes a form of chemotaxis at the nanoscale, the mechanism behind which is currently under debate. One proposed explanation is based on an active process[87,93], and relies on the idea that enzymes perform "leaps" every time they catalyze a reaction which propels them ballistically over short timescales. Another explanation[39,62] relies on the competition between two passive effects: diffusiophoresis (Section 1.1.2) and a change in enzyme diffusion coefficient upon the reversible binding with its substrate[†]. As opposed to the leap

---

[†]In general, the enhanced diffusion of enzymes[94] is a controversial topic. Its very existence is still currently

hypothesis, these two phenomena are both equilibrium, and do not necessitate the enzyme to perform catalysis. One argument in favor of the latter mechanism is that it explains the seemingly contradictory behaviors of the enzyme urease, in different experiments chemotax either towards higher[91] or towards lower[93] substrate concentrations. The equilibrium-effects-based theory describes enzyme chemotaxis as resulting from the competition between two contributions, and features a crossover between positive and negative chemotaxis at a critical concentration[62] which reconciles these two observations. Overall, while experimental data clearly indicates that enzymes perform chemotaxis, the mechanism behind this is still unclear, and needs further theoretical and experimental efforts to be fully uncovered. Possible biological consequences of enzyme chemotaxis are discussed in Section 1.3.2.

1.2   Field-mediated interactions of active particles

We have so far focused on the response of individual particles, either biological or artificial, to external concentration gradients. If the particles are chemically active, for instance catalyst-coated colloids, then they also create such gradients, in turn inducing a response in other particles. Several catalytically active and chemotactic particles then develop effective interactions, mediated by the concentration fields upon which they act[68].

To understand the elementary features of these interactions, we write a simple model. Consider an isolated active particle with a local surface activity $a(r_S)$ corresponding to the rate of production (if $a > 0$) or consumption (if $a < 0$) of a field Φ that can describe the concentration of a solute for chemotactic colloids or cells[69] or a temperature difference for thermophoretic colloids[97]. For simplicity, we assume that the field obeys diffusive dynamics de-

---

debated, as different single-molecule measurements either observe it[95] or don't[96]. Its origins are also still being discussed[94], with the leaps invoked in the study of enzyme chemotaxis also being proposed as a mechanism[87].
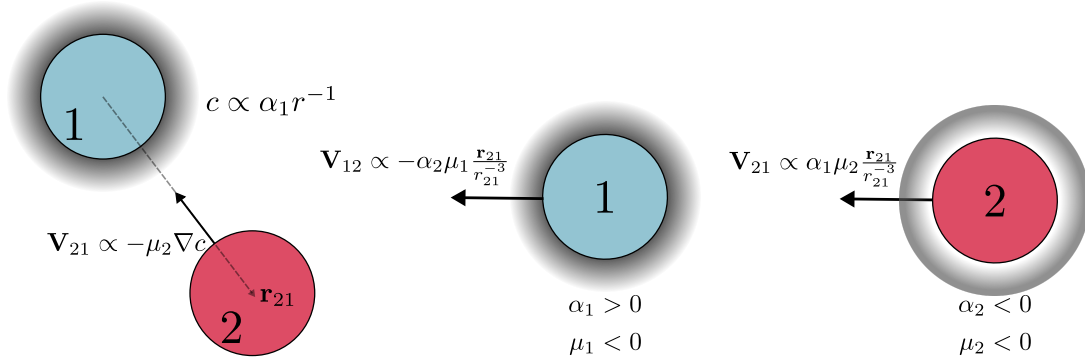
scribed as partial differential equation[67]

$$\partial_t \Phi = D_\Phi \nabla^2 \Phi, \qquad (1.5)$$

where D_Φ is the diffusion coefficient of the field, with the boundary condition

$$-D_\Phi \boldsymbol{n} \cdot \nabla c(\boldsymbol{r}_\mathrm{s}) = a(\boldsymbol{r}_\mathrm{s}), \qquad (1.6)$$

where $\boldsymbol{n}$ is the normal vector to the sphere surface, which describes the activity of the particle.

Figure 1.5: Chemical-field-mediated interactions between two catalytically active and chemotactic colloids. **Left**: particle 1 (light blue) produces a chemical at a rate α_1 through its chemical activity, perturbing the associated concentration field c. Particle 2, which is at a distance $\boldsymbol{r}_{21}$ from particle 1, responds to this perturbation through its chemotactic mobility μ_2. **Right**: the parameters of particles 1 and 2 are chosen so that 1 produces the chemical field, 2 consumes it, and they both chemotax towards higher concentrations. This leads to motion of particle 1 towards particle 2, and particle 2 away from 1, constituting an example of chasing interactions.

Eq. (1.5) can be solved in order to obtain the perturbation of the field created by the particle. For an isotropically coated spherical colloid designated as "particle 1", we calculate the steady-state profile of the field by setting the left-hand term in Eq. (1.5) to zero, yielding the Laplace

equation which has the textbook solution

$$\Phi(r) = \frac{\alpha_1}{4\pi D_\Phi} \frac{1}{r},$$
(1.7)

where $\alpha_1 = a_1 4\pi R^2$ is the overall activity of particle 1 and r the distance to its center (Fig. 1.5). A second phoretic particle placed at a distance $\boldsymbol{r}_{21}$ (oriented towards the center of particle 2, see Fig. 1.5, left) develops a phoretic response given by Eq. (1.1) (Fig. 1.5) which reads:

$$\boldsymbol{V}_{21} = \frac{\alpha_1 \mu_2}{4\pi D_\Phi} \frac{\boldsymbol{r}_{21}}{r_{21}^3}.$$
(1.8)

The expression given in Eq. (1.8) involves some key simplifying assumptions. One condition for its validity is that the particles are far enough to neglect near-field chemical and hydrodynamic effects, which can change their qualitative behavior at low separations[98]. If the active particles have anisotropic activities and mobilities, for instance if they have a Janus geometry, a rotational response additionally needs to be calculated[99]. As we calculated the field profile given by Eq. (1.7) in the steady state, Eq. (1.8) also implicitly involves a quasi-static approximation which breaks down in the limit of a slow-diffusing chemical[100].

Eq. (1.8) reveals two key features of phoretic interactions: they are *long-ranged* and *non-reciprocal*. In the absence of screening, which can originate from the degradation of a chemical if Φ is a concentration field[37], the interaction between the two colloids decays as a power law and corresponds to a scale-free, and therefore long-ranged, interaction. The long-ranged nature of field-mediated interactions can be exploited by chemotactic cells to signal each other over long distances, and leads to system-wide instabilities in mixtures of active colloids (Section 1.2.3). From Eq. (1.8), we also see that the direction of the induced velocity $\boldsymbol{V}_{21}$ depends

on the sign of the product $\alpha_1\mu_2$. If $\alpha_1\mu_2 < 0$, particle 2 moves towards particle 1, corresponding to an attractive interaction, while if $\alpha_1\mu_2 > 0$, particle 2 moves away from particle 1, and the interaction is repelling. On the other hand, the nature of the response of particle 1 to particle 2 is determined by the sign of $\alpha_2\mu_1$, which in general is different from $\alpha_1\mu_2$: the interaction between the two particles is then non-reciprocal (Fig. 1.5). In particular, if the two particles' responses have opposite signs, they behave as predator and prey[101].

1.2.1   Non-reciprocal interactions

One of the foundations of classical mechanics is Newton's third law, often summarized as "action equals reaction". It states that, if a body A applies a force $\boldsymbol{F}_{AB}$ on another body B, then B applies an equal and opposite force on A: $\boldsymbol{F}_{BA} = -\boldsymbol{F}_{AB}$. A feature of active matter systems which has been the source of recent interest[102] is the ability of their components to break this action-reaction symmetry, which is only possible in non-equilibrium conditions[103] ‡.

Active chemotactic particles interacting through concentration fields constitute an example of multi-species mixtures whose components interact non-reciprocally[75,105,106]. Other multi-species systems which break action-reaction symmetry have been shown to self-organize into so-called chiral phases[104], for instance corresponding to the emergence of spontaneous rotation in Vicsek-like flocking models. Another recent body of work concerns descriptions of scalar fields which interact through short-ranged, non-reciprocal interactions[107–109] and can form self-propelled moving bands and oscillating spots.

---

‡Action-reaction symmetry is only broken at the level of the effective interactions between components, i.e. once the interactions between the active particles and the surrounding medium which mediates the effective interactions have been coarse-grained[104]. Newton's third law is still obeyed if the whole system is described.

Non-reciprocity can also be present in single-component systems, i.e. in which all agents have the same properties. One such example is the case of "social-like" interactions, in which individuals react to another agent only if the latter is located in a limited vision cone[110–112], similar to models used to describe the collective behavior of human crowds[113]. Agents with social-like interactions can form cohesive groups[114] or to organize into different patterns based on the size of their vision cones[110]. In the context of a modified XY model, they can also form a long-ranged phase, seemingly breaking the Mermin-Wagner theorem[112]. An analogous mode of interaction can be obtained for thermophoretic Janus colloids under directional illumination, which shade the colloids below them in a non-reciprocal manner[97]. Interestingly, vision-cone-based interactions have also been implemented in a suspension of colloids which can be programmed with arbitrary interactions, constituting an ideal experimental system for the aforementioned models[114].

1.2.2 SMALL SCALE BEHAVIOR OF ACTIVE PHORETIC PARTICLES: COLLOIDAL MOLECULE FORMATION

The non-reciprocity of the interactions between active chemotactic particles have far-reaching consequences, which we will explore at two levels of description: first systems of low particle number or density, and, in the next paragraph, denser mixtures with a larger particle number.

Consider a dilute mixture of two species of active particles which chase after each other, i.e. particles of species 1 goes towards particles of species 2, which in turn move away from particles of species 1[101]. Such a system can be for instance realized using spherical, uniformly coated colloids which obey Eq. (1.8) with $\alpha\mu$ products of opposite signs. In this situation, particle-based models can still be approached from an analytical angle[72,73]. In some parameter regimes,

14

the particles can assemble into objects with dynamics emerging from the chasing interactions. The formation of such structures was theoretically formulated for uniformly coated chemotactic colloids,[72,73], and has been experimentally observed in systems of active droplets[106] and light-controlled active colloids[75,105]. These "colloidal molecules" develop different modes of motion depending on their stoichiometry (the ratio between species populations) and the spatial arrangement of their constituents, with observed behaviors including spinning, linear translation, rotational movement, and periodic beating[72,73,75].

Janus particles, meanwhile, have an intrinsic polarity which leads to orientational interactions and consequently to richer dynamics[99]. For instance, a pair of Janus colloids can form bound states in which they move in a correlated manner and orbit around each other over long time scales[99,115].

1.2.3 Large-scale behavior: the Keller-Segel model and beyond

Large or dense systems of chemotactic particles can be described using coarse-grained theories involving a particle density field, the most famous example of which is the Keller-Segel model of slime mold aggregation[37].

Chemical-field-mediated interactions are an essential tool for the collective organization of microorganisms. Many social species secrete chemoattractant signals to guide other cells to them, such as the amoeba *Dictyostelium discoideum*[31]. In the Keller-Segel model, these amoebae are described by a time- and space-dependent concentration $\rho(\boldsymbol{r}, t)$, and locally produce the signaling chemical acrasin (concentration $c(\boldsymbol{r}, t)$) at a rate $\alpha > 0$. The production of acrasin is counteracted by its degradation at a rate k_{deg} by an enzyme which the amoebae slowly secrete. The cells follow acrasin concentration gradients by developing a chemotactic

velocity given by Eq. (1.1) with a mobility $\mu < 0$ which, according to Eq. (1.8), tends to bring them together. The coupled dynamics of the amoeba and acrasin concentration fields can then be written in its simplest form [§] as [37]:

$$
\begin{aligned}
\partial_t \rho &= \nabla \cdot [D_\rho \nabla \rho + \mu \rho \nabla c] \\
\partial_t c &= D_c \nabla^2 c + \alpha \rho - k_{\text{deg}} c,
\end{aligned}
\tag{1.9}
$$

where D_ρ is the diffusion coefficient of the active particles and k_{deg} is a rate of spontaneous field degradation.

A linear stability analysis of Eq. (1.9) shows that perturbing an initially homogeneous density of cells and acrasin can lead to an instability in which the amoebae aggregate if $\mu\alpha/(D_\rho k_{\text{deg}}) < -1$ [37]. As reflected by this condition, the mechanism behind aggregation is that amoebae, by following the acrasin concentration gradient ($\mu\rho\nabla c$ term), tend to increase their density ρ and thus the local attractant production $\alpha\rho$, leading to a positive feedback loop. Chemotactic aggregation is meanwhile inhibited by the cell diffusive flux $-D_\rho\nabla\rho$ and the acrasin degradation $-k_{\text{deg}} c$ which both smooth out concentration gradients and must then be overcome for the amoebae to aggregate.

The Keller-Segel model also qualitatively captures other collective behaviors of microorganisms, such as the migration of bacteria in concentration gradients [116,117], and has also been applied to the collective dynamics of fast-aligning autophoretic Janus particles [82,118]. Many variations of Eq. (1.9) have been studied which add biologically and physically relevant ingredients [119], for instance excluded volume effects to avoid a blowup of the cell density field ρ [120].

[§]Compared to the original equations written by Keller and Segel, we neglected for simplicity the dependence of the quantities α, μ and k_{deg} on the concentrations ρ and c. We invite the reader to read the original publication [37] for the analysis of the full equation.

The mean-field nature of Eq. (1.9)[121] also implies that the Keller-Segel model does not account for stochastic effects. To incorporate these, stochastic field equations must be derived from the Langevin dynamics of individual chemotactic particles[121,122], in the context of which additional physical ingredients have been considered, for instance the birth and death[123,124] or the polarity[125] of chemotactic cells.

Another example of chemical signaling is provided by some species of bacteria which both secrete and follow a slow-diffusing polymer trail[126]. The deposition of these trails strongly influences the motion of individual bacteria[127] and leads to collective dynamics[126] which drive the formation of multicellular structures[100]. A similar trail-leaving mechanism was recently reproduced in an artificial system of micelles which leave behind a chemo*repellent*, leading to caged dynamics[128]. More indirectly, field-mediated interactions are also achieved through quorum sensing, a phenomenon in which bacteria measure their density by secreting and sensing a signaling molecule[129]. It is used a switch for collective behavior[130]: above a concentration threshold, bacteria start regulating the expression of various genes, including some related to motility[131–133]. A simple concentration-based motility response has been reproduced in systems of Janus colloids[134], providing a model system for the study of quorum-sensing.

Besides biological and bio-inspired systems, artificial colloids with field-mediated interactions also exhibit fascinating collective dynamics. A possible behavior, first observed in monodisperse suspensions of Janus swimmers, is dynamic clustering: the formation of clusters which grow to a fixed size, dynamically exchange particles with their surroundings, merge, and break apart[38,118,135–137]. Suspensions of phoretic or chemotactic active particles can also undergo large-scale instabilities[97] which can result in the formation of self-propelled aggregates, as demonstrated for thermophoretic Janus colloids[138] and isotropically coated catalytic parti-

cles[139]. For the particular case of Janus particles, a more careful treatment of the orientational dynamics through a gradient expansion procedure leads to a wide variety of collective behaviors[80,140], in particular oscillatory dynamics.

1.3   DENSE, ACTIVE INTRACELLULAR MATTER

Our focus over the last two sections has mostly been on microscopic objects, typically cells and colloids. The physical phenomena we previously described also apply to lower length scales, more specifically to chemotactic enzymes (Section 1.1.3) which thus should be able to develop field-mediated interactions similar to the ones described in Section 1.2.1. In order to understand the possible consequences of these effects in biological systems, we describe here how the intracellular environment is shaped by various active processes.

The inside of a cell is a dense and dynamic environment, in which a large variety of processes must occur simultaneously in a space- and time-localized manner[141]. Control over these processes is intrinsically active, typically fueled by adenosine triphosphate (ATP) hydrolysis, and involves, among many other examples, the dynamic formation and dissolution of membraneless organelles (Section 1.3.1), the spatial localization of catalytic enzymes for increased reaction efficiency (Section 1.3.2), and a variety of efficient intracellular transport processes.

A famous example of intracellular transport is the use by eukaryotic cells of ATP-powered molecular motors, which glide along cytoskeletal filaments in order to quickly and selectively move objects between organelles[85]. Prokaryotes do not possess these motor proteins and must then mostly rely on diffusion for intracellular transport[142]. However, the bacterial cytoplasm is particularly crowded[143], which would lead to glassy dynamics at equilibrium and strongly hinder the motion of objects inside bacterial cells[144]. Metabolic activity has

been found to restore efficient intracellular transport by fluidizing the cytoplasm,[144], a phenomenon which is currently studied using non-motile active matter models[145,146].

1.3.1 BIOMOLECULAR CONDENSATES

As a part of their functioning, cells must perform a staggering variety of biochemical processes, many of which compete for the same resources or necessitate different chemical environments. In order to simultaneously support all these processes, cells are divided into compartments, also called organelles. Many of these compartments are separated from the cell cytoplasm by a lipid membrane, most famously the eukaryotic nucleus in which DNA transcription occurs[141].

A second class of organelles, which has garnered significant amounts of attention over the past decade, is membraneless[147]. These structures, called *biomolecular condensates*[148], have liquid-like rheological properties such as flowing, surface tension, and coalescence[149]. They are formed through liquid-liquid phase separation[149–151], which allows the cell to control their assembly and disassembly through active processes[152]. For instance, the formation of condensates can be triggered by increasing the concentration or the transcription rate of RNAs[153,154]. Both the formation and dissolution of condensates are also possible by tuning the interactions between their components, which cells can dynamically do through post-transcriptional modifications[155].

Strikingly, whereas droplets formed through equilibrium liquid-liquid phase separation undergo a coarsening process which results in a single large droplet, biomolecular condensates grow until they reach a fixed size[156]. This arrested coarsening phenomenon can be explained by adding out-of-equilibrium chemical reactions to models of liquid-liquid phase

separation[156], suggesting that condensates are intrinsically active objects. Out-of-equilibrium condensates, also called *active droplets* or *active emulsions*, can additionally be positioned by external concentration gradients[157], echoing the spatial localization of biomolecular condensates[149], and can in some conditions undergo division[158,159], hinting at a possible role in the origin of life.

Condensates concentrate dozens[160] to hundreds[161] different protein, DNA, and RNA species, which, according to the theory of multi-component phase separation, allows for varied morphologies[151,162]. The interplay between cell biology, soft matter, and out-of-equilibrium statistical physics is then very strong in these systems: as an illustration, the complex geometries obtained by multicomponent liquid-liquid phase separation can be exploited to spatially arrange successive steps of self-assembly chemical reactions in a structure akin to a molecular assembly line[163].

1.3.2 COLLECTIVE BEHAVIOR OF ENZYMES

Catalytic enzymes are the workhorse of metabolism, participating in intricate biochemical reaction pathways which involve up to an order of ten steps and as many intermediates[141]. As a part of their function as reaction crucibles, it is then natural to expect biomolecular condensates to include enzymes, the intrinsically active nature of which influences their behavior.

Many enzymes are already known to self-assemble into transient structures called *metabolons*, first conceptualized by Paul Srere[164], in the presence of their substrate[165]. While the characterization of their role is still an ongoing task, one broadly accepted function of metabolons is *substrate channeling*, the efficient transfer of a reaction intermediate between two successive enzymes in a chain of reactions[166].

Substrate channeling has initially been studied in the context of complexes of physically linked enzymes, this particular case being called direct channeling, and involving the directed transfer of a reaction intermediate from one enzyme to the active site of the next through a physical "tunnel"[167]. Counterintuitively, this process only transiently increases a pathway's output rate, and does not increase the reaction output at the steady state[165,168]. Instead, direct channeling is effective at preventing the escape of reaction intermediates[168], which could serve to avoid their use in unwanted reaction pathways or their spontaneous degradation during diffusive transfer[167].

Another kind of substrate channeling, more relevant to condensate-sized clusters , is probabilistic channeling[165], in which different enzymes participating in the same pathway colocate to efficiently transfer an intermediate. This mode of substrate channeling has been shown to increase efficiency of metabolic pathways[169] and to provide a mechanism for the selection of a path in a branching point[169,170].

A particularly relevant metabolon in the context of this section is the purinosome[171], which concentrates the enzymes involved in the ten-step de novo purine biosynthesis pathway. Purinosomes have all the hallmarks of biomolecular condensates: they are spherical, membrane-less structures with a 0.1 - 1 micron radius[172,173] and liquid-like properties[174]. While the properties and the biological functions of the purinosome are still not fully understood, its existence hint at an important role of enzymes in the formation and function of condensates[171].

Recent works have started exploring the possible consequences of the presence of enzymes inside condensates. In an experimental realization of enzyme-containing, condensate-like droplets[175], it was found that enzymes had a significantly increased reaction rate compared to an homogeneous phase. This, coupled with very low activity levels outside droplets, high-
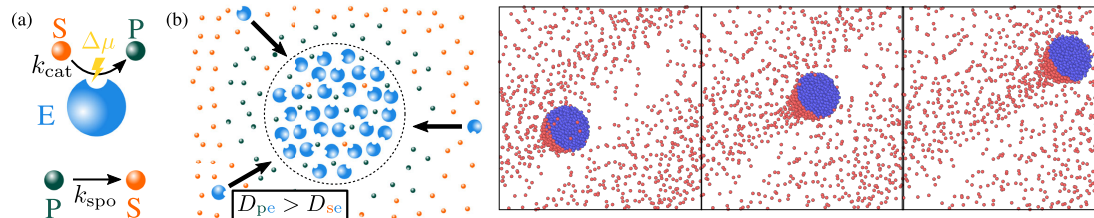
Figure 1.6: Enzyme aggregation driven by out-of-equilibrium catalytic activity. **Left**: By driving the conversion of a substrate S into its product P out of equilibrium (a), enzymes E can create gradients which leads to their self-organization into a condensate-like cluster (b). **Right**: The non-reciprocal interactions described by Eq. (1.8) can lead to aggregation of a mixture of two catalytically active species, one which produces a chemical and the other which consumes it, for instance representing two successive enzymes in a metabolic pathway. Brownian dynamics simulations show the active particles form a cluster which, due to the chasing nature of the interactions (Fig. 1.5), spontaneously breaks symmetry and self-propels. Left panel reproduced from "Catalysis-Induced Phase Separation and Autoregulation of Enzymatic Activity", Matthew W. Cotton, Ramin Golestanian, and Jaime Agudo-Canalejo, Phys. Rev. Lett. 129, 158101 (2022). Licensed under a Creative Commons Attribution 4.0 International License. Original article available at `https://doi.org/10.1103/PhysRevLett.129.158101`. Link to license: `https://creativecommons.org/licenses/by/4.0/legalcode`

lights the usefulness of enzyme-rich condensates as fast and selective reaction crucibles. Enzymatic activity inside of condensates can also lead to the emergence of qualitatively new behaviors, being experimentally found to induce hydrodynamic flow inside droplets[175], and theoretically predicted to lead to diffusiophoresis-like interfacial effects and the ability to divide through a shape instability[176].

Besides the emergence of new effects in already-formed droplets, enzymes might also be involved in the formation and control of membraneless organelles. By catalyzing chemical reactions, they offer for instance a mechanism for the size control of condensates, and can arrest their coarsening by generating diffusive fluxes[177]. While condensate formation is generally understood to be a result of attractive equilibrium interactions[151], theoretical models have predicted that enzymes can drive the assembly of condensates purely thanks to their catalytic activity[178] (Fig. 1.6, left). This catalysis-induced phase separation results in a droplet with reduced chemical reaction flux compared to an homogeneous phase, thus constituting

a possible self-regulation mechanism of enzymatic activity.

The chemotactic properties of enzymes (Section 1.1.3) might play a role in their biological activity, e.g. by driving their collective motion towards regions of low substrate concentration[179] which would, according to the Michaelis-Menten law[141], decrease their catalytic activity. Recent experimental[92,180] and theoretical[139] work has meanwhile shown that chemotaxis can promote the assembly of enzymes involved in successive catalysis steps (Fig. 1.6, right). This motivates further investigation into the role of chemotaxis in condensate formation and function, both as a physical and a biological problem.

1.4 Thesis outline: spatio-temporal self-organization of chemophoretic agents

The spatial self-organization of catalytically active particles is, at the same time, a fascinating physical problem to tackle, and an important phenomenon for cellular function.

A possible approach to this problem is to modify the Keller-Segel equations Eq. (1.9) to describe a mixture of several active and chemotactic species with long-range and non-reciprocal interactions similar to Eq. (1.8). A mixture of M enzyme species interacting through a single chemical field without degradation obeys the system of equations[139]:

$$
\begin{aligned}
\partial_t \rho_m &= \nabla \left[D_{\mathfrak{p}} \nabla \rho_m + \mu_m \rho_m \nabla c \right] \\
\partial_t c &= D \nabla^2 c + \sum_{m=1}^{M} \alpha_m \rho_m.
\end{aligned}
\tag{1.10}
$$

Performing a linear stability analysis around a homogeneous set of catalyst concentrations ρ_{0m}, it was found[139] that the catalytic mixture undergoes self-organization through a macro-

scopic instability if $\sum_{m=1}^{M} \alpha_m \mu_m \rho_{0m} < 0$, i.e. if the mixture is overall self-attracting. At the onset of instability, two species with the same mobility sign were found to aggregate, while species with opposite mobility signs were found to separate. Particle-based Brownian dynamics simulations (Fig. 1.6, right) showed that an unstable mixture of two non-reciprocally-interacting particles can organize into a self-propelled, comet-like structure.

This thesis extends the Keller-Segel-like formalism developed in Ref. 139 by taking into account a number of key physical ingredients that are essential to biologically relevance, and which lead to new phenomenology. The rest of the thesis is structured as follows:

In Chapter 2, we take a more detailed description of the catalytic particles, taking into account the dependence of the reaction speed on the substrate concentration and the size dispersity of different catalytic species. We find that these ingredients lead to a rich phenomenology, which we characterize analytically. This chapter is reproduced from Ouazan-Reboul *et. al.*, Eur. Phys. J. E, 44 9 (2021) 113 ¶.

In Chapter 3, we consider the possible role of catalytic and chemotactic particles in an origin of life scenario. We assume the existence of a primitive metabolic cycle involving an arbitrary number of catalytic species with identical parameters, and characterize analytically and numerically its ability to self-organise into protocell-like structures. This chapter is reproduced from a revised version of the preprint Ouazan-Reboul et al, ArXiv:2303.09832 (2023) ‖, currently under review at Nature Communications.

In Chapter 4, we also study the self-organization of a simple metabolic cycle, which con-

---

‖Revised manuscript reused with the permission of the authors

tains a fixed number of species with arbitrary parameters, allowing for a larger variation of interaction patterns. We discover that these general interaction rules allow for the self-organization of catalytic species which are all self-repelling, which constitutes a new behavior in such systems. This chapter is reproduced from the preprint Ouazan-Reboul et al, ArXiv:2303.09832 (2023) [**], currently under review at Physical Review Letters.

In Chapter 5, we further characterize the system first described in Chapter 4. We exhaustively study all the possible interaction networks that three-species metabolic cycles can develop, and classify them according to their ability to become unstable and the associated instability conditions. This chapter is reproduced from the preprint Ouazan-Reboul et al, ArXiv:2305.05472 (2023) [**], which has been submitted to the New Journal of Physics.

2

Non-equilibrium phase separation in mixtures of catalytically active particles: size dispersity and screening effects

Regular Article - Living Systems

Non-equilibrium phase separation in mixtures of catalytically active particles: size dispersity and screening effects

Vincent Ouazan-Reboul[1], Jaime Agudo-Canalejo[1], and Ramin Golestanian[1,2,a]

[1] Max Planck Institute for Dynamics and Self-Organization, Am Fassberg 17, D-37077 Göttingen, Germany
[2] Rudolf Peierls Centre for Theoretical Physics, University of Oxford, Oxford OX1 3PU, UK

Abstract Biomolecular condensates in cells are often rich in catalytically active enzymes. This is particularly true in the case of the large enzymatic complexes known as metabolons, which contain different enzymes that participate in the same catalytic pathway. One possible explanation for this self-organization is the combination of the catalytic activity of the enzymes and a chemotactic response to gradients of their substrate, which leads to a substrate-mediated effective interaction between enzymes. These interactions constitute a purely non-equilibrium effect and show exotic features such as non-reciprocity. Here, we analytically study a model describing the phase separation of a mixture of such catalytically active particles. We show that a Michaelis–Menten-like dependence of the particles' activities manifests itself as a screening of the interactions, and that a mixture of two differently sized active species can exhibit phase separation with transient oscillations. We also derive a rich stability phase diagram for a mixture of two species with both concentration-dependent activity and size dispersity. This work highlights the variety of possible phase separation behaviours in mixtures of chemically active particles, which provides an alternative pathway to the passive interactions more commonly associated with phase separation in cells. Our results highlight non-equilibrium organizing principles that can be important for biologically relevant liquid-liquid phase separation.

1 Introduction

Enzymes, which are chemically active proteins that catalyse metabolic reactions, have been found to exhibit non-equilibrium dynamical activity [1]. As part of their biological function, they are also known to self-organize into clusters called metabolons, which contain different enzymes that participate in the same catalytic pathway [2]. One possible theoretical explanation for this process is based on the ability of enzymes to chemotax in the presence of gradients of their substrate, which has been experimentally observed in recent years for a variety of enzymes [3–7]. The mechanisms underlying enzyme chemotaxis, however, are as of yet still unclear, with diffusiophoresis and substrate-induced changes in enzyme diffusion being possible candidates [7–11]. In a recent publication [12], it was shown that the interplay between catalytic activity and chemotaxis can lead to effective non-reciprocal interactions [13–15] between enzyme-like particles, resulting in an active mechanism for the phase separation of such particles. This active phase separation is distinct from the non-equilibrium phase separation models that have been more com-

monly put forward in the cell biological context [16], where the interactions between the different components are equilibrium ones, and the non-equilibrium aspect comes from fuelled chemical reactions that act as a source or sink of some of the phase-separating components. In contrast, in the model of Ref. [12], the phase-separating components are conserved, and it is the effective interactions between them that represent an intrinsically out-of-equilibrium phenomenon. For the particular case of a suspension of a single type of enzymes, the resulting aggregation process was later studied theoretically in more detail in Ref. [17]. An interesting non-biological model system to study these effects is provided by catalyst-coated synthetic colloids [18,19] and chemically active droplets [20], which have experimentally been shown to form aggregates *via* chemical-mediated effective interactions [21–26].

Here, we will generalize the model studied in Ref. [12], by accounting for size polydispersity of the catalytically active particles involved in the mixture, as well as for the dependence of catalytic activity on the concentration of substrate. We show that taking into account the dependence on substrate concentration leads to screening effects, which put a stricter activity threshold for the occurrence of a spatial instability. Moreover, we show that a mixture of different-sized catalytically

[a] e-mail: ramin.golestanian@ds.mpg.de (corresponding author)

active particles can undergo both local and system-wide self-organization, with the latter possibly showing oscillatory phenomena. A model that simultaneously takes into account both of these effects is finally shown to exhibit a rich phase diagram, ranging from non- to partially to fully oscillatory.

The paper is organized as follows. In Sect. 2, we explain the model describing the chemically active particles, and summarize previous results on the simplest version of this model [12]. In Sect. 3, we reveal a screening effect created by a dependence of the catalytic activity on the concentration of substrate, and conclude that this effect leads to an instability threshold and a local (as opposed to system-wide) instability. Then, in Sect. 4, we study the effect of a difference in the sizes of different particle species, which enters the theory as a difference in their diffusion coefficient. We show that under these conditions, the stability phase diagram of the particle mixture shows an extended instability region corresponding to a local instability, and can also exhibit transient oscillations during a system-wide instability. Finally, in Sect. 5, we consider both screening and size dispersity effects combined, which leads to a complex stability phase diagram, which includes fully, partially, and non-oscillatory local instabilities.

## 2 Linear stability analysis of a chemically active mixture

2.1 Model for chemically active particles

We study chemically active particles (for instance, enzymes or catalyst-coated colloids) whose chemical activity is characterized by a parameter α, which is the rate at which they consume ($\alpha < 0$) or produce ($\alpha > 0$) a given chemical. If we denote c the concentration of this chemical species, the presence of an isolated active particle creates a long-ranged perturbation to the concentration field of the chemical, which in steady state goes as $\delta c \propto \frac{\alpha}{r}$ (Fig. 1a).

The considered active particles are also chemotactic: in a concentration gradient of the chemical they act on, they develop a velocity $\mathbf{v} \propto -\mu \nabla c$ (Fig. 1b), which drives them towards high concentrations if $\mu < 0$ (chemotaxis), and low concentrations if $\mu > 0$ (antichemotaxis). Synthetic colloids can be engineered to be chemotactic, for instance using phoretic effects [27,28]. Meanwhile, many enzymes have been reported to chemotax in gradients of their substrate [3–7], with a variety of mechanisms having been proposed to explain the phenomenon [1,7–11].

These two properties give rise to effective particle-particle interactions mediated by the chemical field, which takes the form of a velocity developed by particle i in the presence of particle j given by [12–14]

$$\mathbf{v}_{ij} \propto -\frac{\alpha_j \mu_i}{r_{ij}^3}\mathbf{r}_{ij} \tag{1}$$
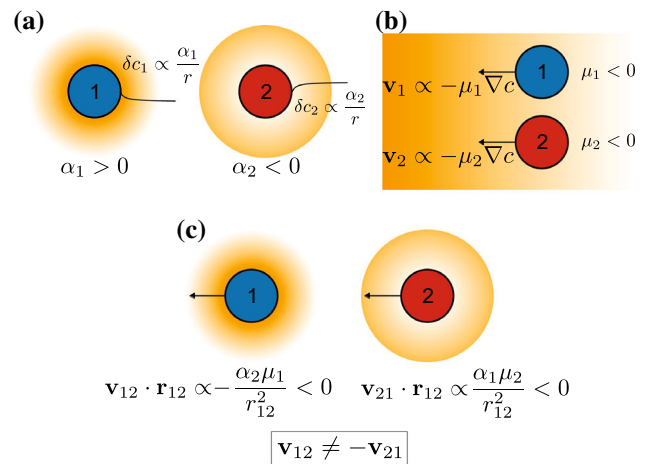
Fig. 1 Model for chemically active particles. **a** Chemical activity: particles 1 and 2 respectively produce and consume a chemical species (orange), perturbing its concentration profile around them. **b** Chemotaxis: the two species develop a velocity in response to concentration gradients of the same chemical they act on, in this case towards higher concentrations. **c** Particle–particle interactions arising from the combination of these two properties. Each particle both perturbs the chemical field and responds to the other's perturbation, leading to non-reciprocal interactions characteristic of active mixtures. In this case, species 1 is repelled by species 2, which is itself attracted by 1, giving rise to a chasing interaction

with $\mathbf{r}_{ij} = \mathbf{r}_i - \mathbf{r}_j$ the inter-particle distance vector. Note that as the perturbation of and the response to the concentration field obey to different parameters, this interaction is in general non-reciprocal: $\mathbf{v}_{ji} \neq -\mathbf{v}_{ij}$, leading for instance to the possibility of chasing interactions (Fig. 1c). This non-reciprocity, characteristic of active matter systems [12–15,29–32], can give rise to interesting many-body phenomena, which we will study here.

2.2 Linear stability analysis

We wish to study the ability of a mixture of these active particles to self-organize. To do so, we consider M species of particles, each with an activity α_m and a mobility μ_m, and described by a concentration field $\rho_m(\mathbf{r}, t)$. All the species act on the same chemical field, which we may refer as the messenger chemical. The active species concentrations evolve according to the Smoluchowski equation:

$$\partial_t \rho_m(\mathbf{r}, t) = \nabla \cdot [D_m \nabla \rho_m + \mu_m(\nabla c(\mathbf{r}, t))\rho_m(\mathbf{r}, t)] \tag{2}$$

with D_m the diffusion coefficient of species m and $c(\mathbf{r}, t)$ the concentration of the chemical.

The concentration of the chemical, meanwhile, obeys a reaction–diffusion equation:

$$\partial_t c\left(\mathbf{r}, t\right) = d\nabla^2 c + \sum_{m=1}^{M}\left(\alpha_m(c)\rho_m\left(\mathbf{r}, t\right)\right) \qquad (3)$$

where we allow for the activity of the active particles to be a function of the chemical concentration, and with d the diffusion coefficient of the chemical.

We perform a linear stability analysis by considering perturbations around a spatially homogeneous steady state, writing: $\rho\left(\mathbf{r}, t\right) = \rho_{0,m} + \delta\rho\left(\mathbf{r}, t\right)$ and $c\left(\mathbf{r}, t\right) = c_H(t) + \delta c\left(\mathbf{r}, t\right)$ with $c_H(t)$ the (potentially time dependent) homogeneous concentration of the messenger chemical. Indeed, this concentration may be time-dependent in cases where the stationarity condition $\sum_m \alpha_m(c_H)\rho_{0,m} = 0$ cannot be satisfied, as may occur in systems with nonzero net catalytic activity such as e.g. producer-only or consumer-only mixtures.

We then expand (2) and (3) to the first order in the perturbations, while also performing a quasi-static approximation $\partial_t \delta c\left(\mathbf{r}, t\right) \simeq 0$ in (3). This approximation corresponds to the assumption that the chemical diffuses over timescales much shorter than those associated with the motion of the active particles, both through diffusion and chemotaxis; as well as with the changes in the overall chemical concentration in mixtures with net catalytic activity. We also expand the activities to the first order in concentration: $\alpha_m(c) \simeq \alpha_m(c_H(t)) + (\partial_c\alpha_m)|_{c_H}\delta c\left(\mathbf{r}, t\right)$, approximating for instance a Michaelis–Menten-like dependence on the concentration c for the activities.

Note that in systems with net catalytic activity, the parameters $\alpha_m \equiv \alpha_m(c_H(t))$ and $(\partial\alpha_m) \equiv (\partial_c\alpha_m)|_{c_H(t)}$ have an implicit time dependence. Depending on the sign of the total activity $\sum_m \alpha_m\rho_{0,m}$, the system either homogeneously consumes or produces the messenger chemical, leading to activity parameters that evolve in time. Only in the special case $\sum_m \alpha_m\rho_{0,m} = 0$, we find a "neutral" mixture with no net production or consumption of the chemical. As we only care about the stability of the system in a given homogeneous state, we will ignore this time dependence in the following. The time dependence can be brought back into the picture *a posteriori*, for a chosen functional dependence $\alpha_m(c)$, by considering the trajectories that such a system would describe in parameter space over time.

We look for solutions of the form:

$$\begin{aligned}
\delta\rho_m\left(\mathbf{r}, t\right) &= \sum_{\mathbf{q},\lambda}\delta\rho_{m,\mathbf{q},\lambda}\ e^{\lambda t + i\mathbf{q}\cdot\mathbf{r}} \\
\delta c\left(\mathbf{r}, t\right) &= \sum_{\mathbf{q},\lambda}\delta c_{\mathbf{q},\lambda}\ e^{\lambda t + i\mathbf{q}\cdot\mathbf{r}}
\end{aligned} \qquad (4)$$

where the $\mathbf{q}, \lambda$ indices will be omitted in what follows, for readability. By plugging these expressions into the linearized evolution equations, we find the eigenvalue problem:

$$\begin{aligned}
\lambda\delta\rho_m = -\frac{q^2}{dq^2 + \eta}\sum_{n=1}^{M}[&\alpha_n\mu_m\rho_{0,m} \\
&+ D_m(dq^2 + \eta)\delta_{mn}]\delta\rho_n
\end{aligned} \qquad (5)$$

with $\eta \equiv -\sum_m(\partial\alpha_m)\rho_{0,m}$ a screening parameter, that is present only when the activities are concentration-dependent. We note that this screening parameter is generally positive. Indeed, by analogy with Michaelis–Menten kinetics, the activity of a producer does not depend on the concentration of its product, and thus $\partial\alpha_m \equiv 0$ when $\alpha_m > 0$, while the activity of a consumer increases with substrate concentration, and thus $\partial\alpha_m < 0$ when $\alpha_m < 0$.

Note also that screening may arise in a different way, if we consider that the chemical may undergo spontaneous decay. Such a situation can be taken into account by adding a term $-\kappa c$ in the right-hand side of (3), in which case one finds that the screening parameter is rescaled to $\eta \to \eta + \kappa$.

Equation (5) features the growth rate λ of a given mode as the eigenvalue, whose sign will inform us about the stability of the system. If at least one eigenvalue is positive, the homogeneous state is unstable and the system shows spatial self-organization, typically into dense clusters as seen in particle-based Brownian dynamics simulations of the system [12].

At the onset of such an instability, the eigenvector components $\delta\rho_m$ inform us about the stoichiometry of the growing perturbation, that is, which species tend to aggregate together (and in which proportion), and which species tend to separate.

2.3 Simplest case: similarly sized species without screening

We summarize here the result of the stability analysis for a particularly simple case which was previously studied in Ref. [12]. If we consider species with concentration-independent activities ($\eta = 0$) and equal sizes ($D_1 = D_2 = \cdots = D_M = D$), (5) reduces to an eigenproblem involving a rank one matrix, with $M - 1$ degenerate eigenvalues λ_- and one unique eigenvalue λ_+:

$$\begin{aligned}
\lambda_- &= -Dq^2 \\
\lambda_+ &= -Dq^2 - \sum_{m=1}^{M}\frac{\alpha_m\mu_m\rho_{0,m}}{d}
\end{aligned} \qquad (6)$$

Of the two, only λ_+ can be positive, according to the criterion:

$$\sum_{m=1}^{M}\alpha_m\mu_m\rho_{0,m} < 0 \qquad (7)$$

corresponding to the mixture of active particles being overall self-attractive. Notice that the only requirement is for the overall sum to be negative, implying that any arbitrarily small amount of attraction is sufficient to trigger an instability. This is a consequence of the long-ranged, unscreened nature of the interactions.

When condition (7) is satisfied, the $q^2 = 0$ mode is the fastest-growing one, and the instability is therefore always system-wide. The corresponding eigenvector is:

$$(\delta\rho_1, \delta\rho_2, \ldots, \delta\rho_M) = (\mu_1\rho_{0,1}, \mu_2\rho_{0,2}, \ldots, \mu_M\rho_{0,M}) \tag{8}$$

The stoichiometry at instability onset is then determined by the mobilities, independently of the activities. In particular, species with equal sign of the mobility tend to aggregate together, whereas those with opposite sign tend to separate.

The behaviour of a two-species mixture can be captured in a two-dimensional phase diagram, plotted in $(|\alpha_i|\mu_i\rho_{0,i})$ coordinates for given signs of the activities, i.e. independently for mixtures of producers and consumers, or for mixtures of two consumers (Fig. 2).

In the following, we will show that accounting for screening effects due to concentration-dependent activities as well as for different-sized particles leads to significant departures from this simple behaviour, including the existence of a minimum activity threshold for an instability to occur, and the possibility of oscillatory instabilities.

3 Screening-induced stability threshold

3.1 Arbitrary number of species

In the presence of screening ($\eta > 0$), but for identically sized particles ($D_1 = D_2 = ... = D_M = D$), the eigenvalue problem (5) becomes:

$$\lambda\delta\rho_m = -\frac{q^2}{dq^2 + \eta} \sum_{n=1}^{M} [\alpha_n\mu_m\rho_{0,m} + D(dq^2 + \eta)\delta_{mn}]\delta\rho_n \tag{9}$$

which, as in the case described in Sect. 2.3, can be reduced to a rank one matrix eigenvalue problem, with eigenvalues:

$$\lambda_-(q^2) = -Dq^2$$

$$\lambda_+(q^2) = -Dq^2 - \frac{q^2}{dq^2 + \eta} \sum_{m=1}^{M} \alpha_m\mu_m\rho_{0,m} \tag{10}$$

Once again, only λ_+ can positive, but this time under the condition:

$$\sum_{m=1}^{M} \alpha_m\mu_m\rho_{0,m} < -\eta D \tag{11}$$

This instability criterion corresponds to a stricter version of (7), with the activity dependence on concentration appearing as a screening term. As a consequence, there is now a threshold value of overall self-attraction required for an instability to occur.

An intuitive way of understanding the more stringent instability criterion is as arising from a feedback effect affecting consumer species, which are the only ones contributing to η. Indeed, these are self-attracting only if they verify $\mu > 0$, i.e. if they are antichemotactic. This implies that in the context of self-attraction, these particles migrate towards zones of lower chemical concentration, which in turn lowers their activity, and thus their self-attraction. In the self-repelling case, the opposite happens, with a positive feedback on the self-interaction which amplifies the inter-particle repulsion as particles get further away from each other.

Another key difference to the case without screening is that the unstable eigenvalue now has a non-monotonic dependence on the wave number q^2. Indeed, we now find $\lambda_+(q^2 = 0) = 0$ always, and the eigenvalue is maximum at

$$q^2 = d^{-1}\left(\sqrt{\frac{-\eta\sum_m \alpha_m\mu_m\rho_{0,m}}{D}} - \eta\right) \tag{12}$$

which gives a finite wave length to the fastest-growing perturbations. With regard to the stoichiometry of the instability, we will show later that the sign of the eigenvector components is still determined by the sign of the mobilities, as before.

3.2 Two species: phase diagram

Figure 3 shows the phase diagram for a mixture of two similarly sized particles with screening. Comparing it to Fig. 2, we see that the instability line is shifted, corresponding to the screening-induced instability threshold. Moreover, the eigenvalue plots also highlight the fact that while the lower eigenvalues show the same behaviour in both cases, in the screened case, the upper eigenvalue is zero at $q^2 = 0$ and goes through a maximum at a finite q^2, while in the unscreened case, it monotonically decreases from a nonzero value at $q^2 = 0$.

4 Differently sized particles: local instability and oscillations

4.1 Macroscopic and local instabilities

We now turn to the case of concentration-independent activity ($\eta = 0$), but differently sized particle species. The eigenvalue problem (5) becomes:

$$\lambda\delta\rho_m = -\sum_{n=1}^{M}\left[\frac{\alpha_n\mu_m\rho_{0,m}}{d} + D_mq^2\delta_{mn}\right]\delta\rho_n \tag{13}$$
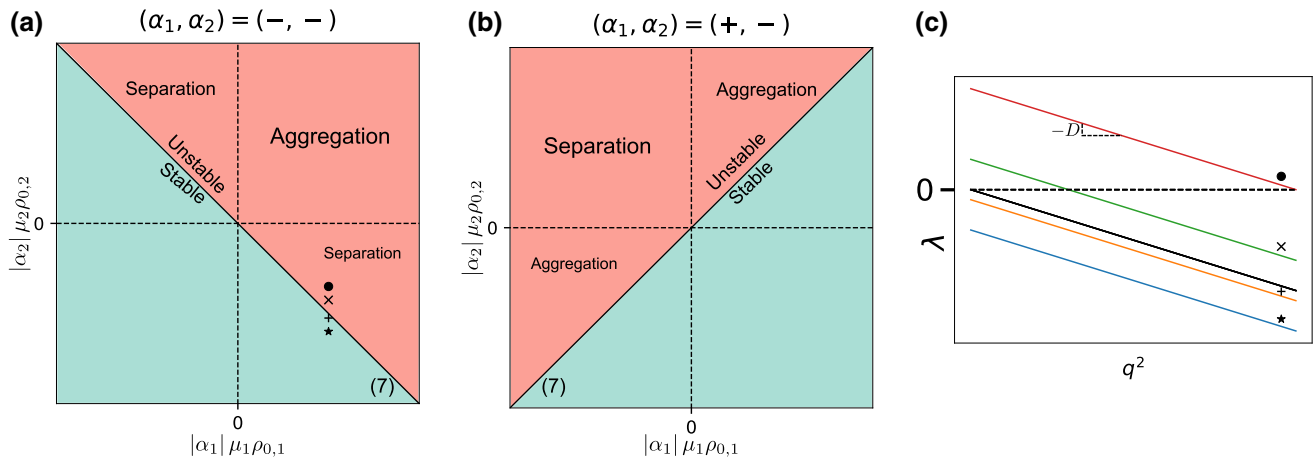
Fig. 2 Behaviour of a mixture of two same-sized species with concentration-independent activities [12]. **a** Phase diagrams for two consumers. **b** Phase diagram for one producer, one consumer. In (**a**) and (**b**), numbers in parentheses refer to the corresponding equations in the text. **c** Selected eigen- value plots as a function of the squared wave vector q^2. Coloured lines corre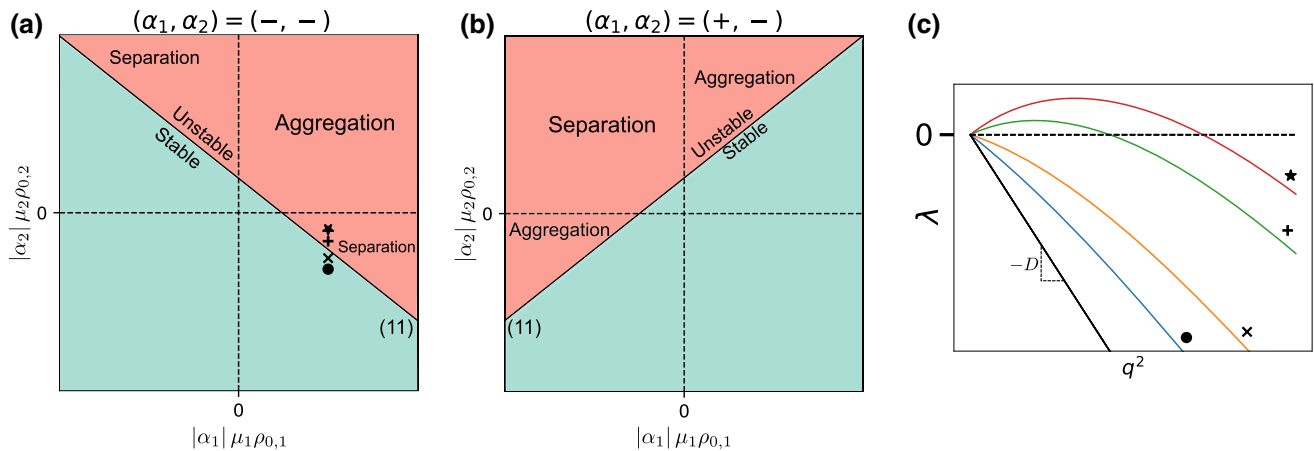spond to the upper eigenvalues of the phase diagram points marked in (**a**). Black line corresponds to the lower eigenvalue, shared by all points in the phase diagram

Fig. 3 Behaviour of a mixture of two same-sized species with concentration-dependent activities. **a** Phase diagram for two consumers. **b** Phase diagram for one producer, one consumer. In (a) and (b), numbers in parentheses refer to the corresponding equations in the text. **c** Eigenvalue plots as a function of the squared wave vector q^2. Coloured lines correspond to the upper eigenvalue, taken at several loca- tions in (a) Black line represents the lower eigenvalue, which does not depend on phase space location

involving an arbitrary matrix, now that the diffusion coefficients D_m are species-dependent. The problem is then intractable in general, and we turn to the two- species case, which is solvable analytically. From here on, we choose the convention $D_1 > D_2$ without loss of generality.

Solving for λ, we find the eigenvalues:

$$\lambda_\pm(q^2) = -\frac{1}{2d}\left(\gamma_1 + \gamma_2 + (D_1 + D_2)dq^2\right)$$
$$\pm \frac{1}{2d}\sqrt{\left[\gamma_1 - \gamma_2 + (D_1 - D_2)dq^2\right]^2 + 4\gamma_1\gamma_2}$$

$$(14)$$

with $\gamma_m = \alpha_m \mu_m \rho_{0,m}$ the self-interaction of species m. The instability conditions can be obtained by develop-

ing the eigenvalues to the first order in q^2:

$$\lambda_+(q^2) = -\frac{\gamma_1 D_2 + \gamma_2 D_1}{\gamma_1 + \gamma_2}q^2 + O(q^4)$$
$$\lambda_-(q^2) = -\frac{\gamma_1 + \gamma_2}{d} - \frac{\gamma_1 D_1 + \gamma_2 D_2}{\gamma_1 + \gamma_2}q^2 + O(q^4)$$

$$(15)$$

λ_- is unstable when $\gamma_1 + \gamma_2 \leq 0$, or equivalently

$$\alpha_1\mu_1\rho_{0,1} + \alpha_2\mu_2\rho_{0,2} \leq 0 \qquad (16)$$

which coincides with (7), and leads to a system-wide instability (maximum at $q^2 = 0$). However, even when λ_- is negative, the system can still be unstable, as λ_+ can have a positive initial slope when the less strict

condition $\gamma_2 \leq -\frac{D_2}{D_1}\gamma_1$, which we can write as:

$$\alpha_2\mu_2\rho_{0,2} \leq -\frac{D_2}{D_1}\alpha_1\mu_1\rho_{0,1} \qquad (17)$$

is verified. In this case, the instability is only at finite wavelengths as in the screened case, with $\lambda_+(q^2 = 0) = 0$ and maximum λ_+ at a finite value of q^2.

There is therefore a wider range of conditions under which a mixture can become unstable if the particles are differently sized, with the caveat that this extended range only leads to a finite wave length instability rather than a system-wide one.

4.2 Transient oscillations

We can also extract the range of parameters for which the two eigenvalues in (14) become a complex conjugate pair, which results in the condition $\gamma_2 \geq -(D_1/D_2)^2\gamma_1$, or equivalently

$$\alpha_2\mu_2\rho_{0,2} \geq -\left(\frac{D_2}{D_1}\right)^2\alpha_1\mu_1\rho_{0,1} \qquad (18)$$

where the real parts are positive for a finite range of wavevectors whenever (16) is satisfied. The different particle sizes can thus lead to oscillatory instabilities for a finite range of perturbation wave lengths. Note, however, that the most unstable wave length (eigenvalue with largest real part) still always corresponds to a real eigenvalue, suggesting that any oscillatory phenomena will be at most transient.

The overall behaviour of the system is summed up in the phase diagrams and eigenvalue plots of Fig. 4. Note some marked differences with the cases of Sects. 3.2 and 2.3, most importantly the apparition of a variety of unstable regions with distinct behaviours. If $\gamma_1 \geq 0$, $\gamma_2 \leq 0$ (upper-left quadrant in Fig. 4a, upper-right in 4b), λ_+ shows similar behaviour to the screened case, being zero at $q^2 = 0$ with a maximum at finite q^2, while λ_- has a non-null value at $q^2 = 0$ (all lines of Fig. 4d). If (17) is verified, the situation is similar to Fig. 3: λ_+ is the unstable eigenvalue, and leads to a local instability (up- and right-pointing triangles on Fig. 4d). However, if (16) is verified, then λ_- becomes positive and has a positive value at $q^2 = 0$, leading to a situation similar to the one in Fig 2, with one key difference: the positive eigenvalue is non-monotonic, having a maximum at a nonzero wave vector (left-pointing triangle in Fig. 4d). The system should then show an initial, local instability phenomenon followed by system-wide self-organization. If $\gamma_1 < 0$ (right and left halves on Fig. 4a and b respectively), the different-sized species mixture shows an entirely new behaviour, with the eigenvalue being real from $q^2 = 0$ to a finite wave vector, then complex (all lines on Fig. 4c). In the region where the eigenvalues are real, the behaviour of the largest one is similar to Fig. 2, being non-null at $q^2 = 0$ and monotonically decreasing. This behaviour carries over to the real part

of the complex eigenvalue, which decreases monotonically as well, implying that the instability will always be system-wide with the $q^2 = 0$ mode dominating. We distinguish between the non- and partly oscillatory sections of the phase diagram by considering whether or not there exists a region where the eigenvalue is complex with a positive real part (star label in Fig. 4d is non-oscillatory, plus and cross labels are oscillatory). Finally, the stoichiometry sign for non-oscillatory instabilities is the same as in Sect. 2.3, as will be shown in the next section.

5 Variety of behaviours for differently sized species with screened interactions

5.1 Local instability

Finally, we turn to the most general version of the eigenvalue problem (5). Once again, it is analytically intractable for an arbitrary species number M, and we turn to the $M = 2$ case. The solution to (5) writes:

$$\lambda_{\pm} = \frac{1}{2}\frac{q^2}{dq^2 + \eta}\Bigg\{-(\gamma_1 + \gamma_2) - (D_1 + D_2)(dq^2 + \eta)$$
$$\pm\sqrt{[\gamma_1 - \gamma_2 + (D_1 - D_2)(dq^2 + \eta)]^2 + 4\gamma_1\gamma_2}\Bigg\} \qquad (19)$$

We can look for an instability condition either by proceeding as in 4.1 and developing the expressions to first order, or by calculating the range of squared wave vectors for which the eigenvalues are positive. Imposing $\lambda_+ \geq 0$ leads to two possible conditions, which correspond to two distinct instability lines. Since only one of the conditions needs to be satisfied in order for the instability to occur, we only need to consider the largest of the two instability lines in a given region. The two lines intersect at the branching point given by

$$\left((\alpha_1\mu_1\rho_{0,1})_B, (\alpha_2\mu_2\rho_{0,2})_B\right) = \left(\frac{-\eta D_1^2}{D_1 - D_2}, \frac{\eta D_2^2}{D_1 - D_2}\right) \qquad (20)$$

leading to the two instability conditions

$$\alpha_2\mu_2\rho_{0,2} \leq -\alpha_1\mu_1\rho_{0,1} - \eta(D_1 + D_2) \qquad (21)$$

for $\alpha_1\mu_1\rho_{0,1} \leq (\alpha_1\mu_1\rho_{0,1})_B$, and

$$\alpha_2\mu_2\rho_{0,2} \leq -\frac{D_2}{D_1}\alpha_1\mu_1\rho_{0,1} - \eta D_2 \qquad (22)$$

for $\alpha_1\mu_1\rho_{0,1} \geq (\alpha_1\mu_1\rho_{0,1})_B$. These two lines recover both the screening-induced shift of the instability line,

Fig. 4 Behaviour of a mixture of two differently sized species with concentration-independent activities. **a** Phase diagram for two consumers. **b** Phase diagram for one producer, one consumer. In (a) and (b), numbers in parentheses refer to the corresponding equations in the text. **c** Eigenvalue plots along the transition from stable (blue) to partially oscillatory (orange, green) to real unstable (red). Full lines correspond to the eigenvalue real parts, dashed lines to the imaginary part. **d** Eigenvalue plots along the transition from stable (blue) to local (orange, green) and then to macroscopic (red) instability
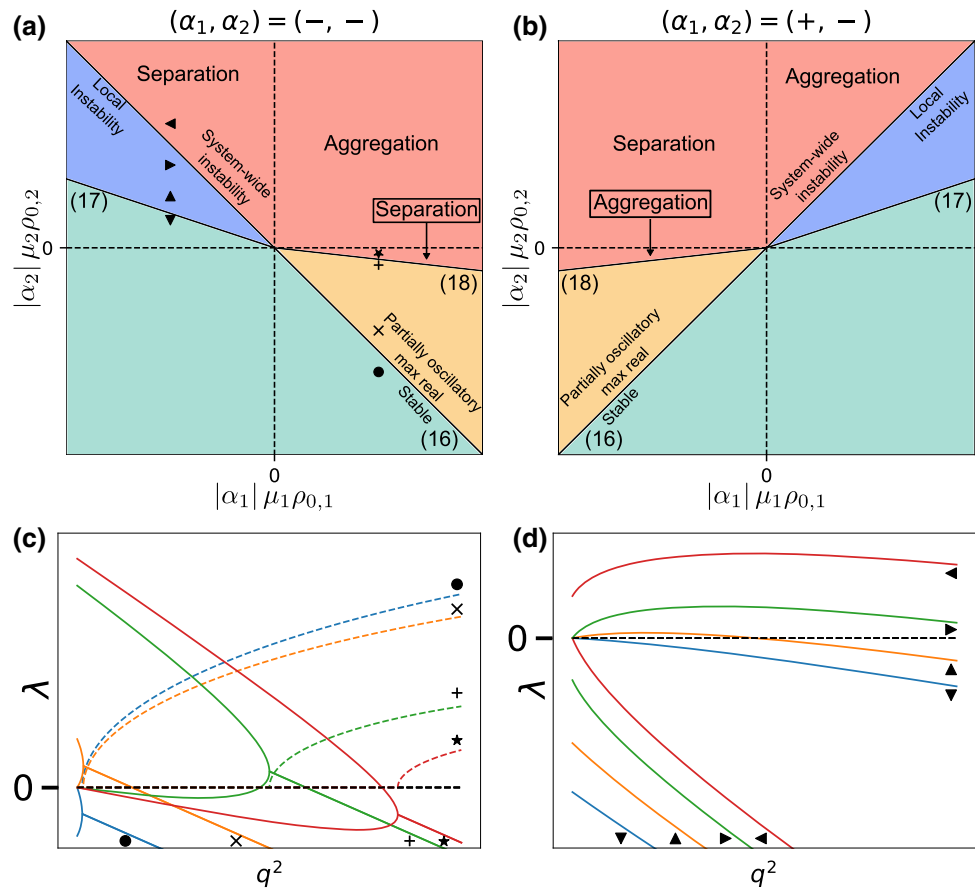
as well as the extension of the instability region caused by the different species sizes. However, as opposed to the eigenvalues (14), here both eigenvalues are null at $q^2 = 0$: the eigenvalue has the same behaviour in the extended instability region as in the standard one, and the instability is always local.

5.2 Partial and fully oscillatory instabilities

Proceeding similarly to Sect. 4.2, we now look for complex eigenvalues. In phase space, the parameters allowing for complex solutions correspond to a "fork" which opens in the instability line for $\gamma_1 \leq \gamma_{1,B}$, from the branching point defined in (20). By comparing the maximal unstable wavevector to the range of wavevectors for which the eigenvalues are complex, we find a variety of possible behaviours. When the condition

$$\alpha_2\mu_2\rho_{0,2} > \left(\sqrt{-\alpha_1\mu_1\rho_{0,1}} - \sqrt{\eta(D_1 - D_2)}\right)^2 \quad (23)$$

is verified, the full range of wavevectors that are unstable (eigenvalue with positive real part) have complex conjugate eigenvalues, and we term this a "fully oscillatory" instability. Another kind of instability, which we call "partially oscillatory", is observed if condition (23)

is not satisfied and instead:

$$\alpha_2\mu_2\rho_{0,2} > -\left(\frac{D_2}{D_1}\right)^2 \alpha_1\mu_1\rho_{0,1} \quad (24)$$

in which case there are two ranges of unstable wave vectors, one with real and one with complex conjugate eigenvalues, each of which features a local maximum of the real part of the eigenvalue. Far away from the lower bound given by (24), the fastest growing mode is still complex, and so the instability process should still be mainly oscillatory. Below a line which can be calculated numerically, as we approach the lower bound given by (24), the two maxima cross over, and the global maximum of the real part occurs for a real eigenvalue, so that the non-oscillatory instability should dominate. Finally, if the condition (24) is not satisfied, then all unstable modes are real and the instability should display no oscillations whatsoever.

The behaviour of the system is shown in Fig. 5. As we now have incorporated both screening and size dispersity effects, the resulting behaviour can be seen as a mix of the two individual cases. Contrast the phase diagram and plotted eigenvalues of Fig. 5 to the ones in Fig. 3: thanks to the screening effects, we recover the shifted instability line and the fact that the eigenvalues are null at $q^2 = 0$, stopping system-wide instabilities from occurring. On the other hand, similarly to Fig. 4, the
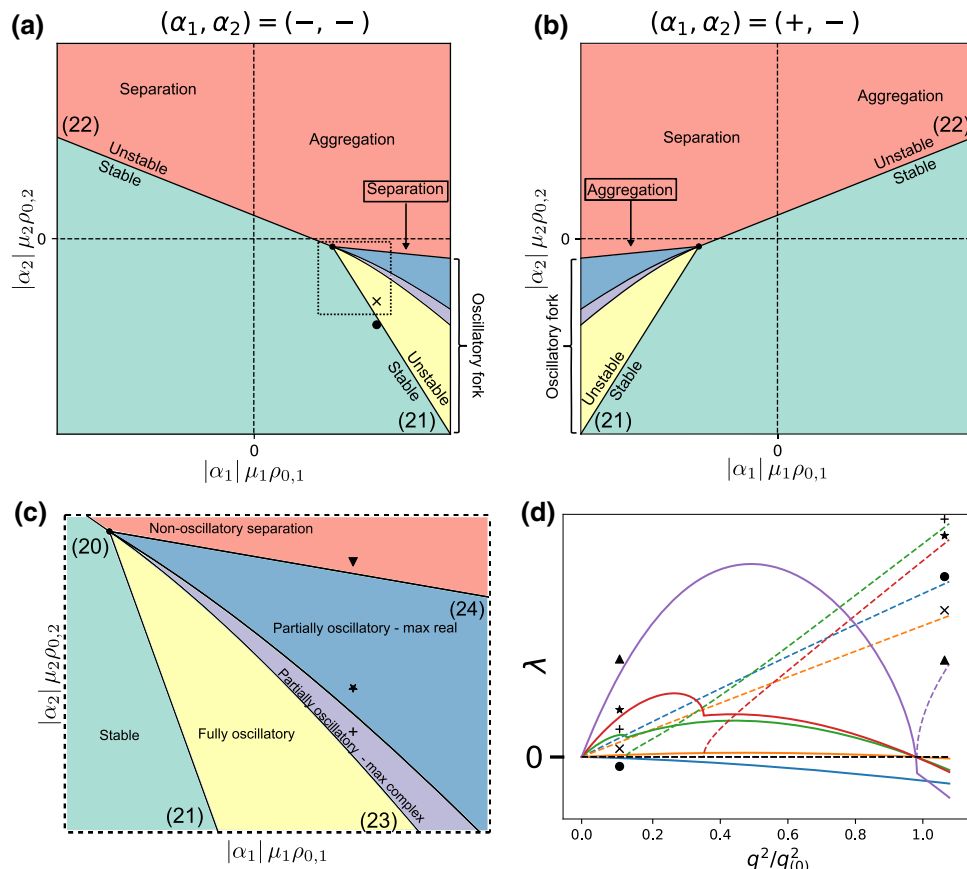
Fig. 5 Behaviour of a mixture of two differently sized species with concentration-dependent activities. **a** Phase diagram for two consumers. **b** Phase diagram for one producer, one consumer. **c** Structure of the phase diagram near the branching point for two consumers, corresponding to the zoomed-in dashed square in (a). In (a), (b) and (c), numbers in parentheses refer to the corresponding equations in the text. **d** Eigenvalue plots (see (a) and (c) for marker locations in phase space) along the transition from stable (blue) to fully oscillatory (orange) to partially oscillatory with dominant oscillatory modes (green) and then dominant non-oscillatory modes (red), and finally to non-oscillatory (purple). Only the upper eigenvalue is plotted, for readability. Full lines correspond to the eigenvalue real parts, dashed lines to the imaginary part. Wave vectors are normalized by the largest unstable wave vector $q_{(0)}^2$, if applicable

eigenvalues can be complex, but with major differences. Instead of necessarily having a real positive region, the eigenvalues in Fig. 5 can be complex with a positive real part over the whole range of unstable wave vectors, corresponding to a fully oscillatory instability. Moreover, in the partially oscillatory regime, the upper eigenvalue exhibits two maxima, one in the real region and one in the complex region, whereas in the case without screening it only had a maximum at $q^2 = 0$. This implies that in this regime, the maximally growing mode can be either oscillatory or non-oscillatory, based on which of these two maxima is the global one.

5.3 Stoichiometry

We finally turn to the study of the eigenvectors, more precisely the ratio $S_{2/1} \equiv \delta\rho_2/\delta\rho_1$, the sign of which will inform us about the tendency of the two species in an unstable binary mixture to aggregate (if positive) or separate (if negative). We only study the eigenvector corresponding to the upper eigenvalue λ_+, as it is the

one driving the instability. Calculating the eigenvector in (5) leads to the expression:

$$
S_{2/1} = -\frac{1}{2\gamma_2}\frac{\gamma_2\rho_{0,2}}{\gamma_1\rho_{0,1}}\left[(\gamma_1 - \gamma_2) + (D_1 - D_2)(dq^2 + \eta)\right.
$$
$$
\left. +\sqrt{[\gamma_1 - \gamma_2 + (D_1 - D_2)(dq^2 + \eta)]^2 + 4\gamma_1\gamma_2}\right]
$$
(25)

It can be shown that the term in brackets keeps a constant sign as a function of q^2. By distinguishing between the $\gamma_2 > 0$ and $\gamma_2 < 0$ cases, we can systematically calculate the sign of $S_{1/2}$ in the regions where the eigenvalue is real and unstable, leading to the conclusion:

$$
\text{sign}(S_{2/1}) = \text{sign}(\mu_2/\mu_1)
$$
(26)

Thus, similar to the simple case studied in Sect. 2.3, the sign of the stoichiometry only depends on the sign of the mobilities, with species having the same mobility

sign tending to aggregate, and species having opposite mobility signs tending to separate. Note that this result applies to all the cases studied in this paper. The phase diagrams in Figs. 3, 4 and 5 are then plotted using the same procedure as in Sect. 2.3: the instability lines are functions of the $\alpha_m \mu_m \rho_{0,m}$, and the stoichiometry depends on the mobilities signs only, so the phase diagrams can be plotted as a function of $|\alpha_m| \mu_m \rho_{0,m}$ for fixed signs of the activities.

6 Discussion

In this work, we have explored a general model for the stability of a mixture of active particles based on the linear stability analysis of continuum equations. The model studied was a generalization of a simpler model introduced in Ref. [12], in which case the mixture was found to show a system-wide instability if it was overall self-attracting. We have shown that if the catalytic activities of the particles have a dependence on the concentration of their substrate, the interactions become screened, leading to the emergence of a minimum threshold of self-attraction for the instability to occur, and to the inhibition of system-wide instabilities, which become local (finite wave length). Accounting for dispersity in the sizes of the active particles, meanwhile, can either lead to the same system-wide instability observed in the simple model, or to the apparition of an extended, local instability regime with a less strict requirement for the instability. The existence of size dispersion also allows for the possibility of system-wide, transient oscillations during a global instability. Finally, combining both screening and size dispersity effects leads to a wide variety of behaviours. Due to the screening, the instability can only be local, but oscillations are also possible and, depending on the location in phase space, can either represent the dominant unstable mode, or transiently coexist with a more dominant non-oscillatory instability. For each of these cases, we have obtained exact analytical conditions that fully describe the resulting phase diagrams and can be used as guidance in future experimental or simulation studies. In all the studied cases, the stoichiometry of the growing instability is purely a function of the signs of the species' mobilities, implying that chemotactic species and antichemotactic species tend to separate from each other and aggregate among themselves.

The instabilities that we predict here at the linear level may also be explored beyond this regime, by means of numerical solution of the continuum equations, or particle-based simulations. Such simulations will allow for the study of the kinetics of the self-organization process, as well as the resulting steady-state configurations of the system. Of particular interest is the presence or absence of transient oscillations in the instability process. While our linear stability analysis can yield complex eigenvalues with positive real part, we cannot conclude whether long-lived oscillations will be observed. In general, the behaviour of the system beyond the

onset of instability will depend on factors outside the scope of this analysis, among others the feedback of changes in substrate concentration on the activity and nonlinear effects not captured at the linear stability level. Another limitation of our model is the quasi-static approximation performed for the messenger chemical, implying that we limit ourselves to cases where the motion of the catalysts is much slower than the diffusion of their substrates and products.

While this paper focused on catalytic particles, many bacteria are known to chemotax in response to chemicals they themselves secrete or consume, leading to pattern formation [33–38]. In particular, Ref. [36] explores the influence of concentration-dependent chemotactic drift, stemming from the microscopic characteristics of bacterial receptors, on pattern formation. Such a concentration-dependent chemotactic mobility could also be incorporated into our model. In turn, our concentration-dependent activity would correspond to cases where the bacteria modulate their production or consumption of chemoattractant or chemorepellant based on local concentration. Our model could further be applied to bacterial ecosystems in which different species of bacteria coexist, resulting in inter-species interactions which may be non-reciprocal.

Coming back to the applications at the subcellular level, a natural step for future work is to allow for the enzymes to participate in catalytic cycles, in which the product of one enzyme becomes the substrate of the next enzyme in the cycle [39], given that such cycles are ubiquitous in metabolic pathways in the cell. Furthermore, it will be interesting to explore the effect of self-organization on the yield of the associated catalytic reactions. In Ref. [12], it was shown that mixtures of producers and consumers tend to form clusters with just the right stoichiometry that allows for perfect channelling of the chemical released by the producers to be taken up by the consumers in the cluster. The effect of concentration-dependent activities on this phenomenon, as well as the implications on the overall catalytic yield remain to be explored. On the experimental side, a deeper exploration of the dynamics during the formation of metabolons or enzyme-rich condensates may help elucidate whether non-equilibrium chemical-mediated interactions are at play, perhaps in conjunction with passive interactions.

References

1. J. Agudo-Canalejo, T. Adeleke-Larodo, P. Illien, R. Golestanian, Acc. Chem. Res. **51**(10), 2365 (2018)
2. L.J. Sweetlove, A.R. Fernie, Nat. Commun. **9**(1), 2136 (2018)
3. H. Yu, K. Jo, K.L. Kounovsky, J.J.D. Pablo, D.C. Schwartz, J. Am. Chem. Soc. **131**(16), 5722 (2009)
4. S. Sengupta, K.K. Dey, H.S. Muddana, T. Tabouillot, M.E. Ibele, P.J. Butler, A. Sen, J. Am. Chem. Soc. **135**(4), 1406 (2013)
5. K.K. Dey, S. Das, M.F. Poyton, S. Sengupta, P.J. Butler, P.S. Cremer, A. Sen, ACS Nano. **8**(12), 11941 (2014)
6. X. Zhao, H. Palacci, V. Yadav, M.M. Spiering, M.K. Gilson, P.J. Butler, H. Hess, S.J. Benkovic, A. Sen, Nat. Chem. **10**(3), 311 (2018)
7. A.Y. Jee, Y.K. Cho, S. Granick, T. Tlusty, Proc. Natl. Acad. Sci. **115**(46), E10812 (2018)
8. J. Agudo-Canalejo, P. Illien, R. Golestanian, Nano Lett. **18**(4), 2711 (2018)
9. T. Adeleke-Larodo, J. Agudo-Canalejo, R. Golestanian, J. Chem. Phys. **150**(11), 115102 (2019)
10. J. Agudo-Canalejo, R. Golestanian, Eur. Phys. J. Special Topics. **229**(17), 2791 (2020)
11. M. Feng, M.K. Gilson, Annu. Rev. Biophys. **49**(1), 87 (2020)
12. J. Agudo-Canalejo, R. Golestanian, Phys. Rev. Lett. **123**, 018101 (2019)
13. R. Soto, R. Golestanian, Phys. Rev. Lett. **112**(6), 068301 (2014)
14. R. Soto, R. Golestanian, Phys. Rev. E **91**(5), 052304 (2015)
15. S. Saha, S. Ramaswamy, R. Golestanian, New J. Phys. **21**(6), 063006 (2019)
16. C.A. Weber, D. Zwicker, F. Jülicher, C.F. Lee, Rep. Prog. Phys. **82**(6), 064601 (2019)
17. G. Giunta, H. Seyed-Allaei, U. Gerland, Commun. Phys. **3**(1), 1 (2020)
18. R. Golestanian, Phys. Rev. Lett. **108**, 038303 (2012)
19. S. Saha, R. Golestanian, S. Ramaswamy, Phys. Rev. E **89**, 062316 (2014)
20. M. Schmitt, H. Stark, Phys. Fluids **28**(1), 012106 (2016)
21. J. Palacci, S. Sacanna, A.P. Steinberg, D.J. Pine, P.M. Chaikin, Science **339**(February), 936 (2013)
22. R. Niu, T. Palberg, T. Speck, Phys. Rev. Lett. **119**(2), 028001 (2017). https://doi.org/10.1103/PhysRevLett. 119.028001
23. T. Yu, P. Chuphal, S. Thakur, S.Y. Reigh, D.P. Singh, P. Fischer, Chem. Commun. **54**, 11933 (2018)
24. H. Massana-Cid, J. Codina, I. Pagonabarraga, P. Tierno, Proc. Natl. Acad. Sci. U.S.A. **115**(42), 10618 (2018)
25. F. Schmidt, B. Liebchen, H. Löwen, G. Volpe, J. Chem. Phys. **150**, 094905 (2019)
26. C.H. Meredith, P.G. Moerman, J. Groenewold, Y.J. Chiu, W.K. Kegel, A. van Blaaderen, L.D. Zarzar, Nat. Chem. **12**(12), 1136 (2020)
27. J.L. Anderson, Annu. Rev. Fluid Mech. **21**(1969), 61 (1989)
28. R. Golestanian, T.B. Liverpool, A. Ajdari, New J. Phys. **9**, 126 (2007)
29. A.V. Ivlev, J. Bartnick, M. Heinen, C.R. Du, V. Nosenko, H. Löwen, Phys. Rev. X **5**(1), 011035 (2015)
30. S. Saha, J. Agudo-Canalejo, R. Golestanian, Phys. Rev. X **10**(4), 041009 (2020)
31. Z. You, A. Baskaran, M.C. Marchetti, Proc. Natl. Acad. Sci. **117**(33), 19767 (2020)
32. M. Fruchart, R. Hanai, P.B. Littlewood, V. Vitelli, Nature **592**(7854), 363 (2021)
33. R. Erban, H. Othmer, Multiscale Modeling & Simulation, v.3 **3**, 362–394 (2005)
34. A. Sengupta, S. van Teeffelen, H. Löwen, Phys. Rev. E **80**, 031122 (2009)
35. A. Sengupta, T. Kruppa, H. Löwen, Phys. Rev. E **83**, 031914 (2011)
36. M. Meyer, L. Schimansky-Geier, P. Romanczuk, Phys. Rev. E **89**, 022711 (2014)
37. S. Mahdisoltani, R.B.A. Zinati, C. Duclut, A. Gambassi, R. Golestanian, Phys. Rev. Res. **3**, 013100 (2021)
38. A. Gelimson, R. Golestanian, Phys. Rev. Lett. **114**, 028101 (2015)
39. V. Ouazan-Reboul, J. Agudo-Canalejo, R. Golestanian, In preparation (2021)

3

Self-organization of primitive metabolic cycles due to non-reciprocal interactions

This chapter is reproduced from a revised version of the preprint Ouazan-Reboul et al, ArXiv:2304.09925 (2023)[182], currently under review at Nature Communications. I took part in the design of the research, performed the analytical calculations, designed the numerical simulation code, analyzed and interpreted the numerical data, and participated in the redaction of the paper.

The movies described in the main text and supplementary information are available at the following link: https://owncloud.gwdg.de/index.php/s/t2Ka6zxJsZq8Xee

Self-organization of primitive metabolic cycles due to non-reciprocal interactions

Vincent Ouazan-Reboul,[1] Jaime Agudo-Canalejo,[1] and Ramin Golestanian[1, 2]

[1]*Max Planck Institute for Dynamics and Self-Organization, Am Fassberg 17, D-37077, Göttingen, Germany*

[2]*Rudolf Peierls Centre for Theoretical Physics, University of Oxford, OX1 3PU, Oxford, UK*

ABSTRACT

One of the greatest mysteries concerning the origin of life is how it has emerged so quickly after the formation of the earth. In particular, it is not understood how the intricate structures of metabolic cycles, which power the non-equilibrium activity of cells and support their functions under homeostatic conditions, have come into existence in the first instances. These structures have emerged from a dilute primordial soup of chemicals that have turned out to be suitable partners in certain reactions in the roles of reactants and catalysts. While it is generally expected that non-equilibrium conditions would have been necessary for the formation of these primitive metabolic structures, the focus has so far been on externally imposed non-equilibrium conditions, such as temperature or proton gradients. Here, we propose an alternative paradigm in which naturally occurring non-reciprocal interactions between catalysts that can potentially partner together in a cyclic reaction lead to their rapid recruitment into self-organized functional structures. We uncover different classes of self-organized cycles that form through exponentially rapid coarsening processes, depending on the parity of the cycle and the nature of the interaction motifs, which are all generic but have readily tuneable features. Our results also shed light on possibilities that may be explored in designing efficient synthetic cycles.

MAIN TEXT

Since Oparin [1] proposed a picture to describe how early forms of living matter might have emerged from what Haldane described as the prebiotic soup [2], there has been a significant amount of progress in our understanding of the physical aspects of the origin of life [3]. Recent examples of such studies include spontaneous emergence of catalytic cycles [4, 5], spontaneous growth and division of chemically active droplets [6–8], programmable self-organization of functional structures under non-equilibrium conditions [9, 10], and controllable realization of metabolically active condensates [11]. A striking generic observation that has emerged in a variety of different scenarios is that the introduction of non-equilibrium activity in the form of catalytic activity, or a primitive form of metabolism, can be a versatile driving force for functional structure formation [12–17] with manifestations of lifelike behaviour [18–26]. It has also

been demonstrated that the structured catalytic activity that would support the required non-equilibrium processes for primitive cells can be successfully coupled with the condensation of appropriate functional nucleotide and peptide components in membrane-free systems [27–29], as well as lipid components in protocells with functionalized membranes [30, 31].

Living systems necessarily involve a set of auto-catalytic chemical reactions [32], which have been theoretically shown to spontaneously emerge in a population of polypeptide-like structures that could assemble in a primordial soup setting [33–36]. A candidate metabolic cycle that may have served a key role in the early stages of life formation is the citric acid cycle, which consists of 11 catalysts and exhibits evolutionary robustness and universality [37, 38]. Candidates for pre-RNA and protein autocatalytic chemical networks have been identified from early microbial organisms [39], and mixtures of RNA fragments have been experimentally observed to organize into self-replicating and catalyzing reaction networks [40–43].

The physicochemically motivated ideas initiated by Oparin and Haldane were critically debated for much of the past century by proponents of the perspective that (genetic) information should be considered as the main organizer of matter that forms life [32, 44, 45]. As a modern interpretation of these considerations, we note that the current accepted paradigm assumes that the ingredients that would later join up to form intricate components of living systems first come together by *ad hoc* physical forces without any input from the *information* that will eventually be at work in their hierarchical self-organization. The information-based organization is expected to occur when the system has already made physical condensates. However, this paradigm has so far been unable to answer two important questions. Firstly, as we know from the physics of phase separation, physically formed condensates such a coacervates are fundamentally very slow, almost glass-like, in their dynamics, even if they are driven by external non-equilibrium forces like temperature and proton gradients. Therefore, the idea that such dense and glassy condensates that are formed randomly would have been able to intelligently evolve to form information-based functional structures via random searches does not appear to plausibly match the time scale that has taken life to emerge after the formation of the earth. It is not clear how this important problem has been solved at the origin of life. Secondly, it is an established fact that the physics of condensation is governed
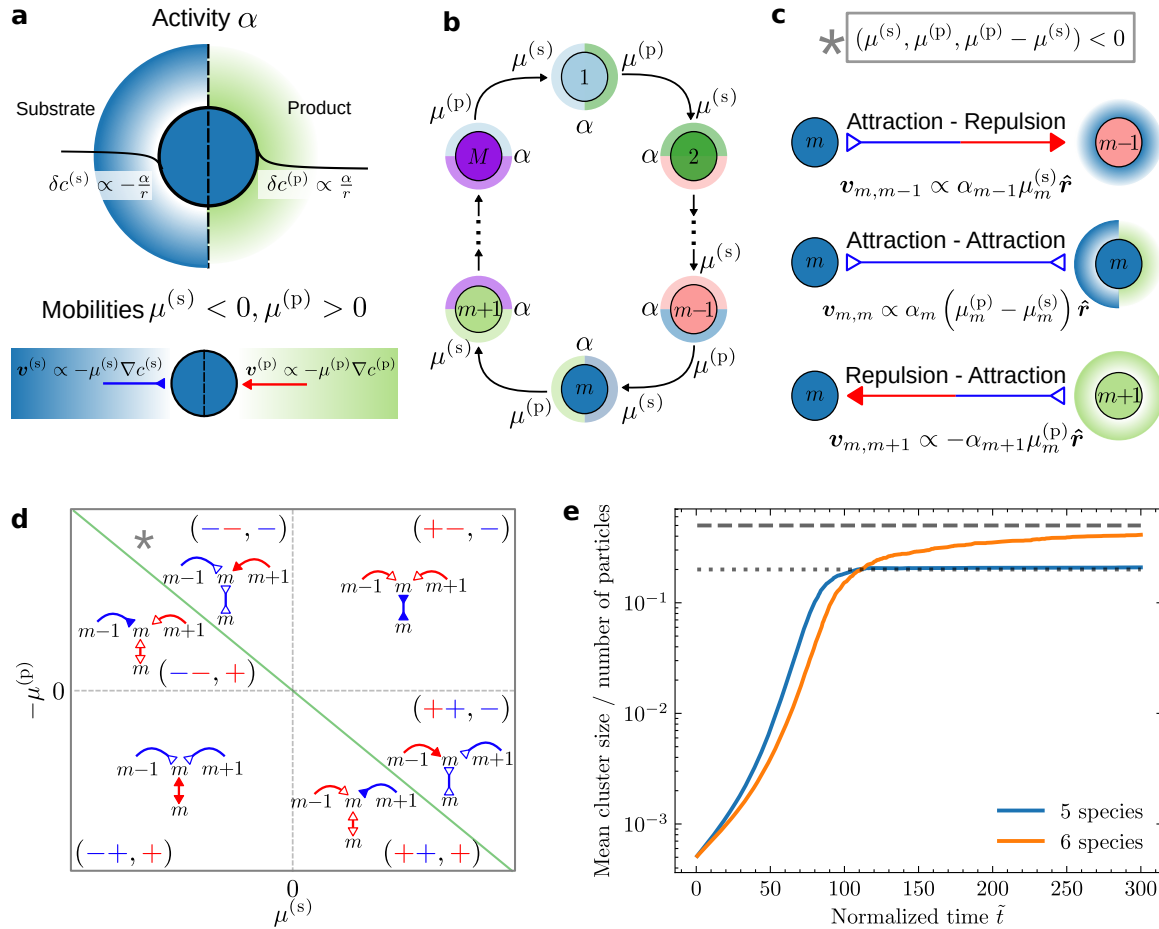
FIG. 1. **Properties and interactions of catalytically-active particles.** **(a)**: The particles convert substrate (s) into product (p) with a rate given by the activity α (top) and respond to gradients of these chemicals with mobilities $\mu^{(s)}$ and $\mu^{(p)}$ (bottom). **(b)**: M active particle species are arranged in a model catalytic cycle, in which the product of species m is the substrate of species $m+1$. **(c)**: Non-reciprocal interactions between particles of the same or adjacent species. Direction and colour of arrows indicate the attractive (blue, inwards arrowhead) or repulsive (red, outwards arrowhead) nature of the interaction. **(d)**: Phase diagram of interaction motifs. Each region constrains the mobilities so that one interaction has a higher magnitude than the others, as highlighted by a full arrowhead. The grey asterisk indicates the location in parameter space of the interactions pictured in (c). The green line separates the self-attracting and self-repelling regions. The sign triplets correspond to the signs of $(\mu^{(s)}, \mu^{(p)}, \mu^{(p)} - \mu^{(s)})$. **(e)**: Cluster growth dynamics for a cycle of $M = 5$ (blue, see Fig. 3a and Movie 7) and $M = 6$ (orange, see Fig. 3b and Movie 3) species, showing super-exponential coarsening dynamics of the condensate formation. For $M = 5$ species, the mean cluster size saturates at a value corresponding to the total particle population divided by M (grey dotted line). For $M = 6$, it saturates at half the particle population (dashed grey line).

by relatively slow power law coarsening dynamics such as the Lifshitz-Slyozov ($\sim t^{1/3}$) law [46], even in externally driven non-equilibrium cases. Then, it is hard to imagine how such a process has given rise to such a rapid formation of intelligent life through slow coarsening into inherently slow condensates.

In connection with the above considerations and to broaden the scope of the research on the physical aspects of the origin of life, we pose the following question: how can we envisage pathways in which the information contained in chemical reaction networks from which primitive forms of metabolism can emerge would lead to structural self-organization of the corresponding components?

Here, we propose a strategy that can achieve this task by employing the naturally occurring non-reciprocal interactions between catalysts that can form a cyclic reaction network. We show that model catalytically-active particles participating in a metabolic cycle are able to spontaneously self-organize into condensates, which may aggregate or separate depending on the number of particle species involved in the cycle, and exhibit chasing, periodic aggregation and dispersal, as well as self-stirring, thus providing a generic mechanism for spontaneous formation of metabolically-active protocells. While the observed (super-) exponential coarsening law offers a significantly faster alternative for the formation of condensates (see Fig. 1), the information-driven dynamics leads

to formation of structurally active and functional condensates that exhibit lifelike behaviour already at the outset.

Non-reciprocal interactions have been shown to generically emerge in active matter in the context of non-equilibrium phoretic interactions between catalytically active colloids and enzymes [47]. Let us consider a set of M species of chemically-active particles (Fig. 1a, top), representing catalyst molecules or enzymes. Each of the particles converts a substrate (s) into a product (p) at a rate α. At steady state, they create perturbations in the concentration field of the corresponding substrate that decays with distance r as $\delta c^{(s)} \propto -\alpha/r$, and a corresponding change in the concentration of the corresponding product as $\delta c^{(p)} \propto \alpha/r$ (Methods). These particles are also chemotactic (Fig. 1a, bottom): when subjected to a concentration gradient of their substrate, they develop a velocity $\boldsymbol{v} \propto -\mu^{(s)} \nabla c^{(s)}$ with $\mu^{(s)}$ the chemotactic mobility for the substrate, which is negative or positive if the particle is attracted to or repelled from the substrate, respectively. Similarly, the particles are able to chemotax in response to gradients of their products, with a mobility $\mu^{(p)}$.

To create a model for primitive metabolism, we consider a simplified catalytic cycle (Fig. 1b), in which the substrate of the catalyst species m, which we denote as chemical (m), is the product of species $m - 1$. To close the cycle, species 1 has the product of species M as its substrate. For simplicity, we take all catalyst species to have the same parameters α, $\mu^{(s)}$ and $\mu^{(p)}$, and to be present in the system at identical initial concentrations. The cycle can achieve a steady state without net chemical production or consumption. Due to their chemical activity and chemotactic mobilities, the particle species can interact with one another through chemical fields (Fig. 1c). For instance, if we consider two particles of species m and $m - 1$, then the particle of species $m - 1$ creates, through its chemical activity, a concentration gradient of the substrate of the particle of species m, to which the latter responds by developing a velocity directed towards the particle of species $m - 1$, $\boldsymbol{v}_{m,m-1} \propto \alpha\mu^{(s)}\hat{\boldsymbol{r}}$, where $\hat{\boldsymbol{r}}$ is the unit vector pointing from the particle that creates the perturbation to the particle that responds to the perturbation (Methods). On the other hand, the particle of species m consumes the product of $m - 1$, and thus the particle of species $m - 1$ develops a velocity $\boldsymbol{v}_{m-1,m} \propto -\alpha\mu^{(p)}\hat{\boldsymbol{r}}$ towards the other particle. As a consequence, the interactions between the particles of species m and $m - 1$ are non-reciprocal, i.e. $\boldsymbol{v}_{m,m-1} \neq -\boldsymbol{v}_{m-1,m}$ (see Fig. 1d for different possibilities). This effective violation of action-reaction symmetry is a signature of non-equilibrium activity, leading to non-trivial many-body behaviour as has been shown for chemically-active particles interacting through a single chemical [24, 48], active mixtures interacting through generic short-range interactions [49, 50], complex plasmas [51], and other systems [52–54]. Particles of the same species also self-interact

by consumption of their substrate and creation of their product, with a velocity $\boldsymbol{v}_{m,m} \propto \alpha(\mu^{(p)} - \mu^{(s)})\hat{\boldsymbol{r}}$. We note that these effective non-reciprocal interactions mediated by chemical fields are long-ranged, with the induced velocities going as $1/r^2$ (Methods).

We consider the evolution equations for the concentration fields of the active species ρ_m and their substrates $c^{(m)}$, given by the coupled system of $2M$ equations

$$\partial_t \rho_m(\boldsymbol{r}, t) = \nabla \cdot [D_{\mathrm{p}}\nabla\rho_m + (\mu^{(s)}\nabla c^{(m)} + \mu^{(p)}\nabla c^{(m+1)})\rho_m],$$
$$(1a)$$

$$\partial_t c^{(m)}(\boldsymbol{r}, t) = D\nabla^2 c^{(m)} + \alpha\left(\rho_{m-1} - \rho_m\right). \qquad (1b)$$

Equation (1a) describes the conserved dynamics of the catalysts, with a diffusion term involving a species-independent coefficient D_{p} and a chemotactic drift term in response to both substrate and product gradients. The substrate concentrations evolve according to the reaction-diffusion equation (1b), with a diffusion coefficient D, and a reaction term corresponding to the activity of the catalysts.

The time evolution of equation (1) naturally leads to the formation of clusters, akin to active phase separation [24, 48]. The clusters are formed through a particularly fast and efficient coarsening process that exhibits exponential growth rather than the commonly occurring power law form, associated with processes such as Ostwald ripening, as can be seen in Fig. 1e (see Methods). This behaviour can be characterized using a simple scaling argument. When particles are collapsing onto a cluster, the rate of growth for the cluster can be estimated as $\frac{dN}{dt} = \oint_S \rho\boldsymbol{v} \cdot d\boldsymbol{S}$ where the velocity $\boldsymbol{v} = -\mu\nabla c$ can be expressed in terms of the particle concentration by using Gauss theorem and the relation $-\nabla^2 c = \alpha\rho/D$, which yields $\frac{dN}{dt} = \frac{\mu\alpha}{D}\rho N$. This expression can be integrated to obtain $N(t) = N_0 \exp\left(\frac{\mu\alpha}{D}\int_0^t dt_1\rho\right) \simeq N_0 \exp\left(\frac{\mu\alpha}{D}\rho t\right)$, which predicts an exponential growth law for constant ρ and allows for super-exponential growth if the density increases with time, which matches well with the results presented in Fig. 1e. This observation suggests that non-equilibrium phoretic interactions have the ability to guide formation of dense clusters in a fast and efficient manner, and as such, can be strong candidates for creating the appropriate conditions for the emergence of early functionalized protocells.

A linear stability analysis on equation (1) (Methods) around a spatially-homogeneous solution leads to the following eigenvalue equation for the macroscopic (long-wavelength) particle density modes

$$-\sum_{n=1}^{M} \Lambda_{m,n}\delta\rho_n = \lambda\delta\rho_m. \qquad (2)$$

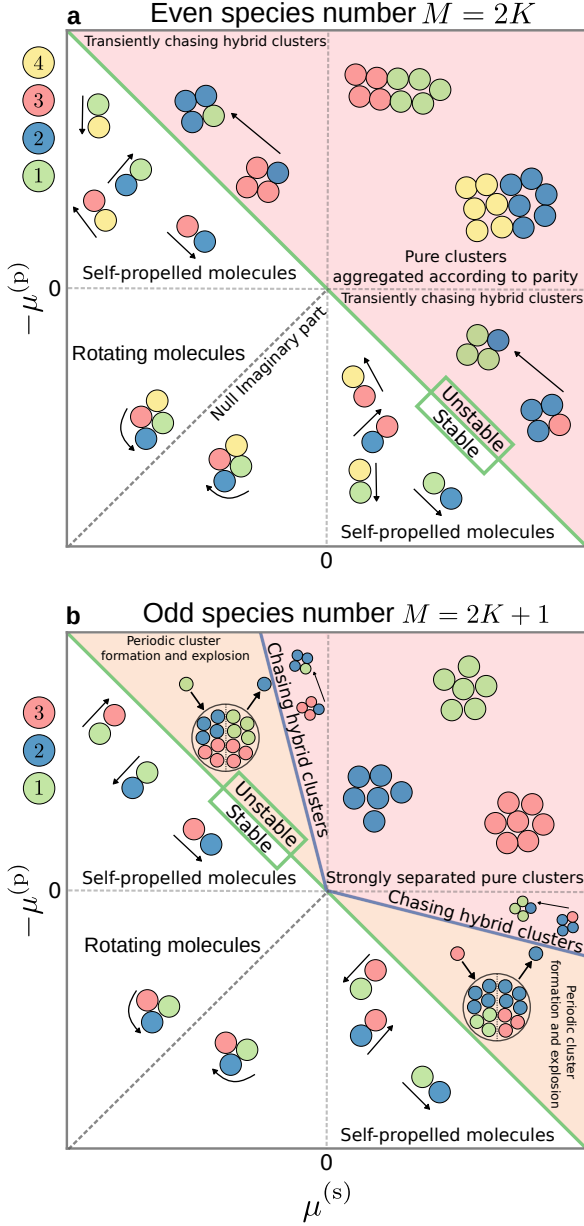The matrix $\Lambda_{m,n}$ describes the velocity response of

a Even species number $M = 2K$

Transiently chasing hybrid clusters

Self-propelled molecules

Pure clusters aggregated according to parity

Transiently chasing hybrid clusters

Null Imaginary part

Rotating molecules

Unstable / Stable

Self-propelled molecules

b Odd species number $M = 2K + 1$

Periodic cluster formation and explosion

Chasing hybrid clusters

Unstable / Stable

Self-propelled molecules

Strongly separated pure clusters

Chasing hybrid clusters

Rotating molecules

Periodic cluster formation and explosion

Self-propelled molecules

$-\mu^{(\mathrm{p})}$

$\mu^{(\mathrm{s})}$

FIG. 2. **Stability diagrams for catalytic cycles.** The cycles contain an even (**a**) or an odd (**b**) number of catalytic species. The interaction motifs in each quadrant of the parameter space are the same as those displayed in Fig. 1d. Details of the behaviour in each phase are given in the text. In both the self-propelled and rotating molecule phases, the molecules exchange particles with one another. Molecule rotation does not occur along the dashed lines corresponding to null imaginary part in the unstable eigenvalue.

species m to species n, and is defined as follows

$$
\begin{cases}
\Lambda_{m,m-1} = \alpha \mu^{(\mathrm{s})} \rho_0 / D, \\
\Lambda_{m,m} = \alpha \left(\mu^{(\mathrm{p})} - \mu^{(\mathrm{s})} \right) \rho_0 / D, \\
\Lambda_{m,m+1} = -\alpha \mu^{(\mathrm{p})} \rho_0 / D, \\
\Lambda_{m,n \notin \{m,m\pm 1\}} = 0,
\end{cases}
\tag{3}
$$

where ρ_0 represents the initial homogeneous concentrations. By definition, $\Lambda_{m,n}$ is negative, or positive, if m is attracted to, or repelled from, n, respectively. The form of $\Lambda_{m,n}$ suggests a classification scheme as there are six possible interaction motifs (Fig. 1d), representing the interactions of each species with itself as well as with its two neighbours in the catalytic cycle. The signs of the interactions are represented diagrammatically, following the conventions defined in Fig. 1c and d.

The eigenvalues λ_ℓ ($\ell \in \{1, \ldots, M\}$) allow us to predict the stability of the system: $\mathrm{Re}(\lambda) > 0$ for any eigenvalue λ indicates an instability, whereas $\mathrm{Re}(\lambda) < 0$ for all eigenvalues implies a stable homogeneous state. The eigenvector $\delta\rho_m^\ell$, in turn, gives the stoichiometry at the onset of instability, i.e. the ratio of the different species within the growing perturbation, which may be positive, for species that aggregate together, or negative, for species that separate.

The topology of the catalytic cycle strongly influences its self-organization. As a point of comparison, we consider a non-cyclic system, in which M catalytic species all act on a single chemical field. In this case, all the coefficients of the interaction matrix are equal to $\alpha\mu\rho_0$, leading to a system with only one nonzero eigenvalue $\lambda = -M\alpha\mu\rho_0/D$. The corresponding instability condition is $\alpha\mu < 0$, and the instability is equivalent to the Keller-Segel model [24, 55]. The model catalytic cycle studied here, however, presents a different category. As the interaction matrix (3) is a circulant matrix, its eigenvalues are easily calculated as

$$
\begin{cases}
\mathrm{Re}(\lambda_\ell) & = -\frac{\alpha\rho_0}{D} \left(\mu^{(\mathrm{p})} - \mu^{(\mathrm{s})} \right) \left[1 - \cos(2\pi\ell/M) \right], \\
\mathrm{Im}(\lambda_\ell) & = \frac{\alpha\rho_0}{D} \left(\mu^{(\mathrm{s})} + \mu^{(\mathrm{p})} \right) \sin(2\pi\ell/M),
\end{cases}
\tag{4}
$$

(see Supplementary Information for graphical representations of the eigenvalue spectra for different species numbers). There are now $M - 1$ nonzero eigenvalues, which come as pairs of complex conjugate numbers with the possible exception of $\lambda_{M/2}$ for M even. In stark contrast with the non-cyclic system, the complex character of these eigenvalues opens the door to oscillatory behaviour. The instability condition, obtained by imposing that the real part of at least one eigenvalue is larger than zero, in turn corresponds to

$$
\mu^{(\mathrm{p})} - \mu^{(\mathrm{s})} < 0, \tag{5}
$$

i.e. the catalytic species have to be self-attracting for an instability to occur. This is represented in the phase diagrams of Fig. 2: all interaction networks above the green line are unstable. If the condition is not satisfied, the system remains homogeneous, with several possible states: the particles can form transient self-propelled molecules (Extended Data Fig. E2a, Movie 1, see Methods for the parameters of all Movies), or form more long-lived, rotating molecules (Extended Data Fig. E2b, Movie 2) which exchange particles without growing, as found in particle-
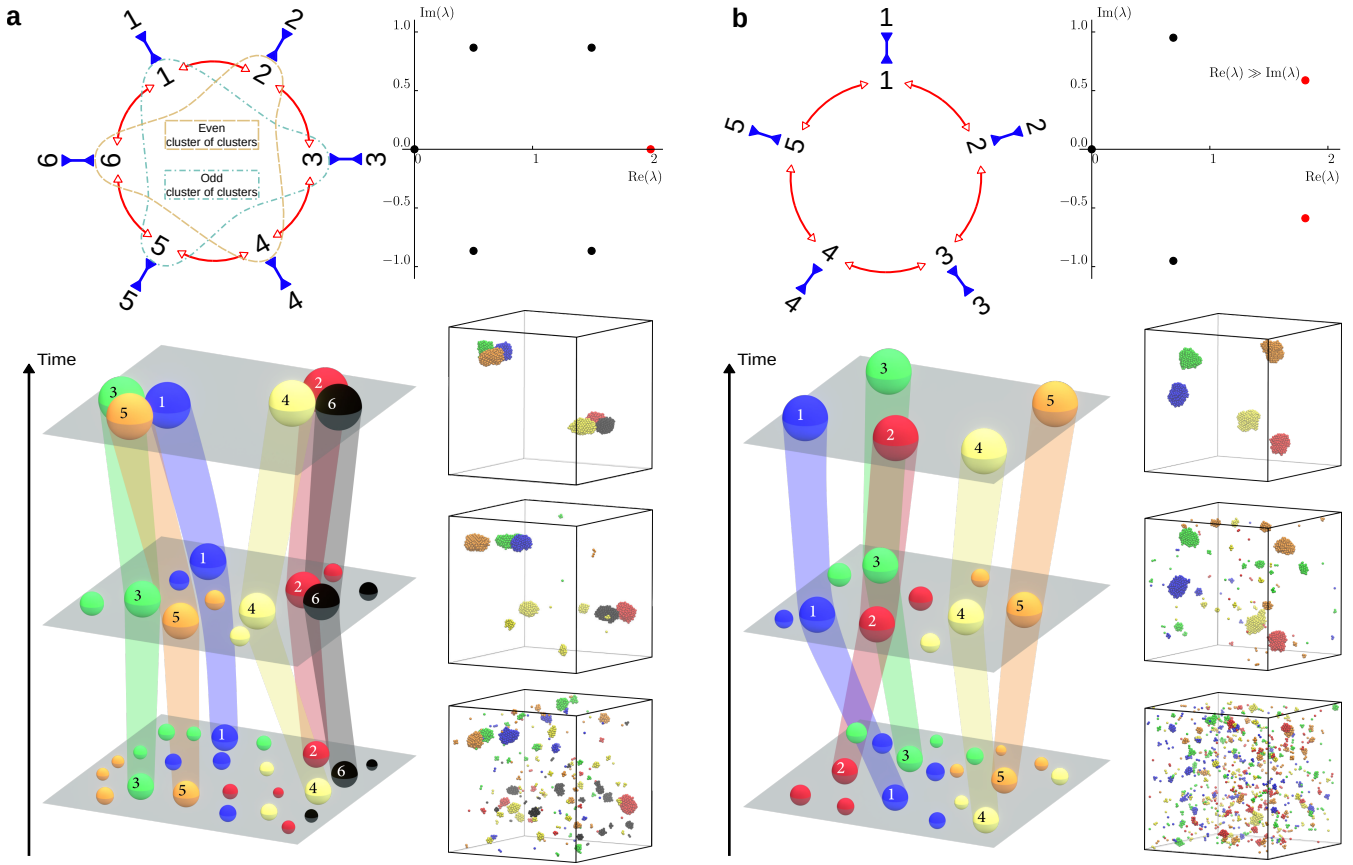
FIG. 3. **Aggregation dynamics for self-attracting, cross-repelling species.** The cycles contain an even (**a**) or an odd (**b**) number of catalytic species. Top left: interactions between the active species. All species are self-attracting and repel both neighbours in the cycle (corresponding to the top-right quadrants in Fig. 2a,b). Top right: corresponding eigenvalue spectrum, in units of $-(\mu^{(p)} - \mu^{(s)})\alpha\rho_0/D$ for the real part and $-(\mu^{(s)} + \mu^{(p)})\alpha\rho_0/D$ for the imaginary part. The eigenvalue (or complex conjugate pair) with the largest real part is shown in red. In (**b**), the corresponding conjugate pair has an imaginary part much smaller than its real part, so that the dynamics of the system are non-oscillatory. Bottom: Schematic representations of the time evolution of the aggregation dynamics (left) and corresponding snapshots of molecular dynamics simulations (right, see Movies 3 and 7 for even and odd cases, respectively) are shown side by side. Dashed lines in (**a**) indicate the parity-based aggregation that occurs for an even number of species.

based Brownian dynamics simulations of the same system (Methods).

Remarkably, we find key differences between cycles with even or odd number of species. In the case of an even species number $M = 2K$, the eigenvalue with largest real part (which dominates the instability) is real and given by

$$\lambda_K = -2\frac{\alpha\rho_0}{D}\left(\mu^{(p)} - \mu^{(s)}\right), \qquad (6)$$

implying that the instability is non-oscillatory with the corresponding eigenvector

$$\delta\rho^K = (1, -1, 1, -1, \cdots, -1). \qquad (7)$$

Thus, at onset of instability, all the species with equal parity tend to aggregate together and to separate from the species of opposite parity (Fig. 2a, above the green line). Brownian dynamics simulations show that this prediction carries over to the final phase-separated state; an example is shown in Fig. 3a (Movie 3). These simulations show an initial exponential growth of M clusters, each containing all the particles of a given species. The steady state for an even number of self-attracting, cross-repelling species is two large "clusters of clusters", one encompassing clusters of the even-labelled species, the other of the odd-labelled species. Both the transient and the steady state are captured by the growth dynamics shown in Fig. 1e, with the average cluster size initially growing exponentially and saturating at half of the total particle population.

A variety of behaviour is observed in the case with chasing interactions among neighbours, based on the relative values of the chasing strength $|\mu^{(s)} + \mu^{(p)}|$ as compared to the self-attraction strength $|\mu^{(p)} - \mu^{(s)}|$. If both values are of the same order of magnitude, the system behaves simi-
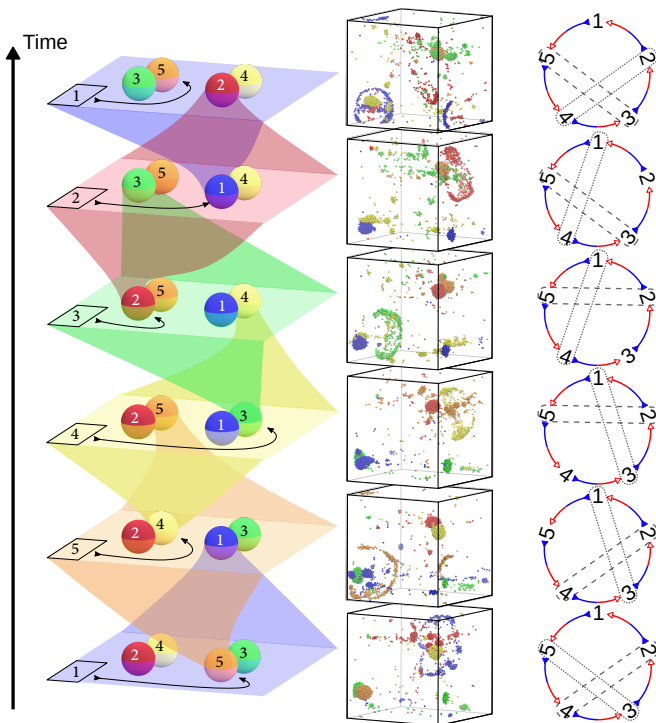
FIG. 4. **Oscillatory dynamics for an odd number of species with chasing cross-interactions**. A schematic representation of the oscillatory dynamics (left), snapshots of molecular dynamics simulations (middle, see also Movie 8), and a diagram of the corresponding species interactions and pairing (right) are shown side by side. Here, dashed and dotted lines represent respectively the pairs on the left and right of the schematic representation. The eigenvalues of the system are as in Fig. 3b, but now $\mathrm{Re}(\lambda) < \mathrm{Im}(\lambda)$ for the most unstable conjugate pair, so that the dynamics of the system are oscillatory.

larly to the cross-repelling case, except that the resulting clusters can chase each other or rotate in place (Extended Data Fig. E1a and Movie 4). For the cases where the value of the self-attraction is much lower than the chasing strength, fully-hybrid clusters containing all species of the same parity form over longer timescales, as opposed to "clusters of clusters" as in the cross-repelling case (Movie 5). Finally, for almost negligible self-attraction transient oscillations are observed before cluster formation (Extended Data Fig. E1b, Movie 6).

For cycles with an odd number of species $M = 2K+1$, the largest real part corresponds to the complex conjugate pair of eigenvalues (see Supplementary Information)

$$\lambda_{K+\frac{1}{2}\pm\frac{1}{2}} = -\frac{\alpha\rho_0}{D}\left(\mu^{(\mathrm{p})} - \mu^{(\mathrm{s})}\right)\left[1 + \cos\left(\frac{\pi}{2K+1}\right)\right]$$
$$\mp i\frac{\alpha\rho_0}{D}\left(\mu^{(\mathrm{s})} + \mu^{(\mathrm{p})}\right)\sin\left(\frac{\pi}{2K+1}\right),$$
(8)

suggesting the potential for long-lived oscillations, or even oscillatory steady states, with the real part corre-

sponding to the growth rate of the perturbation and the imaginary part to its oscillation frequency.

The corresponding eigenvectors $\delta\rho^{K+\frac{1}{2}\pm\frac{1}{2}}$ are also a pair of complex conjugates, with components given by

$$\delta\rho_m^{K+\frac{1}{2}\pm\frac{1}{2}} = (-1)^{m-1}\left[\cos\left(\frac{(m-1)\pi}{2K+1}\right) \pm i\sin\left(\frac{(m-1)\pi}{2K+1}\right)\right],$$
(9)

for $m = 1,...,2K+1$. The species are out of phase by $2\pi/(2K+1)$ with respect to their second-nearest neighbour during the oscillations. Since the number of species is odd, parity-based cluster aggregation is not possible: if two clusters attempt to come together, a third will systematically come to break them apart. For cross-repelling species, this leads to a segregation into single-species clusters which separate in a way that minimizes their overall repulsion (Fig. 3b, Movie 7). Similarly to the even case with $M = 2K$, this behavior is captured by the growth statistics displayed in Fig. 1e, where mean cluster size exhibits an initial exponential growth and saturates at a value corresponding to the formation of M individual clusters.

In the case of chasing cross-interactions, oscillations become visible when the growth rate is slower than the oscillation frequency, which corresponds to the condition

$$-\mu^{(\mathrm{p})} \lesssim -\mu^{(\mathrm{s})}\left[\frac{1 + \cos\left(\frac{\pi}{2K+1}\right) \mp \sin\left(\frac{\pi}{2K+1}\right)}{1 + \cos\left(\frac{\pi}{2K+1}\right) \pm \sin\left(\frac{\pi}{2K+1}\right)}\right], \quad (10)$$

which defines the orange region in Fig. 2b. We note that this inequality only sets an order of magnitude for the transition from oscillatory to non-oscillatory dynamics, rather than a sharp boundary. The behaviour of the system again depends on the relative values of the self attraction magnitude $|\mu^{(\mathrm{p})} - \mu^{(\mathrm{s})}|$ and the chasing strength $|\mu^{(\mathrm{p})} + \mu^{(\mathrm{s})}|$. When self-attraction is weaker than the chasing strength (i.e. close to the instability line), Brownian dynamics simulations indeed show a persistent oscillatory dynamical behaviour with the following choreography for the case in which each species chases after the previous one: a single-species cluster of a species m forms transiently, and is then "invaded" by species $m+1$, leading to an explosion that disperses species m back into the solution. Species m then invades a cluster of species $m-1$, and so on, in a sequential order until M explosion events have occurred and the cycle starts again. In the case with $M = 5$ (Fig. 4 and Movie 8; see Supplementary Information for a quantification of the oscillation dynamics), we observe that the system comes back to a state similar to the initial one, except for a swap in the locations of the clusters. This change occurs because the clusters of the second-nearest-neighbour species in the cycle tend to form pairs. One component of one of these pairs is replaced in every explosion event by the species preceding it in the cycle, such that, after five explosions, the pairs have been switched in space. The reverse dy-

namics (species m invading species $m + 1$) are observed if the signs of $\mu^{(s)}$ and $\mu^{(p)}$ are reversed, so that each species chases the next one in the cycle.

For even weaker self-attraction or stronger chasing, the clusters do not have time to form. In this case, oscillations are observed in a dilute mixture of catalytic particles, where clusters are replaced by transient zones of higher concentration (Movie 9). This can create a self-stirring solution, favouring the mixing and assembly of solution components in time scales considerably shorter than those allowed by passive diffusion. Lastly, if the perturbation growth rate is instead larger than its oscillation frequency (red region in Fig. 2b), then the dynamics leads to formation of stable clusters. We have observed in simulations the formation of chasing hybrid clusters similar to the case with even number of species (Extended Data Fig. E3, Movie 10).

These results can be contrasted with the behaviour of reaction-diffusion systems, which can also undergo instabilities as first formulated by Turing [56], and extensively studied for both non-mass-conserving [57–59] and mass-conserving [60, 61] reactions. Such systems have been shown to exhibit pattern formation, macroscopic phase separation, or travelling wave fronts. In contrast, the model we study in this work is able to exhibit a larger variety of complex behaviour, because of the non-reciprocal interactions.

Our work shows that catalytically-active and chemotactic particles participating in a primitive metabolic cycle exhibit a variety of structural complex collective behaviour. Due to the nature of the gradient-mediated interactions involved, such particles are able to interact over large distances, and undergo spontaneous and exponentially rapid cluster formation that serves to support their metabolic function. This feature can help overcome the barrier of the time needed for the right types of molecules to meet by chance at sufficiently high concentrations in the first place, and selectively drives the formation of functional metabolic condensates based on the information embedded in the chemical reaction network kinship of the components. This suggests that naturally occurring phoretic transport mechanisms might be able to equip the biological paradigm of liquid-liquid phase separation with an information-controlled strategy for metabolic structure formation. Moreover, since the overall chemical activity of enzymes can be enhanced with suitable clustering behaviour [14, 62], the ability to engineer complex clustering features such as those reported here may help improve the design and efficiency of synthetic reaction networks.

Depending on the parity of the number of different species involved in the cycle and on their chemotactic parameters, these clusters might consist of a single or several species, thereby accommodating a range of design strategies for metabolic structure formation. If the number of species in the cycle is odd, chasing interactions may emerge at the macroscopic level, similar to those that have been observed in recent experiments [25, 26], although in this case leading to long-lived, system-wide oscillations. Our work suggests that a metabolic cycle consisting of an odd number of catalysts may have an advantage (over a cycle with an even number of catalysts) due to the formation of the explosive oscillatory stationary state. It remains to be seen whether the fact that the universal citric acid cycle consists of eleven catalysts can in some way be related to this observation. The observed variety of emergent structural behaviour with highly precise control over the composition of the constituents of the metabolically active clusters hints at a significant possible role for catalytically active molecules at the origin of life: the molecules that are metabolically connected to each other will preferentially and efficiently form active clusters together, hence serving as potential candidates for the nucleation of early forms of life.

What is remarkable about our proposal to use non-reciprocal interactions in this context is that such interactions generically emerge in non-equilibrium systems with chemical catalytic activity [63], which are abundantly present in the cell (enzymes involved with metabolic activity) and can be easily synthesized in artificial systems (catalytic colloids) for controlled *in vitro* experiments. In this sense, the theoretical developments that have led to significant progress in the field of active matter in the laboratory setting can now be used to guide new experimental strategies for research in the field of origin of life. Our work offers a theoretical and conceptual platform towards developing this possibility.

AUTHOR CONTRIBUTIONS STATEMENT

V.O-.R., J.A-.C., and R.G. designed the research, conducted the research, analyzed the data, and wrote the paper.

COMPETING INTERESTS STATEMENT

The authors declare no competing financial interests.

[1] A. I. Oparin, *The Origin of Life* (MacMillan, New York, 1938).

[2] J. B. S. Haldane, *Genesis of Life* (Bates D. R. (ed) The Planet Earth. Pergamon Press, London, 1957).

[3] F. Dyson, *Origins of Life* (Cambridge University Press, 1999).

[4] Z. Zeravcic, V. N. Manoharan, and M. P. Brenner, Colloquium: Toward living matter with colloidal particles, Rev. Mod. Phys. **89**, 031001 (2017).

[5] Z. Zeravcic and M. P. Brenner, Spontaneous emergence of catalytic cycles with colloidal spheres, Proc. Natl. Acad. Sci. U.S.A. **114**, 4342 (2017).

[6] D. Zwicker, R. Seyboldt, C. A. Weber, A. A. Hyman, and F. Jülicher, Growth and division of active droplets provides a model for protocells, Nat. Phys. **13**, 408 (2017).

[7] M. Tena-Solsona, J. Janssen, C. Wanzke, F. Schnitter, H. Park, B. Rieß, J. M. Gibbs, C. A. Weber, and J. Boekhoven, Accelerated ripening in chemically fueled emulsions, ChemSystemsChem **3**, e2000034 (2021).

[8] M. Matsuo and K. Kurihara, Proliferating coacervate droplets as the missing link between chemistry and biology in the origins of life, Nat. Commun. **12**, 5487 (2021).

[9] A. McMullen, M. M. Basagoiti, Z. Zeravcic, and J. Brujic, Self-assembly of emulsion droplets through programmable folding, Nature **610**, 502 (2022).

[10] S. Osat and R. Golestanian, Non-reciprocal multifarious self-organization, Nature Nanotechnology (2022).

[11] A. Testa, M. Dindo, A. A. Rebane, B. Nasouri, R. W. Style, R. Golestanian, E. R. Dufresne, and P. Laurino, Sustained enzymatic activity and flow in crowded protein droplets, Nat. Commun. **12**, 6293 (2021).

[12] R. Soto and R. Golestanian, Self-assembly of catalytically active colloidal molecules: Tailoring activity through surface chemistry, Phys. Rev. Lett. **112**, 068301 (2014).

[13] J. Agudo-Canalejo, P. Illien, and R. Golestanian, Phoresis and Enhanced Diffusion Compete in Enzyme Chemotaxis, Nano. Lett. **18**, 2711 (2018).

[14] G. Giunta, H. Seyed-Allaei, and U. Gerland, Cross-diffusion induced patterns for a single-step enzymatic reaction, Commun Phys **3**, 1 (2020).

[15] M. W. Cotton, R. Golestanian, and J. Agudo-Canalejo, Catalysis-induced phase separation and autoregulation of enzymatic activity, Phys. Rev. Lett. **129**, 158101 (2022).

[16] A.-D. C. Nguindjel, P. J. de Visser, M. Winkens, and P. A. Korevaar, Spatial programming of self-organizing chemical systems using sustained physicochemical gradients from reaction, diffusion and hydrodynamics, Physical Chemistry Chemical Physics **24**, 23980 (2022).

[17] A. D. Pizarro, C. L. A. Berli, G. J. A. A. Soler-Illia, and M. G. Bellino, Droplets in underlying chemical communication recreate cell interaction behaviors, Nat. Commun. **13**, 3047 (2022).

[18] R. Golestanian, Collective behavior of thermally active colloids, Phys. Rev. Lett. **108**, 038303 (2012).

[19] J. Palacci, S. Sacanna, A. P. Steinberg, D. J. Pine, and P. M. Chaikin, Living crystals of light-activated colloidal surfers, Science **339**, 936 (2013).

[20] J. A. Cohen and R. Golestanian, Emergent cometlike swarming of optically driven thermally active colloids, Phys. Rev. Lett. **112**, 068302 (2014).

[21] O. Pohl and H. Stark, Dynamic clustering and chemotactic collapse of self-phoretic active particles, Phys. Rev. Lett. **112**, 238303 (2014).

[22] S. Saha, R. Golestanian, and S. Ramaswamy, Clusters, asters, and collective oscillations in chemotactic colloids, Phys. Rev. E **89**, 062316 (2014).

[23] R. Soto and R. Golestanian, Self-assembly of active colloidal molecules with dynamic function, Phys. Rev. E **91**, 052304 (2015).

[24] J. Agudo-Canalejo and R. Golestanian, Active Phase Separation in Mixtures of Chemically Interacting Particles, Phys. Rev. Lett. **123**, 018101 (2019).

[25] Y. Qiao, M. Li, R. Booth, and S. Mann, Predatory behaviour in synthetic protocell communities, Nat. Chem. **9**, 110 (2017).

[26] C. H. Meredith, P. G. Moerman, J. Groenewold, Y.-J. Chiu, W. K. Kegel, A. van Blaaderen, and L. D. Zarzar, Predator–prey interactions between droplets driven by non-reciprocal oil exchange, Nat. Chem. **12**, 1136 (2020).

[27] S. Koga, D. S. Williams, A. W. Perriman, and S. Mann, Peptide–nucleotide microdroplets as a step towards a membrane-free protocell model, Nat. Chem. **3**, 720 (2011).

[28] E. Sokolova, E. Spruijt, M. M. K. Hansen, E. Dubuc, J. Groen, V. Chokkalingam, A. Piruska, H. A. Heus, and W. T. S. Huck, Enhanced transcription rates in membrane-free protocells formed by coacervation of cell lysate, Proc. Natl. Acad. Sci. U.S.A. **110**, 11692 (2013).

[29] B. Drobot, J. M. Iglesias-Artola, K. Le Vay, V. Mayr, M. Kar, M. Kreysing, H. Mutschler, and T.-Y. D. Tang, Compartmentalised RNA catalysis in membrane-free coacervate protocells, Nat. Commun. **9**, 3643 (2018).

[30] N. P. Kamat, S. Tobé, I. T. Hill, and J. W. Szostak, Electrostatic localization of RNA to protocell membranes by cationic hydrophobic peptides, Angewandte Chemie International Edition **54**, 11735 (2015).

[31] L. Jin, N. P. Kamat, S. Jena, and J. W. Szostak, Fatty acid/phospholipid blended membranes: A potential intermediate state in protocellular evolution, Small **14**, 1704077 (2018).

[32] M. Eigen, Selforganization of matter and the evolution of biological macromolecules, Die Naturwissenschaften **58**, 465 (1971).

[33] S. A. Kauffman, Autocatalytic sets of proteins, J. Theor. Biol. **119**, 1 (1986).

[34] M. Steel, The emergence of a self-catalysing structure in abstract origin-of-life models, Appl. Math. Lett. **13**, 91 (2000).

[35] F. J. Dyson, A model for the origin of life, Journal of Molecular Evolution **18**, 344 (1982).

[36] S. Jain and S. Krishna, A model for the emergence of cooperation, interdependence, and structure in evolving networks, Proceedings of the National Academy of Sciences **98**, 543 (2001).

[37] H. J. Morowitz, J. D. Kostelnik, J. Yang, and G. D. Cody, The origin of intermediary metabolism, Proceedings of the National Academy of Sciences **97**, 7704 (2000).

[38] E. Smith and H. J. Morowitz, Universality in intermediary metabolism, Proceedings of the National Academy of Sciences **101**, 13168 (2004).

[39] J. C. Xavier, W. Hordijk, S. Kauffman, M. Steel, and W. F. Martin, Autocatalytic chemical networks at the origin of metabolism, Proc. Roy. Soc. B-Biol. Sci. **287**, 20192377 (2020).

[40] D. P. Horning and G. F. Joyce, Amplification of RNA by an RNA polymerase ribozyme, Proc. Natl. Ac. Sci. U.S.A. **113**, 9786 (2016).

[41] P. G. Higgs and N. Lehman, The RNA World: Molecular cooperation at the origins of life, Nat. Rev. Genet. **16**, 7 (2015).

[42] P. Nghe, W. Hordijk, S. A. Kauffman, S. I. Walker, F. J. Schmidt, H. Kemble, J. A. M. Yeates, and N. Lehman, Prebiotic network evolution: Six key parameters, Mol. BioSyst. **11**, 3206 (2015).

[43] N. Vaidya, M. L. Manapat, I. A. Chen, R. Xulvi-Brunet, E. J. Hayden, and N. Lehman, Spontaneous network formation among cooperative RNA replicators, Nature **491**, 72 (2012).

[44] F. Crick, The origin of the genetic code, Journal of Molecular Biology **38**, 367 (1968).

[45] R. Falk and A. Lazcano, The forgotten dispute: A.I. Oparin and H.J. Muller on the Origin of Life, History and Philosophy of the Life Sciences **34**, 373 (2012).

[46] I. Lifshitz and V. Slyozov, The kinetics of precipitation from supersaturated solid solutions, Journal of Physics and Chemistry of Solids **19**, 35 (1961).

[47] R. Golestanian, Phoretic Active Matter, in *Active matter and nonequilibrium statistical physics*, Lecture Notes of the 2018 Les Houches Summer School (Oxford University Press, London, England, 2022).

[48] V. Ouazan-Reboul, J. Agudo-Canalejo, and R. Golestanian, Non-equilibrium phase separation in mixtures of catalytically active particles: Size dispersity and screening effects, Eur. Phys. J. E **44**, 113 (2021).

[49] S. Saha, J. Agudo-Canalejo, and R. Golestanian, Scalar Active Mixtures: The Nonreciprocal Cahn-Hilliard Model, Phys. Rev. X **10**, 041009 (2020).

[50] Z. You, A. Baskaran, and M. C. Marchetti, Nonreciprocity as a generic route to traveling states, Proc. Natl. Acad. Sci. U.S.A. **117**, 19767 (2020).

[51] A. V. Ivlev, J. Bartnick, M. Heinen, C.-R. Du, V. Nosenko, and H. Löwen, Statistical Mechanics where Newton's Third Law is Broken, Phys. Rev. X **5**, 011035 (2015).

[52] S. A. M. Loos and S. H. L. Klapp, Irreversibility, heat and information flows induced by non-reciprocal interactions, New Journal of Physics **22**, 123051 (2020).

[53] M. Fruchart, R. Hanai, P. B. Littlewood, and V. Vitelli, Non-reciprocal phase transitions, Nature **592**, 363 (2021).

[54] A. Dinelli, J. O'Byrne, A. Curatolo, Y. Zhao, P. Sollich, and J. Tailleur, Non-reciprocity across scales in active mixtures (2022).

[55] E. F. Keller and L. A. Segel, Initiation of slime mold aggregation viewed as an instability, J. Theor. Biol. **26**, 399 (1970).

[56] A. M. Turing, The chemical basis of morphogenesis, Philos. T. Roy. Soc. B **237**, 37 (1952).

[57] P. K. Maini, K. J. Painter, and H. N. P. Chau, Spatial pattern formation in chemical and biological systems, J Chem. Soc. Faraday T. **93**, 3601 (1997).

[58] P. K. Maini, T. E. Woolley, R. E. Baker, E. A. Gaffney, and S. S. Lee, Turing's model for biological pattern formation and the robustness problem, Interface Focus **2**, 487 (2012).

[59] K. J. Painter, P. K. Maini, and H. G. Othmer, Stripe formation in juvenile Pomacanthus explained by a generalized Turing mechanism with chemotaxis, Proc. Natl. Acad. Sci. U.S.A. **96**, 5549 (1999).

[60] F. Brauns, H. Weyer, J. Halatek, J. Yoon, and E. Frey, Wavelength Selection by Interrupted Coarsening in Reaction-Diffusion Systems, Phys. Rev. Lett. **126**, 104101 (2021).

[61] J. Halatek and E. Frey, Rethinking pattern formation in reaction–diffusion systems, Nat. Phys. **14**, 507 (2018).

[62] F. Hinzpeter, F. Tostevin, and U. Gerland, Regulation of reaction fluxes via enzyme sequestration and co-clustering, J. R. Soc. Interface **16**, 20190444 (2019).

[63] J. Agudo-Canalejo, T. Adeleke-Larodo, P. Illien, and R. Golestanian, Enhanced Diffusion and Chemotaxis at the Nanoscale, Acc. Chem. Res. **51**, 2365 (2018).

[64] P. Strating, Brownian dynamics simulation of a hard-sphere suspension, Phys. Rev. E **59**, 2175 (1999).

METHODS

Linear stability analysis. We consider a system of M catalytically-active particles described by concentration fields $\rho_m(\boldsymbol{r}, t)$. A given species m converts its substrate, chemical (m) described by a concentration field $c^{(m)}(\boldsymbol{r}, t)$, into its product, which will in turn be the substrate $(m+1)$ of the catalytic species $m+1$. This conversion takes place at a rate $\alpha > 0$, which we take to be constant (i.e. catalysis is assumed to take place in the substrate-saturated regime), and equal for all species. The particles are also chemotactic for their substrate and their product, with respective mobilities $\mu^{(s)}$ and $\mu^{(p)}$, again chosen to be equal for all species. We start from the evolution equations for the substrate and product concentrations given in (1). We then consider the effects of a time- and space-dependent perturbation $(\delta\rho_m(\boldsymbol{r}, t), \delta c^{(m)}(\boldsymbol{r}, t))$ around an initially homogeneous state (ρ_0, c_0). We also assume a separation of timescales: as the substrates are typically much smaller than the catalytic particles and thus diffuse faster, we assume that their concentrations equilibrate more quickly to a quasi-steady state for a given configuration of the fields ρ_m, meaning that we set $\partial_t c^{(m)} \simeq 0$. Fourier-transforming the linearized equations with respect to space leads to the following equation for the $\delta c^{(m)}$ mode with wavevector $\boldsymbol{q}$:

$$Dq^2 \delta c^{(m)}(\boldsymbol{q}, t) = \alpha\left(\delta\rho_{m-1}(\boldsymbol{q}, t) - \delta\rho_m(\boldsymbol{q}, t)\right). \quad (11)$$

Reintroducing this perturbation into the linearized equation (1a), which we Laplace-transform with respect to time, leads to the system of equations for the different modes with growth rate λ and wavevector $\boldsymbol{q}$:

$$
\begin{aligned}
(\lambda + D_{\mathrm{p}}q^2)\delta\rho_m(\boldsymbol{q}, \lambda) = &-\frac{\alpha\rho_0}{D}\big[\mu^{(s)}\delta\rho_{m-1}(\boldsymbol{q}, \lambda) \\
&+ (\mu^{(p)} - \mu^{(s)})\delta\rho_m(\boldsymbol{q}, \lambda) - \mu^{(p)}\delta\rho_{m+1}(\boldsymbol{q}, \lambda)\big],
\end{aligned} \quad (12)
$$

which is an eigenvalue equation. It is readily seen that the fastest growing mode is the $\boldsymbol{q} = 0$ mode. Therefore, we focus on this mode throughout the paper. The system is unstable when $\mathrm{Re}(\lambda(\boldsymbol{q} = 0)) > 0$. Denoting the interaction matrix as Λ_{mn} (as defined in equation (3)), we obtain the result in equation (2).

Pair interactions between spherical catalytically-active particles. In order to perform Brownian dynamics simulations of the system, we calculate the effective interaction between two spherical catalytically-active particles in the far-field approximation, which we do in two steps.

We first consider an isolated particle of species m, with activity α and radius R, taken to be equal for all species. We place the particle at the origin, and use spherical coordinates. The perturbation $\delta c^{(n)}$ induced by the particle, which is assumed to equilibrate quickly with respect to the motion of all particles, is a solution of the Laplace equation:

$$0 = D\nabla^2 \delta c^{(n)}. \quad (13)$$

The corresponding boundary conditions, however, depend on whether the chemical is the substrate $(n = m)$, the product $(n = m+1)$, or neither. Indeed, the boundary condition is determined by the diffusive fluxes across the particle surface due to its chemical activity, resulting in

$$
-4\pi R^2 D \left.\frac{\partial \delta c^{(n)}}{\partial r}\right|_{r=R} = \begin{cases} -\alpha & \text{if } n = m, \\ \alpha & \text{if } n = m+1, \\ 0 & \text{otherwise.} \end{cases} \quad (14)
$$

The corresponding solutions for the perturbations are given as

$$
\delta c^{(n)}(r) = \begin{cases} -\frac{\alpha}{4\pi D}\frac{1}{r} & \text{if } n = m, \\ \frac{\alpha}{4\pi D}\frac{1}{r} & \text{if } n = m+1, \\ 0 & \text{otherwise.} \end{cases} \quad (15)
$$

Now consider a second particle of species n placed at a location $\boldsymbol{r}$. Its velocity $\boldsymbol{v}_{n,m}(\boldsymbol{r})$ in response to the perturbation created by the particle of species m will be

$$
\boldsymbol{v}_{n,m}(\boldsymbol{r}) = \begin{cases} -\mu^{(s)}\nabla\delta c^{(n)} & \text{if } n = m+1, \\ -\mu^{(p)}\nabla\delta c^{(n+1)} & \text{if } n = m-1, \\ -\mu^{(s)}\nabla\delta c^{(n)} - \mu^{(p)}\nabla\delta c^{(n+1)} & \text{if } n = m, \\ 0 & \text{otherwise.} \end{cases} \quad (16)
$$

Using equation (15), the responses can be explicitly written as

$$
\boldsymbol{v}_{n,m}(\boldsymbol{r}) = \begin{cases} \frac{\alpha\mu^{(s)}}{4\pi D}\frac{\boldsymbol{r}}{r^3} & \text{if } n = m+1, \\ -\frac{\alpha\mu^{(p)}}{4\pi D}\frac{\boldsymbol{r}}{r^3} & \text{if } n = m-1, \\ \frac{\alpha\left(\mu^{(p)} - \mu^{(s)}\right)}{4\pi D}\frac{\boldsymbol{r}}{r^3} & \text{if } n = m, \\ 0 & \text{otherwise,} \end{cases} \quad (17)
$$

which may be directly compared to the interaction matrix in equation (3) of the main text. Note that in general $\boldsymbol{v}_{n,m}(\boldsymbol{r}) \neq -\boldsymbol{v}_{m,n}(-\boldsymbol{r})$ when $n \neq m$, which again highlights the non-reciprocal nature of the interactions.

Brownian dynamics simulations. We perform Brownian dynamics simulations using a custom program written in the Julia language. We simulate N particles equally distributed among M species. Particles are started out randomly distributed in space, corresponding to a homogeneous state.

The equations of motion used in our simulations are

$$
\dot{\boldsymbol{r}}_i(t) = \sum_{\substack{j=1 \\ (j\neq i)}}^{N} \boldsymbol{v}_{S(i),S(j)}(\boldsymbol{r}_i - \boldsymbol{r}_j) + \sqrt{2D_{\mathrm{p}}}\,\boldsymbol{\xi}_i, \quad (18)
$$

Movie number	M	$\tilde{\mu}^{(\mathrm{s})}$	$\tilde{\mu}^{(\mathrm{p})}$	$d\tau$	τ_{tot}
1	5	-1.05	-1	0.001	2666
2	6	-0.5	1	0.0005	900
3	6	0.5	-1	0.0005	900
4	6	-0.5	-1	0.0005	900
5	6	-0.7	-0.8	0.001	8000
6	6	-0.95	-1	0.001	3200
7	5	0.5	-1	0.0005	900
8	5	-0.929	-1.07	0.001	2000
9	5	1.05	1	0.001	2666
10	5	-0.1	-0.2	0.001	6666

TABLE I. Simulation parameters for the movies referenced in the main text.

where $i \in \{1, 2, \ldots, N\}$. Here, $S(i)$ gives the species index corresponding to the particle index i, the velocities calculated using equation (17), D_{p} is the diffusion coefficient of the particles, and $\boldsymbol{\xi}_i$ corresponds to a Gaussian white noise with zero mean and unit variance acting on particle i.

The equations of motion are integrated using a forward Euler scheme. At every integration step, an overlap correction is then performed to account for hard-core repulsion between the spheres, using the "elastic collision method" [64]. We simulate the system in a three dimensional box of side length L with periodic boundary conditions, and interactions are treated according to the minimum image convention. Note that we do not use Ewald summation in our numerical simulations, which would be relevant if our goal was to simulate system sizes considerably larger than currently considered in our study.

The particle diameter, σ, which is taken to be the same for all species, sets the basic length scale of the simulation. We can define reference activity and mobility scales, respectively α_0 and μ_0, from which we build a velocity scale $V_0 = \alpha_0 \mu_0 / (4\pi D \sigma^2)$. From these scales, we can define dimensionless time $\tau = t V_0 / \sigma$, activity $\tilde{\alpha} = \alpha / \alpha_0$, and mobility $\tilde{\mu} = \mu / \mu_0$ scales. Finally, we define a reduced particle diffusion coefficient $\tilde{D}_{\mathrm{p}} = D_{\mathrm{p}} / (V_0 \sigma)$, which serves as an effective noise intensity or temperature.

Simulation parameters. All simulations have been performed with a box size L/σ chosen such that the total volume fraction of the particles is $\phi = 0.005$, as well as the choice of activity $\tilde{\alpha} = 1$, and noise strength

$\tilde{D}_{\mathrm{p}} = 0.02$. Simulations of respectively $M = 5$ ($M = 6$) species are performed with $N/M = 333$ ($N/M = 400$) particles per species. We use the following rule of thumb for parameter choices: the products in the form of $\tilde{\alpha}\tilde{\mu}$ are chosen to be of order unity, while the time step is chosen such that $d\tau \leq 0.001$. The total simulation times are usually of the order of $\tau_{\mathrm{tot}} \approx 10^2 - 10^3$. In the Supplementary Information, we describe each simulation movie. For the specific parameters used in each simulation, see table I.

Cluster growth law determination. In order to qualitatively determine the cluster growth law for both an even (see Fig. 3a of the main text and Movie 7) and an odd (see Fig. 3b of the main text and Movie 3) number of species, we use a simple clustering algorithm implemented in the Julia programming language: starting from each individual particle regarded as a cluster of size 1, we assign two particles to be in the same cluster if their distance is below a threshold, which we choose to be 1.1 times the particle diameter σ. In order to speed up the calculations, we additionally use a link-list algorithm with a cell size 1.1σ, which only requires calculation of the distance of each particle to the particles in its vicinity. We run 100 simulations using the parameters given in the previous subsection for Movies 3 and 7, with a longer total time $\tilde{t}_{\mathrm{total}} = 400$. We then perform an ensemble average on these data to obtain the growth laws shown in Fig. 1e.

DATA AVAILABILITY

The data supporting the main findings of this study are available in the paper and its Supplementary Information. Any additional data can be made available upon request.

CODE AVAILABILITY

The algorithms for the codes supporting the main findings of this study are available in the paper and its Supplementary Information. Any additional information concerning the code can be made available upon request.

EXTENDED DATA
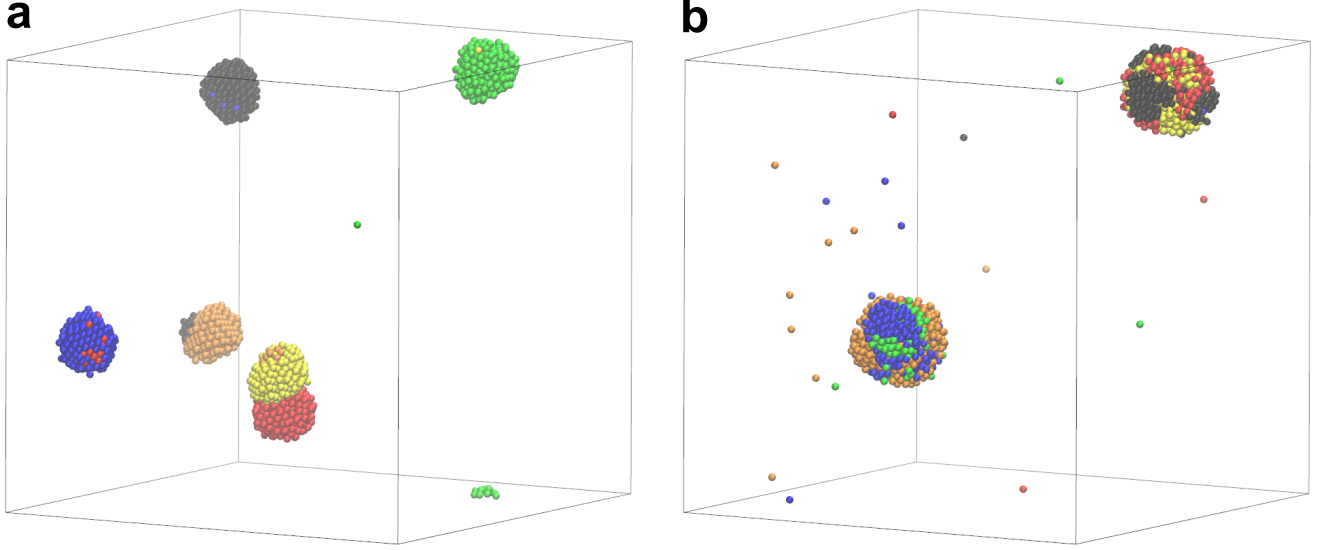
FIG. E1. **Chasing regime for** $M = 6$ **particle species. (a)**: Weak chasing, strong self-attraction regime (Movie 4). Species aggregate in mixed clusters without oscillations. Each cluster is composed of a majority species and a minority species that chases the majority one. Because of their mixed composition, the clusters chase each other over long timescales. Transient aggregation of the clusters is observed. **(b)**: Strong chasing, weak self-attraction regime (Movie 6). After transient oscillations, two clusters form, one containing a mixture of all even species, the other of all odd species.
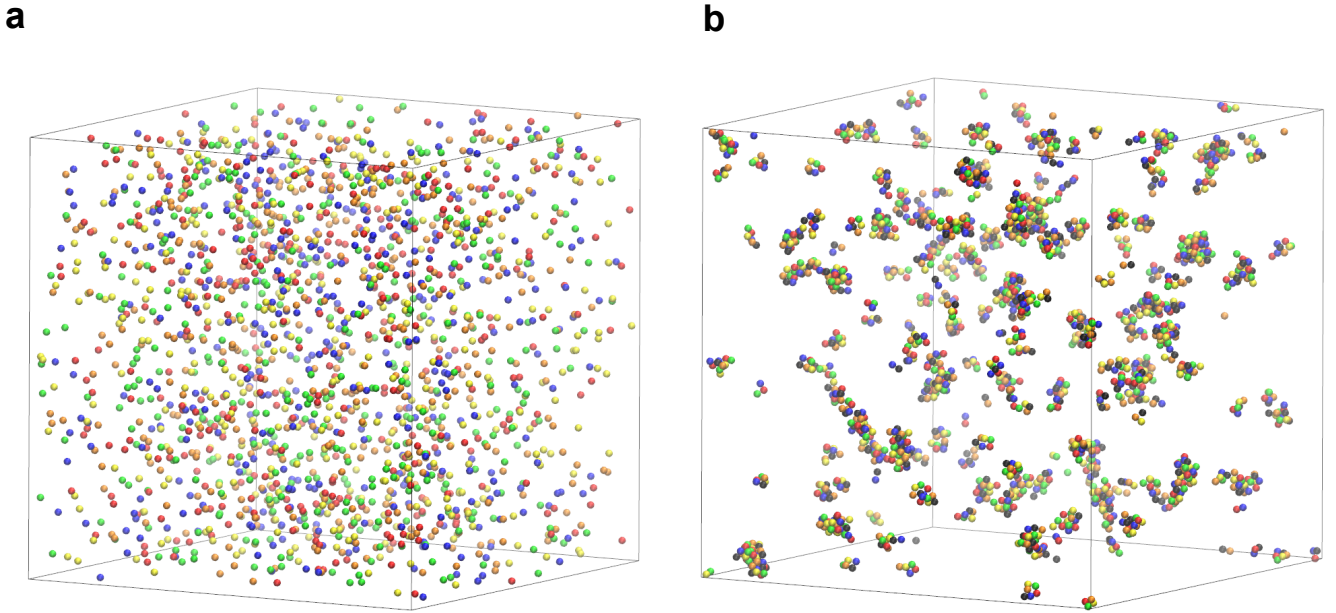
FIG. E2. **Different types of homogeneous steady states. (a)**: Self-repelling, cross-chasing regime (Movie 1). Particles form short-lived, self-propelled molecules, which swap particles with each other. **(b)**: Self-repelling, cross-attracting regime (Movie 2). Particles form larger, long-lived, rotating molecules. If $\mu^{(s)} = -\mu^{(p)}$, rotation is suppressed.
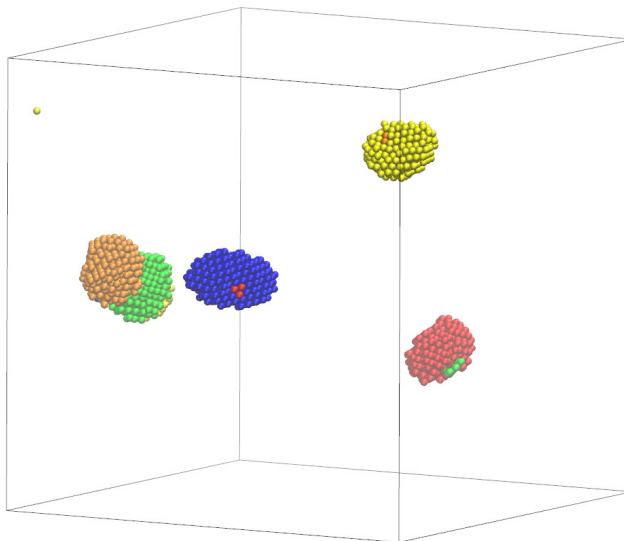
FIG. E3. **Non-oscillatory steady state for** $M = 5$ **particle species.** Species aggregate into mixed clusters, which then chase each other (Movie 10).

Self-organization of primitive metabolic cycles due to non-reciprocal interactions
Supplementary Information

Vincent Ouazan-Reboul,[1] Jaime Agudo-Canalejo,[1] and Ramin Golestanian[1, 2]

[1]*Max Planck Institute for Dynamics and Self-Organization, Am Fassberg 17, D-37077, Göttingen, Germany*

[2]*Rudolf Peierls Centre for Theoretical Physics, University of Oxford, OX1 3PU, Oxford, UK*

CONTENTS

I. EIGENVALUE SPECTRA

In Fig. S1, we plot in the complex plane the spectrum of the stability matrix (equation (3) of the main text) for different numbers of species M, which corresponds to the M eigenvalues given in equation (4) of the main text. These spectra illustrate the key difference between even and odd species numbers, as highlighted in the main text: for cycles involving an even number of species, the fastest growing mode is associated to a real eigenvalue, while for cycles involving an odd number of species, the fastest growing mode is associated to a complex conjugate pair of eigenvalues. In the latter case, the ratio between the magnitudes of the real and imaginary parts (see the full expression given in equation (8) of the main text) determines whether the system exhibits long-lived oscillations.
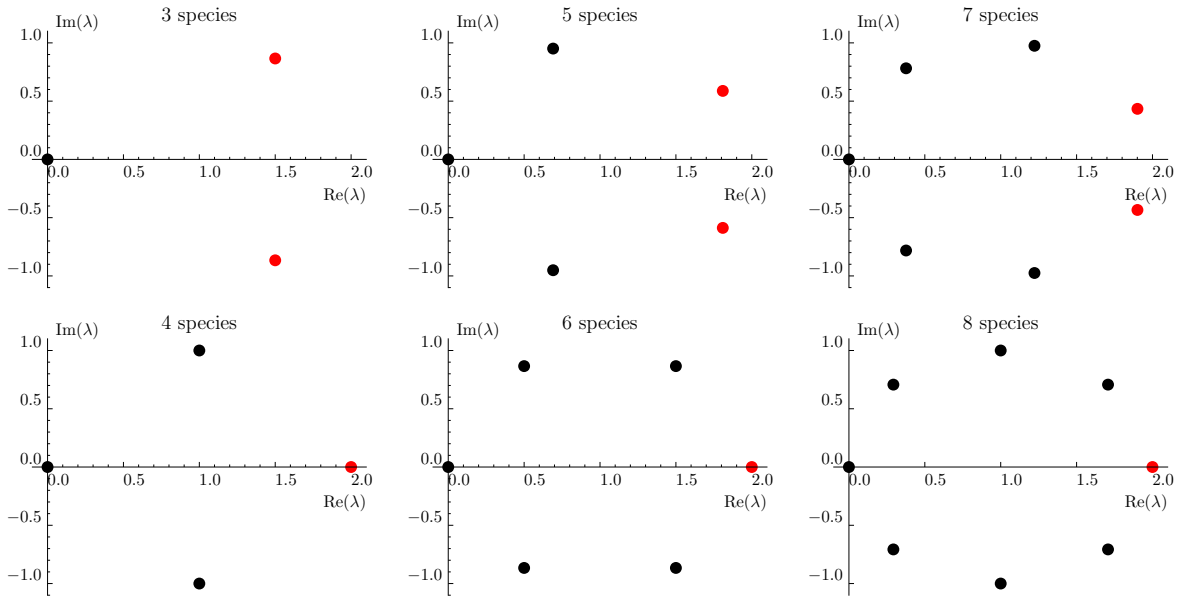

FIG. S1. Eigenvalue spectra for $M = 3$ to 8 species, in units of $-(\mu^{(\mathrm{p})} - \mu^{(\mathrm{s})})\alpha\rho_0/D$ for the real part and $-(\mu^{(\mathrm{s})} + \mu^{(\mathrm{p})})\alpha\rho_0/D$ for the imaginary part. The eigenvalue (for an even number of species) or pair of eigenvalues (for an odd number) with the largest real part is coloured in red.
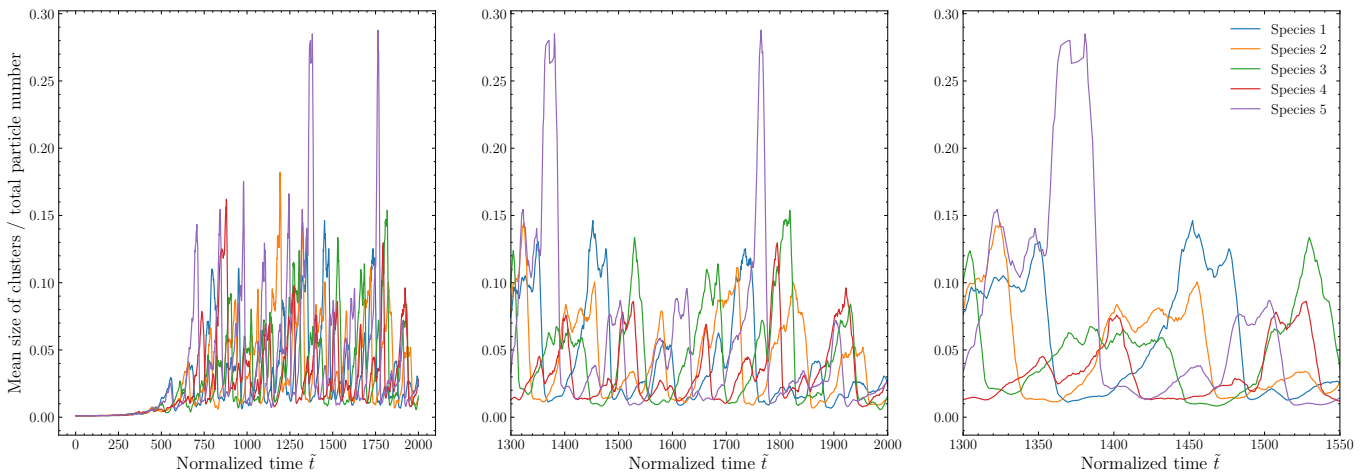
FIG. S2. Oscillation dynamics for $M = 5$ species (see Fig. 4 of the main text and Movie 8). Left: full time span of the simulation. Centre: five oscillation cycles. Right: two oscillation cycles.

II.   OSCILLATORY DYNAMICS FOR AN ODD NUMBER OF CHASING SPECIES

Using the clustering scheme described in Methods, we quantify the oscillation dynamics shown in Fig. 4 of the main text and Movie 8. For each species, we plot in Fig. S2 the normalized mean size of the clusters containing at least one particle of that species, excluding individual particles (i.e. clusters of size 1). A uniform moving average is applied over a 10-point window in order to smooth out high-frequency variations.

In accordance with Fig. 4 of the main text and Movie 8, we observe successive formation and dissolution of large clusters containing a given species, in the order $\cdots \to 5 \to 4 \to 3 \to 2 \to 1 \to 5 \to \ldots$. These formation and explosion events are regularly spaced in time, and can be interpreted as constituting an oscillatory steady state. At their largest, the clusters span 20 to 30 % of the total particle population, reflecting the fact that two clusters of species of the same parity might be in contact right before an explosion event, as shown in Fig. 4 of the main text.

III.   DESCRIPTION OF THE MOVIES

- **Movie 1** Linearly stable mixture of self-repelling species in the chasing regime, resulting in the formation of transient self-propelled colloidal molecules. See Extended Data Fig. 2a.

- **Movie 2** Linearly stable mixture of self-repelling, cross-attracting particle species, which form long-lived rotating molecules. See Extended Data Fig. 2b.

- **Movie 3** Unstable mixture of an even number of self-attracting, cross-repelling particle species undergoing parity-based aggregation. See Fig. 3a of the main text.

- **Movie 4** Linearly unstable mixture of an even number of self-attracting, cross-chasing species for which the magnitude of the chasing interaction is comparable to the self-attraction. The mixture self-organizes into hybrid clusters composed of a majority and a minority species which chase each other. See Extended Data Fig. 1a.

- **Movie 5** Same as Movie 4, but with the magnitude of the chasing interaction being larger than the self-attraction. Two hybrid clusters, each containing all the species of a same parity, form and separate.

- **Movie 6** Same as Movie 4, but with self-attraction negligible compared to chasing interactions. The system behaves similarly to Movie 5, with transient oscillations observed as the clusters form. See Extended Data Fig. 1b.

- **Movie 7** Linearly unstable mixture of an odd number of self-attracting, cross-repelling species. The particles separate into single-species clusters, in order to minimize overall repulsion. See Fig. 3b of the main text.

- **Movie 8** Linearly unstable mixture of an odd number of self-attracting, cross-chasing species, with a magnitude of the self-attraction smaller, but on the same order as the chasing interaction. The system exhibits long-lived

oscillations in which species successively form clusters which then get dissolved and replaced by a chasing species. See Fig. 4 of the main text.

- **Movie 9** Same as Movie 8, but with the self-attraction magnitude taken much lower than the chasing interaction. The system behaves similarly to Movie 8, with the clusters being replaced by regions of transiently increased concentration.

- **Movie 10** Same as Movie 8, but in a parameter regime for which the instability growth rate is larger than its oscillation frequency. The particles phase-separate into hybrid clusters of two species without exhibiting oscillations. See Extended Data Fig. 3.

4

Network effects lead to self-organization in metabolic cycles of self-repelling catalysts

This chapter is reproduced from the preprint Ouazan-Reboul et al, ArXiv:2303.09832 (2023)[183], currently under review at Physical Review Letters. I took part in the design of the research, performed the analytical calculations, designed the numerical simulation code, analyzed and interpreted the numerical data, and participated in the redaction of the paper.

The movies described in the main text and the supplementary information are available at the arxiv repository.

Network effects lead to self-organization in metabolic cycles of self-repelling catalysts

Vincent Ouazan-Reboul,[1] Ramin Golestanian,[1, 2, *] and Jaime Agudo-Canalejo[1, †]

[1] *Max Planck Institute for Dynamics and Self-Organization, Am Fassberg 17, D-37077, Göttingen, Germany*
[2] *Rudolf Peierls Centre for Theoretical Physics, University of Oxford, OX1 3PU, Oxford, UK*

Mixtures of particles that interact through phoretic effects are known to aggregate if they belong to species that exhibit attractive self-interactions. We study self-organization in a model metabolic cycle composed of three species of catalytically-active particles that are chemotactic towards the chemicals that define their connectivity network. We find that the self-organization can be controlled by the network properties, as exemplified by a case where a collapse instability is achieved by design for self-repelling species. Our findings highlight a possibility for controlling the intricate functions of metabolic networks by taking advantage of the physics of phoretic active matter.

Introduction.— Catalyzed chemical reactions are intrinsically and locally out of equilibrium, making catalytic particles a paradigmatic example of systems in which the physics of active matter comes into play [1]. In particular, catalytic activity coupled to a chemotactic, gradient-response mechanism such as diffusiophoresis [2, 3] enables the self-propulsion of individual colloidal particles *via* self-phoresis [4, 5], as well as collective behaviour mediated by effective interactions between active colloids [6–10]. In addition, catalytic activity is essential to the function of biological systems, allowing for the occurrence, as a part of metabolism, of reactions that would otherwise be kinetically inhibited [11]. Metabolic processes often require enzymatic catalysis to occur in a space- and time-localized manner, necessitating some degree of self-organization of the participating enzymes [12–19]. In particular, many enzymes have been shown to spontaneously form transient aggregates, known as metabolons [20].

Simple cases of spontaneous self-organization in mixtures of several catalytic components have been previously studied both in theory [21–26] and in experiment [27–31]. However, the influence of the sometimes complex topology of reaction networks on the self-organization of the metabolic components has not yet been elucidated. Indeed, many catalytic processes of biological and industrial significance—from cellular metabolism [32] to carbon fixation [33]—involve a closed chain of catalytic reactions, where the product of one catalyst is passed on as the substrate of the next one, i.e. a metabolic cycle. Because the spatial arrangement of catalysts may strongly affect the overall rate of the reactions [17, 18, 26], it is important to understand under which conditions such spatial reorganization may happen spontaneously, and whether it can be triggered in generically stable systems via network-mediated effects. In this Letter, we study the chemotactic self-organization of three species of catalytically active particles that participate in a model catalytic cycle. We find that a mixture of only self-repelling catalytic species can undergo self-organization via network effects emerging from the metabolic cycle topology.

Model.—We consider catalytically-active particles which produce and consume a set of chemicals, with activities $\alpha_m^{(k)}$ corresponding to the rate of production (if positive) or consumption (if negative) of chemical k by active species m. These particles are also chemotactic: synthetic colloids typically move *via* hydrodynamic-phoretic mechanisms [1, 27, 28, 31]; whereas the mechanism underlying the observed chemotaxis of biological enzymes is still debated [34–42]. In a concentration gradient of chemical k, species m develops a velocity $\mathbf{v}_m^{(k)} = -\mu_m^{(k)}\boldsymbol{\nabla}c^{(k)}$, where $\mu_m^{(k)}$ is a mobility coefficient. The combination of catalytic and chemotactic activities results in effective interactions between the active species going as $\mathbf{v}_{m,n} \propto \sum_k \alpha_n^{(k)}\mu_m^{(k)}$, where $\mathbf{v}_{m,n}$ represents the velocity of m in response to the presence of n; see Fig. 1(a). Importantly, these interactions are nonrecip-
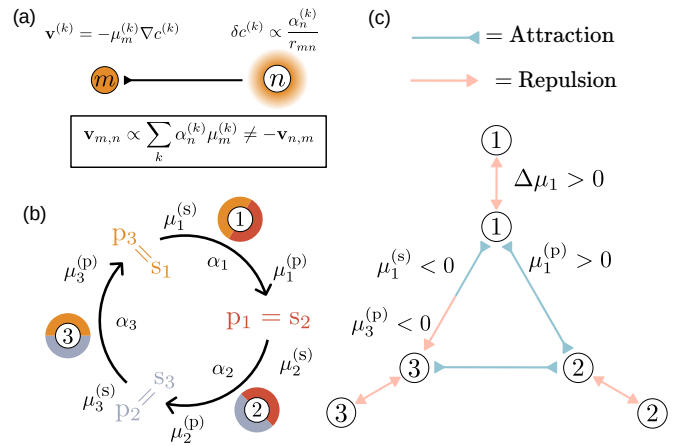
FIG. 1. (a) Emergence of field-mediated, nonreciprocal interactions between particle n, which perturbs the chemical field $c^{(k)}$ around itself, and particle m, which develops a velocity in response to the resulting chemical gradient. (b) Metabolic cycle of three species. Each converts their substrate into a product which acts as the substrate of the next species, and moves in response to gradients of both chemicals. (c) Example of a set of species-species interactions emerging from the combination of effective field-mediated interactions and metabolic cycle topology. With this particular choice of parameters, each species is self-repelling, and the species pair 1-3 exhibits chasing interactions.

rocal, in the sense that we generically have $\mathbf{v}_{m,n} \neq -\mathbf{v}_{m,n}$ [21].

We use a continuum model for the concentration ρ_m of the active species m and the chemical concentration $c^{(k)}$, which reads

$$\partial_t \rho_m(\mathbf{r}, t) = \boldsymbol{\nabla} \cdot \left[D_{\mathrm{p}} \boldsymbol{\nabla} \rho_m + \sum_k \mu_m^{(k)} (\boldsymbol{\nabla} c^{(k)}) \rho_m \right], \quad (1\mathrm{a})$$

$$\partial_t c^{(k)}(\mathbf{r}, t) = D^{(k)} \boldsymbol{\nabla}^2 c^{(k)} + \sum_m \alpha_m^{(k)} \rho_m. \quad (1\mathrm{b})$$

Here, Eq. (1a) is a continuity equation with D_{p} being the diffusion coefficient of the colloidal particles, which we assumed to be equal for all active particles for simplicity, and the drift velocity following the concentration gradients of all chemicals. Moreover, Eq. (1b) is a reaction-diffusion equation for the chemicals, with $D^{(k)}$ representing the diffusion coefficient of chemical (k), and the reaction term accounting for the local activity of all catalytic species.

To determine when such a mixture undergoes an instability, we perform a linear stability analysis of these equations [43]. We find that a perturbation $(\delta\rho_m, \delta c^{(k)})$ around an initially homogeneous state $(\rho_{0m}, c_h^{(k)})$ follows the general eigenvalue equation $-\sum_{n=1}^M \Lambda_{m,n} \delta\rho_n = \left[\lambda + D_{\mathrm{p}} q^2\right] \delta\rho_m$ where $\Lambda_{m,n} = \sum_k \frac{\alpha_n^{(k)} \mu_m^{(k)}}{D^{(k)}} \rho_{0m}$ represents the response of species m to species n, mediated by all

chemical fields, and $\lambda(q)$ is the growth rate of a perturbation with wave number q. The coefficient $\Lambda_{m,n}$ is negative (positive) if species m is attracted to (repelled by) species n. Throughout the rest of this Letter, we rescale the mobility coefficients for brevity, such that $\mu_m^{(k)}/D^{(k)} \to \mu_m^{(k)}$. The system undergoes an instability if any mode has a positive growth rate $\lambda > 0$. We focus on the eigenvalue with the highest growth rate associated with the $q^2 = 0$ mode, corresponding to the longest wavelength, which represents a macroscopic instability.

Metabolic cycles.—We focus on the particular case of metabolic cycles composed of 3 active species (Fig. 1(b)), where species m converts its substrate s_m into its product $\mathrm{p}_m = \mathrm{s}_{m+1}$, with an activity $\alpha_m = \alpha_m^{(m+1)} = -\alpha_m^{(m)} > 0$, as depicted in Fig. 1(b). As the cycle is closed, the species indices are periodic, with species 4 being identical to species 1, and species 0 to species 3.

The species have a chemotactic response to both their substrate and product, with respective mobilities $\mu_m^{(\mathrm{s})} \equiv \mu_m^{(m)}$ and $\mu_m^{(\mathrm{p})} \equiv \mu_m^{(m+1)}$. The resulting interaction matrix has the following (non-vanishing) coefficients (Fig. 1(c)): $\Lambda_{m,m-1} = \alpha_{m-1} \mu_m^{(\mathrm{s})} \rho_{0m}$, $\Lambda_{m,m} = \alpha_m \Delta\mu_m \rho_{0m}$, and $\Lambda_{m,m+1} = -\alpha_{m+1} \mu_m^{(\mathrm{p})} \rho_{0m}$, where $\Delta\mu_m \equiv \mu_m^{(\mathrm{p})} - \mu_m^{(\mathrm{s})}$, and is in general asymmetric, reflecting the non-reciprocal nature of the interactions between the catalytic species.

We now calculate the eigenvalues $\lambda(q=0)$ for $\Lambda_{m,n}$ as defined above, and find two eigenvalues given by [43]

$$\lambda_\pm = -\frac{1}{2} \sum_{m=1}^3 \alpha_m \Delta\mu_m \rho_{0m} \pm \frac{1}{2} \sqrt{\left(\sum_{m=1}^3 \alpha_m \Delta\mu_m \rho_{0m} \right)^2 - 4 \sum_{m=1}^3 \alpha_m \alpha_{m+1} \left(\Delta\mu_m \Delta\mu_{m+1} + \mu_m^{(\mathrm{p})} \mu_{m+1}^{(\mathrm{s})} \right) \rho_{0m} \rho_{0m+1}}, \quad (2)$$

as well as one null eigenvalue $\lambda_0 = 0$. The system will be linearly unstable when (the real part of) the largest eigenvalue λ_+ becomes positive.

Substrate-sensitive species.—A simple class of cycles whose parameter space can be explored in full generality involves those in which the catalytic particles are only chemotactic towards their substrate, i.e. $\mu_m^{(\mathrm{p})} = 0$. We thus have three activities α_m and three substrate mobilities $\mu_m^{(\mathrm{s})}$, with the mobility difference reducing to $\Delta\mu_m = -\mu_m^{(\mathrm{s})}$. Species in such a cycle then only interact with the previous species in the cycle and with themselves, with $\Lambda_{m,m-1} = \alpha_{m-1} \mu_m^{(\mathrm{s})} \rho_{0m}$, $\Lambda_{m,m} = -\alpha_m \mu_m^{(\mathrm{s})} \rho_{0m}$, and $\Lambda_{m,m+1} = 0$. Note that the self-interaction always has the opposite sign to the interaction with the previous species in the cycle, which further limits the possible interaction patterns the catalytic species can exhibit.

In the context of this reduced parameter space, and assuming species 1 is self-repelling (i.e. $\alpha_1 \Delta\mu_1 > 0$), one can solve $\mathrm{Re}(\lambda_+) > 0$ for all parameter values, yield-

ing a comprehensive two-dimensional stability phase diagram as shown in Fig. 2 [43], which depends only the normalized self-interactions $\frac{\alpha_2 \Delta\mu_2 \rho_{02}}{\alpha_1 \Delta\mu_1 \rho_{01}}$ and $\frac{\alpha_3 \Delta\mu_3 \rho_{03}}{\alpha_1 \Delta\mu_1 \rho_{01}}$. The corresponding parameter-free instability line is plotted as a dashed line on Fig. 2, with the dark orange and light orange regions below that line corresponding to unstable metabolic cycles. As the instability line is above the light orange region corresponding to overall self-attracting mixtures in Fig. 2 ($\sum_{m=1}^3 \Lambda_{m,m} < 0$), we uncover that it not necessary for the metabolic cycle to be composed of overall self-attracting species in order to self-organize, as opposed to mixtures involving simpler interaction schemes [22, 25, 44]. This result does not, however, extend to cycles composed only of self-repelling species ($\Lambda_{m,m} > 0$ for all m), which are always stable, as shown by the fact that the corresponding top right quadrant in Fig. 2 is always above the dashed stability line. This implies that some amount of self-attraction is still necessary for the catalytic particles to self-organize
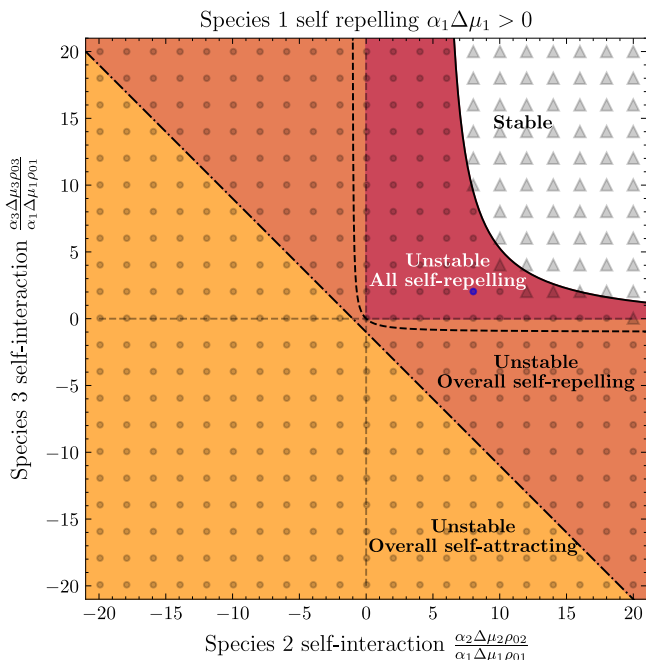
FIG. 2. Stability phase diagram for cycles involving at least one self-repelling species. Species 1 taken to be self-repelling ($\alpha_1\Delta\mu_1 > 0$). Full line: Stability line in normalized self-interaction plane for a specific choice of parameters. Dashed line: Parameter-free instability line below which cycles with null product mobilities $\mu^{(p)}_{1,2,3} = 0$ are unstable. Note that this line always below the the top-right, all-self-repelling quadrant. Dash-dotted line: boundary between an overall self-attracting and self-repelling catalytic mixtures. Gray markers: coordinates of Brownian dynamics simulations, found to be unstable if the marker is a circle or stable if it is a triangle. The blue marker corresponds to the coordinates of the simulation shown in Fig. 3. For the expressions of the stability lines and the values of the parameters, see the Supplemental Material [43].

in this limited interaction topology.

Self-organization of purely self-repelling species—We now consider the general case with both nonzero substrate and product mobilities, for which each species interacts with both the previous and the next species in the cycle according to a pattern set by its substrate mobility $\mu^{(s)}$, its product mobility $\mu^{(p)}$, and their difference $\Delta\mu$. By solving for $\mathrm{Re}(\lambda_+) > 0$ in Eq. (2), we find that a cycle which is overall self-repelling can be made unstable provided the following condition is satisfied

$$\sum_{m=1}^{3} \alpha_m \Delta\mu_m \rho_{0m} \cdot \alpha_{m+1}\Delta\mu_{m+1}\rho_{0m+1}$$
$$< -\sum_{m=1}^{3} \alpha_m \mu^{(s)}_{m+1}\rho_{0m+1} \cdot \alpha_{m+1}\mu^{(p)}_m\rho_{0m}. \tag{3}$$

The condition (Eq. (3)), which involves terms mixing pairs of catalytic species, can be rewritten as

$\sum \Lambda_{m,m}\Lambda_{m+1,m+1} < \sum \Lambda_{m,m+1}\Lambda_{m+1,m}$, and thus sets a bound on the self-interactions of pairs of species relative to their cross-interactions. This inequality implies that, in the case of an overall self-repelling cycle where $\sum_{m=1}^{3} \Lambda_{m,m} > 0$, the presence of species pairs which interact reciprocally offer an alternate route to instability.

We find that a striking new feature of this general case is that cycles composed only of self-repelling species can be unstable according to the condition given in Eq. (3) if any self-repelling species m verifies one of the following inequalities [43]:

$$\alpha_{m+1}\mu^{(p)}_{m+1}\rho_{0m+1} > \alpha_m\Delta\mu_m\rho_{0m}, \tag{4a}$$

$$\mu^{(s)}_m > 0, \tag{4b}$$

$$\frac{1}{\alpha_m\mu^{(s)}_m\rho_{0m}}\Big[\alpha_{m-1}\mu^{(p)}_{m-1}\rho_{0m-1}\alpha_m\mu^{(s)}_m\rho_{0m}$$
$$+ \alpha_{m+1}\mu^{(p)}_{m+1}\rho_{0m+1}\Big(\alpha_m\mu^{(p)}_m\rho_{0m}$$
$$+ \alpha_{m-1}\mu^{(p)}_{m-1}\rho_{0m-1}\Big)\Big] > 0. \tag{4c}$$

This behavior is illustrated, for a particular set of parameters for which species 1 obeys inequalities Eqs. (4a) and (4c), by the stability phase diagram shown in Fig. 2. For this choice of parameters, the stability line is contained in the top-right quadrant, which corresponds to a mixture of three self-repelling species. Thus, in some regions of the parameter space (Fig. 2, dark red), the destabilizing pair interactions are able to overcome self-repulsion, and lead to the formation of a cluster of three species in the absence of self-attraction. We recall that cycles of strictly substrate-sensitive species, which are stable above the dashed line drawn in Fig. 2, exhibit no such region independently of the choice of parameters. An increased complexity of interactions is therefore needed in order to overcome self-repulsion. We have confirmed this analytical prediction using Brownian dynamics simulations (Fig. 2, grey circles and triangles). By scanning the coordinates of Fig. 2 for a set of parameters given in [43], we broadly recover the predicted instability line.

The results of a simulation of an unstable cycle of three self-repelling species, with parameters corresponding to the blue point in Fig. 2 and the interactions shown in Fig. 1(c), are shown in Fig. 3 (see [43] for simulation parameters). In panels (a1) to (a3), we find that each catalytic species taken on its own does not cluster, because of being self-repelling. Panels (b1) and (b3) demonstrate that mixtures of particles belonging to species pairs (1,2) and (3,1), when considered together, are also stable, and lead to the formation of small dynamic molecules. However, as shown in panel (b2), mixtures of particles of species 2 and 3 are unstable, and lead to the formation of a mixed clusters coexisting with a dilute phase. A favourable choice of parameters allows species 2 and 3 to
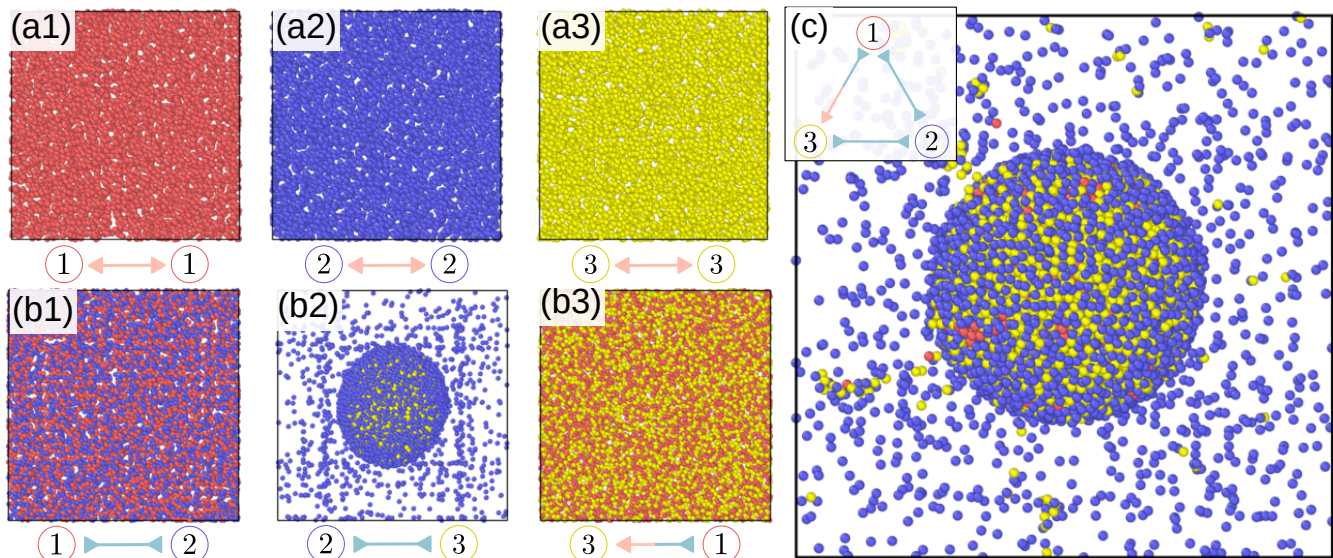
FIG. 3. Instability of a generic three-enzyme cycle triggered by the presence of a single instability-favouring pair. (a1–a3) All particle species are self-repelling, and thus single-species suspensions stay homogeneous. (b1–b3) Of the two-species mixtures, 1-2 and 3-1 mixtures form small molecules but remain homogeneous, while 2-3 is unstable and results in the formation of a 2-3 cluster coexisting with a gas of species 2. (c) Despite all species being self-repelling, the instability of the 2-3 pair causes the instability of the full three-species mixture resulting in the formation of a cluster, which coexists with a gas of species 2. Note that species 1 (red) also participates in the cluster, despite not aggregating with either of the other species (b1, b3). See also Movies 1–7 and the Supplemental Material [43] for a description of the simulation parameters and movies.

destabilize the whole ternary (1,2,3) mixture of catalysts, despite the stabilizing effects of the individual species and the rest of the species pairs. The resulting structure is a cluster mixing all three species coexisting with a dilute phase.

Discussion.—Using a simple model, we have shown that three catalytically active species involved in a model metabolic cycle are able to undergo a self-organizing instability through chemical field-mediated effective interactions. In the case of a cycle involving species which are only chemotactic towards their substrates, we find that while self-organization is possible if the mixture of catalytic species is overall self-repelling, at least one of the species must be self-attracting for the instability to occur. However, in contrast to this case and to what was previously known for phoretic particles [22, 25, 44], we find that the system can self-organize even when all species are self-repulsive through instability-favouring pair interactions, in the general case of species chemotactic to both their substrates and products.

We found here that the topology of interactions between catalytically active particles can lead to entirely new forms of collective behaviour, namely self-organization of self-repelling particles. While we considered minimal catalytic cycles with only three species, our work also shows that the number of species in the cycle can have a strong effect on the resulting dynamics, with cycles of even and odd number of species displaying entirely different behaviour [44]. Future work may con-

sider more complex and biologically relevant topologies of the catalytic network (e.g. branched), as well as the effect of self-organization on the metabolic properties of the system [15, 17–19]. Furthermore, our work may find application in engineering synthetic functional structures with shape-shifting capacity at the molecular scale [45].

* ramin.golestanian@ds.mpg.de
† jaime.agudo@ds.mpg.de

[1] R. Golestanian, Phoretic Active Matter, in *Active Matter and Nonequilibrium Statistical Physics: Lecture Notes of the Les Houches Summer School: Volume 112, September 2018* (Oxford University Press, 2022).

[2] J. Anderson, Colloid Transport by Interfacial Forces, Annu. Rev. Fluid Mech. **21**, 61 (1989).

[3] F. Jülicher and J. Prost, Generic theory of colloidal transport, Eur. Phys. J. E **29**, 27 (2009).

[4] W. F. Paxton, K. C. Kistler, C. C. Olmeda, A. Sen, S. K. St. Angelo, Y. Cao, T. E. Mallouk, P. E. Lammert, and V. H. Crespi, Catalytic nanomotors: autonomous movement of striped nanorods, J. Am. Chem. Soc. **126**, 13424 (2004).

[5] R. Golestanian, T. B. Liverpool, and A. Ajdari, Designing phoretic micro- and nano-swimmers, New J. Phys. **9**,

126 (2007).

[6] I. Theurkauff, C. Cottin-Bizonne, J. Palacci, C. Ybert, and L. Bocquet, Dynamic clustering in active colloidal suspensions with chemical signaling, Phys. Rev. Lett. **108**, 268303 (2012).

[7] I. Buttinoni, J. Bialké, F. Kümmel, H. Löwen, C. Bechinger, and T. Speck, Dynamical clustering and phase separation in suspensions of self-propelled colloidal particles, Phys. Rev. Lett. **110**, 238301 (2013).

[8] S. Saha, R. Golestanian, and S. Ramaswamy, Clusters, asters, and collective oscillations in chemotactic colloids, Phys. Rev. E **89**, 062316 (2014).

[9] O. Pohl and H. Stark, Dynamic clustering and chemotactic collapse of self-phoretic active particles, Phys. Rev. Lett. **112**, 238303 (2014).

[10] B. Liebchen, D. Marenduzzo, and M. E. Cates, Phoretic interactions generically induce dynamic clusters and wave patterns in active colloids, Phys. Rev. Lett. **118**, 268001 (2017).

[11] R. Phillips, J. Kondev, J. Theriot, H. G. Garcia, and N. Orme, *Physical Biology of the Cell*, 2nd ed. (Garland Science, New York, 2012).

[12] C. A. Kerfeld, C. Aussignargues, J. Zarzycki, F. Cai, and M. Sutter, Bacterial microcompartments, Nat. Rev. Microbiol. **16**, 277 (2018).

[13] J.-L. Liu, The cytoophidium and its kind: filamentation and compartmentation of metabolic enzymes, Annu. Rev. Cell Dev. Biol. **32**, 349 (2016).

[14] T. Selwood and E. K. Jaffe, Dynamic dissociating homo-oligomers and the control of protein function, Arch. Biochem. Biophys. **519**, 131 (2012).

[15] J. E. Dueber, G. C. Wu, G. R. Malmirchegini, T. S. Moon, C. J. Petzold, A. V. Ullal, K. L. Prather, and J. D. Keasling, Synthetic protein scaffolds provide modular control over metabolic flux, Nat. Biotechnol. **27**, 753 (2009).

[16] S. Kufer, E. Puchner, H. Gumpp, T. Liedl, and H. Gaub, Single-molecule cut-and-paste surface assembly, Science **319**, 594 (2008).

[17] F. Hinzpeter, F. Tostevin, and U. Gerland, Regulation of reaction fluxes via enzyme sequestration and co-clustering, J. R. Soc. Interface **16**, 20190444 (2019).

[18] F. Hinzpeter, F. Tostevin, A. Buchner, and U. Gerland, Trade-offs and design principles in the spatial organization of catalytic particles, Nat. Phys. **18**, 203 (2022).

[19] Y. Xiong, S. Tsitkov, H. Hess, O. Gang, and Y. Zhang, Microscale colocalization of cascade enzymes yields activity enhancement, ACS Nano **16**, 10383 (2022).

[20] L. J. Sweetlove and A. R. Fernie, The role of dynamic enzyme assemblies and substrate channelling in metabolic regulation, Nat. Commun. **9**, 2136 (2018).

[21] R. Soto and R. Golestanian, Self-assembly of catalytically active colloidal molecules: tailoring activity through surface chemistry, Phys. Rev. Lett. **112**, 068301 (2014).

[22] J. Agudo-Canalejo and R. Golestanian, Active Phase Separation in Mixtures of Chemically Interacting Particles, Phys. Rev. Lett. **123**, 018101 (2019).

[23] J. Grauer, H. Löwen, A. Be'er, and B. Liebchen, Swarm hunting and cluster ejections in chemically communicating active mixtures, Sci. Rep. **10**, 5594 (2020).

[24] G. Giunta, H. Seyed-Allaei, and U. Gerland, Cross-diffusion induced patterns for a single-step enzymatic reaction, Commun. Phys. **3**, 167 (2020).

[25] V. Ouazan-Reboul, J. Agudo-Canalejo, and R. Golesta-nian, Non-equilibrium phase separation in mixtures of catalytically active particles: Size dispersity and screening effects, Eur. Phys. J. E **44**, 113 (2021).

[26] M. W. Cotton, R. Golestanian, and J. Agudo-Canalejo, Catalysis-induced phase separation and autoregulation of enzymatic activity, Phys. Rev. Lett. **129**, 158101 (2022).

[27] T. Yu, P. Chuphal, S. Thakur, S. Y. Reigh, D. P. Singh, and P. Fischer, Chemical micromotors self-assemble and self-propel by spontaneous symmetry breaking, Chem. Commun. **54**, 11933 (2018).

[28] F. Schmidt, B. Liebchen, H. Löwen, and G. Volpe, Light-controlled assembly of active colloidal molecules, J. Chem. Phys. **150**, 094905 (2019).

[29] C. H. Meredith, P. G. Moerman, J. Groenewold, Y.-J. Chiu, W. K. Kegel, A. van Blaaderen, and L. D. Zarzar, Predator–prey interactions between droplets driven by non-reciprocal oil exchange, Nat. Chem. **12**, 1136 (2020).

[30] A. Testa, M. Dindo, A. A. Rebane, B. Nasouri, R. W. Style, R. Golestanian, E. R. Dufresne, and P. Laurino, Sustained enzymatic activity and flow in crowded protein droplets, Nat. Commun. **12**, 6293 (2021).

[31] J. Grauer, F. Schmidt, J. Pineda, B. Midtvedt, H. Löwen, G. Volpe, and B. Liebchen, Active droploids, Nat. Commun. **12**, 6005 (2021).

[32] F. Wu, L. N. Pelster, and S. D. Minteer, Krebs cycle metabolon formation: metabolite concentration gradient enhanced compartmentation of sequential enzymes, Chem. Comm. **51**, 1244 (2015).

[33] T. Schwander, L. Schada von Borzyskowski, S. Burgener, N. S. Cortina, and T. J. Erb, A synthetic pathway for the fixation of carbon dioxide in vitro, Science **354**, 900 (2016).

[34] H. Yu, K. Jo, K. L. Kounovsky, J. J. de Pablo, and D. C. Schwartz, Molecular propulsion: Chemical sensing and chemotaxis of DNA driven by RNA polymerase, J. Am. Chem. Soc. **131**, 5722 (2009).

[35] S. Sengupta, K. K. Dey, H. S. Muddana, T. Tabouillot, M. E. Ibele, P. J. Butler, and A. Sen, Enzyme Molecules as Nanomotors, J. Am. Chem. Soc. **135**, 1406 (2013).

[36] K. K. Dey, S. Das, M. F. Poyton, S. Sengupta, P. J. Butler, P. S. Cremer, and A. Sen, Chemotactic Separation of Enzymes, ACS Nano **8**, 11941 (2014).

[37] X. Zhao, H. Palacci, V. Yadav, M. M. Spiering, M. K. Gilson, P. J. Butler, H. Hess, S. J. Benkovic, and A. Sen, Substrate-driven chemotactic assembly in an enzyme cascade, Nat. Chem. **10**, 311 (2018).

[38] A.-Y. Jee, Y.-K. Cho, S. Granick, and T. Tlusty, Catalytic enzymes are active matter, Proc. Natl. Acad. Sci. U.S.A. **115**, E10812 (2018).

[39] J. Agudo-Canalejo, T. Adeleke-Larodo, P. Illien, and R. Golestanian, Enhanced Diffusion and Chemotaxis at the Nanoscale, Acc. Chem. Res. **51**, 2365 (2018).

[40] J. Agudo-Canalejo, P. Illien, and R. Golestanian, Phoresis and Enhanced Diffusion Compete in Enzyme Chemotaxis, Nano Lett. **18**, 2711 (2018).

[41] J. Agudo-Canalejo and R. Golestanian, Diffusion and steady state distributions of flexible chemotactic enzymes, Eur. Phys. J. Spec. Top. **229**, 2791 (2020).

[42] M. Feng and M. K. Gilson, Enhanced Diffusion and Chemotaxis of Enzymes, Annu. Rev. Biophys. **49**, 87 (2020).

[43] See Supplemental Material at [URL will be inserted by publisher] for details on the linear stability analysis, the enumeration of elementary cycles and their decomposi-

tion into motifs, and the Brownian dynamics simulations, including Refs. [46] and [47] .

[44] V. Ouazan-Reboul, J. Agudo-Canalejo, and R. Golestanian, Self-organization of primitive metabolic cycles due to non-reciprocal interactions, arXiv:2303.09832.

[45] S. Osat and R. Golestanian, Non-reciprocal multifarious self-organization, Nature Nanotechnology **18**, 79 (2022).

[46] P. Strating, Brownian dynamics simulation of a hard-sphere suspension, Phys. Rev. E **59**, 2175 (1999).

[47] M. P. Allen and D. J. Tildesley, *Computer Simulation of Liquids* (Oxford University Press, 2017).

Network effects lead to self-organization in metabolic cycles of self-repelling catalysts
Supplemental Material

Vincent Ouazan-Reboul,[1] Ramin Golestanian,[1, 2, *] and Jaime Agudo-Canalejo[1, †]

[1]*Max Planck Institute for Dynamics and Self-Organization, Am Fassberg 17, D-37077, Göttingen, Germany*

[2]*Rudolf Peierls Centre for Theoretical Physics, University of Oxford, OX1 3PU, Oxford, UK*

CONTENTS

I.   LINEAR STABILITY ANALYSIS FOR THREE-SPECIES CYCLES

To calculate the eigenvalues of the matrix $\Lambda_{m,n}$ in the main text, we construct the associated characteristic polynomial, which reads

$$\chi_{-\Lambda}(\lambda) = \begin{vmatrix} -\alpha_1 \Delta\mu_1 \rho_{01} - \lambda & \alpha_2 \mu_1^{(p)} \rho_{01} & -\alpha_3 \mu_1^{(s)} \rho_{01} \\ -\alpha_1 \mu_2^{(s)} \rho_{02} & -\alpha_2 \Delta\mu_2 \rho_{02} - \lambda & \alpha_3 \mu_2^{(p)} \rho_{02} \\ \alpha_1 \mu_3^{(p)} \rho_{03} & -\alpha_2 \mu_3^{(s)} \rho_{03} & -\alpha_3 \Delta\mu_3 \rho_{03} - \lambda \end{vmatrix}. \tag{S1}$$

Performing the operations $C_1 \leftarrow C_1 + \frac{\alpha_1}{\alpha_2} C_2 + \frac{\alpha_1}{\alpha_3} C_2$ on the columns C_i of the matrix, we obtain

$$\chi_{-\Lambda}(\lambda) = \begin{vmatrix} -\lambda & \alpha_2 \mu_1^{(p)} \rho_{01} & -\alpha_3 \mu_1^{(s)} \rho_{01} \\ -\frac{\alpha_1}{\alpha_2}\lambda & -\alpha_2 \Delta\mu_2 \rho_{02} - \lambda & \alpha_3 \mu_2^{(p)} \rho_{02} \\ -\frac{\alpha_1}{\alpha_3}\lambda & -\alpha_2 \mu_3^{(s)} \rho_{03} & -\alpha_3 \Delta\mu_3 \rho_{03} - \lambda \end{vmatrix}, \tag{S2}$$

which can be further manipulated to give the following polynomial

$$\chi_{-\Lambda}(\lambda) = -\lambda \Big[\lambda^2 + (\alpha_1 \Delta\mu_1 + \alpha_2 \Delta\mu_2 + \alpha_3 \Delta\mu_3)\,\lambda$$
$$+ \alpha_1 \alpha_2 \left(\Delta\mu_1 \Delta\mu_2 + \mu_1^{(p)} \mu_2^{(s)} \right) + \alpha_2 \alpha_3 \left(\Delta\mu_2 \Delta\mu_3 + \mu_2^{(p)} \mu_3^{(s)} \right) + \alpha_3 \alpha_1 \left(\Delta\mu_3 \Delta\mu_1 + \mu_3^{(p)} \mu_1^{(s)} \right) \Big]. \tag{S3}$$

We can now solve $\chi_{-\Lambda}(\lambda) = 0$ to obtain Eq. (2) in the main text and $\lambda = 0$.

———

* ramin.golestanian@ds.mpg.de

† jaime.agudo@ds.mpg.de

II. STABILITY CONDITION FOR SUBSTRATE-SENSITIVE SPECIES

Here we consider the case of a cycle with three species, with activities α_m, substrate mobilities $\mu_m^{(\mathrm{s})}$, and no product mobilities. The corresponding interaction matrix has the two non-null eigenvalues:

$$\lambda_\pm = -\frac{1}{2} \sum_{m=1}^3 \alpha_m \Delta\mu_m \rho_{0m} \pm \frac{1}{2} \sqrt{\left(\sum_{m=1}^3 \alpha_m \Delta\mu_m \rho_{0m} \right)^2 - 4 \sum_{m=1}^3 \alpha_m \Delta\mu_m \rho_{0m} \cdot \alpha_{m+1} \Delta\mu_{m+1} \rho_{0m+1}}, \qquad (\mathrm{S}4)$$

with $\Delta\mu_m = -\mu_m^{(\mathrm{s})}$. In the particular case for which $\alpha_1 \Delta\mu_1 > 0$, solving $\lambda_+ > 0$ leads to two possible parameter-free instability conditions, which can be written as

$$\frac{\alpha_3 \Delta\mu_3 \rho_{03}}{\alpha_1 \Delta\mu_1 \rho_{01}} < -\left(\frac{\alpha_2 \Delta\mu_2 \rho_{02}}{\alpha_1 \Delta\mu_1 \rho_{01}} + 1 \right) \qquad (\mathrm{S}5)$$

and

$$\frac{\alpha_3 \Delta\mu_3 \rho_{03}}{\alpha_1 \Delta\mu_1 \rho_{01}} \left(1 + \frac{\alpha_2 \Delta\mu_2 \rho_{02}}{\alpha_1 \Delta\mu_1 \rho_{01}} \right) < -\frac{\alpha_2 \Delta\mu_2 \rho_{02}}{\alpha_1 \Delta\mu_1 \rho_{01}}, \qquad (\mathrm{S}6)$$

with Eq. (S5) corresponding to an overall self-attracting mixture and Eq. (S6) corresponding to a self-repelling one. We can show that, if $\dfrac{\alpha_2 \Delta\mu_2 \rho_{02}}{\alpha_1 \Delta\mu_1 \rho_{01}} < -1$, then the conditions given in Eq. (S5) and Eq. (S6) are complementary, and the cycle is always unstable. If, however, $\dfrac{\alpha_2 \Delta\mu_2 \rho_{02}}{\alpha_1 \Delta\mu_1 \rho_{01}} \geq -1$, then Eq. (S6) is the least strict stability condition and thus determines the overall stability of the cycle. This boundary is plotted as the dashed line in main text Fig. 2, with cycles having parameters below that line being unstable. It can be shown that the condition given in Eq. (S6) is not achievable for a cycle of three self-repelling species.

III. SELF-REPELLING METABOLIC CYCLES

We use a similar approach to Section II in order to find the instability conditions for a cycle of three self-repelling species with non-null product mobilities $\mu^{(\mathrm{p})}$. We seek to solve $\mathrm{Re}(\lambda_+) > 0$ (see main text Eq. (3)), under the assumption that the mixture of catalysts is self-repelling, i.e. the following condition holds $\sum_{m=1}^3 \alpha_m \Delta\mu_m \rho_{0m} > 0$.

In order to obtain expressions in the normalized self-interaction plane $\left(\dfrac{\alpha_2 \Delta\mu_2 \rho_{02}}{\alpha_1 \Delta\mu_1 \rho_{01}}, \dfrac{\alpha_3 \Delta\mu_3 \rho_{03}}{\alpha_1 \Delta\mu_1 \rho_{01}} \right)$, we rewrite main text Eq. (3) in terms of the $\Delta\mu_m$ and $\mu_m^{(\mathrm{p})}$. For brevity, we introduce the notations $\Delta_m \equiv \dfrac{\alpha_m \Delta\mu_m \rho_{0m}}{\alpha_1 \Delta\mu_1 \rho_{01}}$ and $p_m \equiv \dfrac{\alpha_m \mu_m^{(\mathrm{p})} \rho_{0m}}{\alpha_1 \Delta\mu_1 \rho_{01}}$. This results in the following form for the instability condition

$$(\Delta_2 - p_2 + 1) \Delta_3 < (p_1 - 1) \Delta_2 - \sum_{m=1}^3 p_m p_{m+1} + p_3, \qquad (\mathrm{S}7)$$

which we can plot in normalized self-interaction coordinates Δ_2, Δ_3 by taking p_1, p_2, p_3 as arbitrary parameters. Defining

$$f_{\{p_m\}}(\Delta_2) \equiv \frac{(p_1 - 1)\Delta_2 - \sum_{m=1}^3 p_m p_{m+1} + p_3}{\Delta_2 - p_2 + 1}, \qquad (\mathrm{S}8)$$

and rewriting Eq. (S7) as

$$\begin{cases} \Delta_3 < f_{\{p_m\}}(\Delta_2) \text{ if } \Delta_2 > p_2 - 1, \\ \Delta_3 > f_{\{p_m\}}(\Delta_2) \text{ if } \Delta_2 \leq p_2 - 1, \end{cases} \qquad (\mathrm{S}9)$$
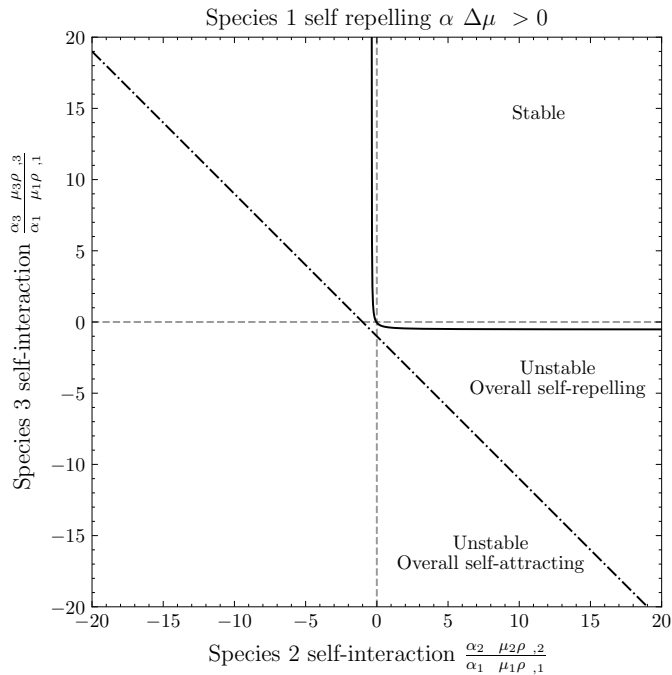
FIG. S1. Phase diagram with parameters $\frac{\alpha_1\mu_1^{(p)}\rho_{01}}{\alpha_1\Delta\mu_1\rho_{01}} = 0.473$, $\frac{\alpha_2\mu_2^{(p)}\rho_{02}}{\alpha_1\Delta\mu_1\rho_{01}} = 0.6315$, and $\frac{\alpha_3\mu_3^{(p)}\rho_{03}}{\alpha_1\Delta\mu_1\rho_{01}} = -2.684$, without an unstable region for all-self-repelling catalytic species.

we can then determine the conditions for which Eq. (S9) can be satisfied if all three species are self-repelling, i.e. $\Delta_2 > 0$ and $\Delta_3 > 0$.

This statement is equivalent to having at least part of the instability line located in the $\Delta_2 > 0, \Delta_3 > 0$ domain of the reduced self-interaction plane in which we plot the instability line. Thus, if there is at least one $\Delta_2 > 0$ such that $f_{\{p_m\}}(\Delta_2) > 0$, an instability can be obtained for a set of three self-repelling species.

The function $f_{\{p_m\}}$ features two asymptotes, a vertical one with value $p_2 - 1$ and a horizontal one with value $p_1 - 1$. If either of these asymptotes are positive, then the existence of a region of $\Delta_2 > 0$ such that $f_{\{p_m\}}(\Delta_2) > 0$ is guaranteed, leading to the first two conditions written in main text Eqs. (4a) and (4b). If the two asymptotes are negative, there is still a possibility for all-self-repelling instabilities, as $f_{\{p_m\}}$ features a zero with value $\Delta_2^{(0)} = (\sum_{m=1}^{3} p_m p_{m+1} - p_3)/(p_1 - 1)$. If $\Delta_2^{(0)} > 0$, f exhibits a sign change in the right half-plane and is guaranteed to be positive-valued in parts of it. We rewrite the $\Delta_2^{(0)} > 0$ inequality in terms of activities, mobilities, and homogeneous concentrations, and present a compact form of it in main text Eq. (4c). As main text Eq. (3) is invariant by cyclic permutation of the catalytic species, the obtained conditions generalize to any of the three species index $m \in \{1, 2, 3\}$, as long as the corresponding species is self-repelling. In the conditions written in main text Eq. (4a-c), we then replace species 1 by an arbitrary species m, species 2 with species $m + 1$, and species 3 with $m - 1$.

In main text Fig. 2, we plot the stability line corresponding to $p_1 = 0.473$, $p_2 = 6.315$, and $p_3 = -5.684$. As $p_1 < 1$ and $p_2 > 1$, the horizontal and vertical asymptotes of the stability function f are, respectively, negative and positive. Furthermore, as the corresponding value of $\Delta_2^{(0)}$ is positive, the stability function exhibits a sign change in the right half-plane. Note that we only plot the stability line for $\Delta_2 > p_2 - 1$, as the values of $f_{\{p_m\}}$ for $\Delta_2 \leq p_2 - 1$ are systematically below the overall-self-attracting line and thus irrelevant.

On the other hand, if we choose for instance $p_1 = 0.473$, $p_2 = 0.6315$, and $p_3 = -2.684$, both asymptotes are negative and the sign change of $f_{\{p_m\}}$ occurs in the right half-plane, as shown in Fig. S1.

IV. BROWNIAN DYNAMICS SIMULATIONS

To study the system beyond the linear regime, we perform Brownian Dynamics simulations. We simulate the dynamics of chemically active and chemotactic spherical particles, the effective interactions among which we derive in the

following. We first consider an isolated particle of species m, with activity α_m and radius R. We place the particle at the origin, and use spherical coordinates. The perturbation $\delta c_m^{(k)}$ induced by the particle to chemical k, which is assumed to equilibrate quickly with respect to the motion of the particle, is given by the solution of the Laplace equation:

$$0 = \nabla^2 \delta c_m^{(k)}. \tag{S10}$$

The corresponding boundary conditions, however, depend on whether the chemical is the substrate of species m (i.e. $k = m$), its product (i.e. $k = m + 1$), or neither. Indeed, the boundary condition must balance the diffusive fluxes across the particle surface with its chemical activity, resulting in:

$$- 4\pi R^2 D^{(k)} \left. \frac{\partial \delta c_m^{(k)}}{\partial r} \right|_{r=R} = \begin{cases} -\alpha_m & \text{if } k = m, \\ \alpha_m & \text{if } k = m + 1, \\ 0 & \text{otherwise.} \end{cases} \tag{S11}$$

The corresponding solutions for the perturbations are then

$$\delta c_m^{(k)}(r) = \begin{cases} -\frac{\alpha_m}{4\pi D^{(k)}} \frac{1}{r} & \text{if } k = m, \\ \frac{\alpha_m}{4\pi D^{(k)}} \frac{1}{r} & \text{if } k = m + 1, \\ 0 & \text{otherwise.} \end{cases} \tag{S12}$$

Now consider a second particle of species n placed at a location $\mathbf{r}$. Its velocity $\mathbf{v}_{n,m}(\mathbf{r})$ in response to the perturbation(s) created by the particle of species m will be:

$$\mathbf{v}_{n,m}(\mathbf{r}) = \begin{cases} -\mu_n^{(\mathrm{s})} \nabla \delta c_m^{(m+1)} & \text{if } n = m + 1, \\ -\mu_n^{(\mathrm{p})} \nabla \delta c_m^{(m)} & \text{if } n = m - 1, \\ -\mu_n^{(\mathrm{s})} \nabla \delta c_m^{(m)} - \mu_n^{(\mathrm{p})} \nabla \delta c_m^{(m+1)} & \text{if } n = m, \\ 0 & \text{otherwise.} \end{cases} \tag{S13}$$

Using Eq. (S12), the responses can be explicitly written as:

$$\mathbf{v}_{n,m}(\mathbf{r}) = \begin{cases} \frac{\alpha_m}{4\pi} \frac{\mu_n^{(\mathrm{s})}}{D^{(n)}} \frac{\mathbf{r}}{r^3} & \text{if } n = m + 1, \\ -\frac{\alpha_m}{4\pi} \frac{\mu_n^{(\mathrm{p})}}{D^{(n+1)}} \frac{\mathbf{r}}{r^3} & \text{if } n = m - 1, \\ \frac{\alpha_m}{4\pi} \left(\frac{\mu_n^{(\mathrm{p})}}{D^{(n+1)}} - \frac{\mu_n^{(\mathrm{s})}}{D^{(n)}} \right) \frac{\mathbf{r}}{r^3} & \text{if } n = m, \\ 0 & \text{otherwise.} \end{cases} \tag{S14}$$

We can then simulate the following equations of motion for N particles:

$$\dot{\mathbf{r}}_i(t) = \sum_{\substack{j=1 \\ (j \neq i)}}^{N} \mathbf{v}_{S(i),S(j)}(\mathbf{r}_i - \mathbf{r}_j) + \boldsymbol{\xi}_m \tag{S15}$$

with $i \in \{1, 2, \ldots, N\}$, $S(i)$ giving the species index corresponding to the particle index i, the velocities calculated using Eq. (S14), and $\boldsymbol{\xi}$ a random velocity corresponding to white noise with intensity $2D_\mathrm{p}$, resulting in diffusion of the particles with diffusion coefficient D_p. Particles start out randomly distributed in space, corresponding to a homogeneous state. The equations of motion are integrated using a forward Euler scheme. At every integration step, an overlap correction is then performed to account for hard-core repulsion between the spheres, using the "elastic collision method" [1] and a cell-list algorithm [2] with cubic cells of side length $2R$ to determine particles' neighbours. We simulate the system in a three-dimensional box of side length L with periodic boundary conditions, and interactions are treated according to the minimum image convention. The particle diameter, $\sigma = 2R$, which is taken to be the same for all species, sets the basic length scale of the simulation. We can redefine the mobility coefficients to include the diffusion coefficient of the corresponding chemical, as $\hat{\mu}_m^{(\mathrm{s,p})} = \mu_m^{(\mathrm{s,p})}/D^{(m,m+1)}$. We can define basic activity and mobility scales, respectively α_0 and $\hat{\mu}_0$, from which we build a velocity scale $V_0 = \alpha_0 \hat{\mu}_0/(4\pi\sigma^2)$. From these scales, we can define dimensionless time $\tau = tV_0/\sigma$, activities $\tilde{\alpha} = \alpha/\alpha_0$, and mobilities $\tilde{\mu} = \hat{\mu}/\hat{\mu}_0$. Finally, we define a reduced

Species m	Activity $\tilde{\alpha}_m$	Substrate mobility $\tilde{\mu}_m^{(s)}$	Product mobility $\tilde{\mu}_m^{(p)}$
1	0.125	-0.5	0.45
2	0.75	$-2.166 + 0.316 \cdot n_2, \ n_2 \in \{1, 2, \ldots, 20\}$	1
3	0.75	$-4.066 + 0.316 \cdot n_3, \ n_3 \in \{1, 2, \ldots, 20\}$	-0.9

TABLE SI. Simulation parameters for main text Fig. 2.

particle diffusion coefficient $\tilde{D}_\mathrm{p} = D_\mathrm{p}/(V_0\sigma)$, equivalent to a noise intensity or temperature.

We numerically verify the stability diagrams shown in Fig. 2 of the main text. To do so, we perform simulations on a twenty by twenty grid in the $\frac{\alpha_2\Delta\mu_2\rho_{02}}{\alpha_1\Delta\mu_1\rho_{01}}, \frac{\alpha_3\Delta\mu_3\rho_{03}}{\alpha_1\Delta\mu_1\rho_{01}}$ plane, which we generate with the parameters given in Table SI.

We then perform Brownian Dynamics simulations for all possible combinations of n_2 and $n_3 \in \{1, 2 \ldots, 20\}$, making for a total of 441 sets of parameters. 5000 particles of each species are simulated, in a box of size $L/\sigma = 54$, corresponding to a total volume fraction $\phi = 0.05$. The simulations are iterated with a time step $\mathrm{d}\tau = 0.005$, for a total time of $\tau_\mathrm{total} = 60$. The effective diffusion coefficient is set at $\tilde{D}_\mathrm{p} = 0.01$. The simulations are run in the Julia programming language. To determine whether the system is unstable, we perform a clustering analysis on the final state of the system using a cell-lists based clustering algorithm [2], and considering that two particles are neighbours if they are within a distance of 1.1σ. A simulation run is considered to be unstable if, at the end of the runtime, any cluster includes more than 20% of the total particle population. We obtain the results shown in Fig. 2 of the main text. Overall, the numerical results agree with the analytical prediction for the instability line.

The results shown in Fig. 3 of the main text correspond to the steady states of simulations ran with the parameters compiled in Table SI with $n_2 = 6$ and $n_3 = 9$ (i.e. $\mu_2^{(s)} = -0.27$ and $\mu_3^{(s)} = -1.22$), with the same $\mathrm{d}\tau$, $\tilde{D}_\mathrm{p}$, and volume fraction ϕ as the previous simulations (which leads to a reduced box size for the single species and species pair simulations), 5000 particles per species, and a total time $\tau_\mathrm{total} = 60$.

We provide the following movies of the Brownian Dynamics simulations:

- **Movie 1**: Homogeneous mixture of species 1, which is linearly stable. See main text Figure 3(a1).

- **Movie 2**: Same as Movie 1, with species 2. See main text Figure 3(a2).

- **Movie 3**: Same as Movie 1, with species 3. See main text Figure 3(a3).

- **Movie 4**: Mixture of species 1 and 2, which is linearly stable. The particles form small, transient assemblies. See main text Figure 3(b1)

- **Movie 5**: Mixture of species 2 and 3, which is unstable, leading to the formation of a cluster containing both species which coexists with a dilute gas phase of species 2. See main text Figure 3(b2)

- **Movie 6**: Mixture of species 3 and 1, which is linearly stable. See main text Figure 3(b3)

- **Movie 7**: Mixture of all three active species, which undergoes self-organization, leading to the formation of a cluster containing all three species which coexists with a gas of species 2. See main text Figure 3(c).

Note that, for movies 5 and 7, and the corresponding panels in main text Figure 3, all the particle coordinates are shifted so that the centre of mass of the mixture is located at the center of the box in the final snapshot. This does not modify the result of the simulations, as they involve periodic boundary conditions, and leads to clearer figures and movies.

[1] P. Strating, Brownian dynamics simulation of a hard-sphere suspension, Phys. Rev. E **59**, 2175 (1999).
[2] M. P. Allen and D. J. Tildesley, *Computer Simulation of Liquids* (Oxford University Press, 2017).

5

Interaction-motif-based classification of self-organizing metabolic cycles

This chapter is reproduced from the preprint Ouazan-Reboul et al, ArXiv:2305.05472 (2023)[184], which has been submitted to the New Journal of Physics. I took part in the design of the research, performed the analytical calculations, designed the numerical simulation code, analyzed and interpreted the numerical data, and participated in the redaction of the paper.

Interaction-motif-based classification of self-organizing metabolic cycles

Vincent Ouazan-Reboul,[1] Ramin Golestanian,[1, 2] and Jaime Agudo-Canalejo[1]

[1] *Max Planck-Institute for Dynamics and Self-Organization, Am Fassberg 17, D-37077, Göttingen, Germany*
[2] *Rudolf Peierls Centre for Theoretical Physics, University of Oxford, OX1 3PU, Oxford, UK*

Particles that are catalytically-active and chemotactic can interact through the concentration fields upon which they act, which in turn may lead to wide-scale spatial self-organization. When these active particles interact through several fields, these interactions gain an additional structure, which can result in new forms of collective behaviour. Here, we study a mixture of active species which catalyze the conversion of a substrate chemical into a product chemical, and chemotax in concentration gradients of both substrate and product. Such species develop non-reciprocal, specific interactions that we coarse-grain into attractive and repulsive, which can lead to a potentially complex interaction network. We consider the particular case of a metabolic cycle of three species, each of which interacts with itself and both other species in the cycle. We find that the stability of a cycle of species that only chemotax in gradients of their substrate is piloted by a set of two parameter-free conditions, which we use to classify the low number of corresponding interaction networks. In the more general case of substrate- and product-chemotactic species, we can derive a set of two high-dimensional stability conditions, which can be used to classify the stability of all the possible interaction networks based on the self- and pair-interaction motifs they contain. The classification scheme that we introduce can help guide future studies on the dynamics of complex interaction networks and explorations of the corresponding large parameter spaces in such metabolically active complex systems.

I. INTRODUCTION

Chemotactic particles, which develop force-free motion in response to gradients, have been shown to develop effective interactions through the fields upon which they act, independently of the particular mechanism through which they move [1]. Such interactions have for instance been observed in diffusiophoretic [2–4] and thermophoretic [5–7] colloids, as well as for chemotactic microorganisms [8, 9]. Field-mediated active interactions have the particularity of being nonreciprocal, meaning that the response of a particle A to the presence of another particle B is different from the response of B to A [10–13]. This feature can lead to new forms of collective behaviour as compared to reciprocally-interacting systems [14, 15]. For example, binary mixtures of catalytically active particles may spontaneously form self-propelled clusters [16]. The models describing active phoretic particles can be extended to the case in which particles act upon and interact through several chemical fields, which introduces a nontrivial topology to the network of interactions among different particle species. This interaction topology can allow the self-organization of a mixture of self-repelling species [17], which is not possible for simpler interaction schemes, and can lead to super-exponential aggregation of complementary catalysts, which could have been relevant in the emergence of living matter [18].

Taking into account the presence of several chemical fields leads to an explosion in the number of possible interaction patterns that active phoretic species can develop, which in turn makes the determination of the conditions in which mixtures of such species can self-organize rather challenging. To overcome this issue, inspiration can be found from the methods used for tackling the protein folding problem, which consists in understanding and characterizing the process through which an initially linear chain of amino acids folds into a dense three-dimensional structure [19], and determining which structure a given sequence folds into. One of the challenges that is encountered in this setting is that proteins are composed of 20 possible amino acid species, leading to a number of possible sequences going as 20^n for a chain of n amino acids, thus making the enumeration of biologically-relevant chains of hundreds of amino acids combinatorially complex. In order to decrease this number, one approach is to coarse-grain the amino acids into a smaller number of categories that have simple interaction rules. This is the basis of the celebrated HP lattice model [20, 21], which considers two categories of hydrophobic and polar amino acids, although it has also been extended to larger alphabets [22–24]. While current state of the art methods can leverage abundant computational power and large data sets, which allows for accurate predictions of the structure of biological proteins [25], simple lattice models have impressive predictive power [26, 27], with the hydrophobic or polar nature of the residues having been shown to have a strong influence on protein structure independently of their particular nature [28]. Moreover, simple proteins having been successfully designed based on the binary alphabet used in the HP model [29].

In this work, we use a similar approach to determine the ability of catalytic species involved in small metabolic cycles to self-organize, coarse-graining their interactions into attractive "A" or repulsive "R" but with the important new element of non-reciprocity. We are able to systematically classify the (linear) stability of homogeneous mixtures of catalytic particles participating in metabolic cycles, and thus their tendency to spatially
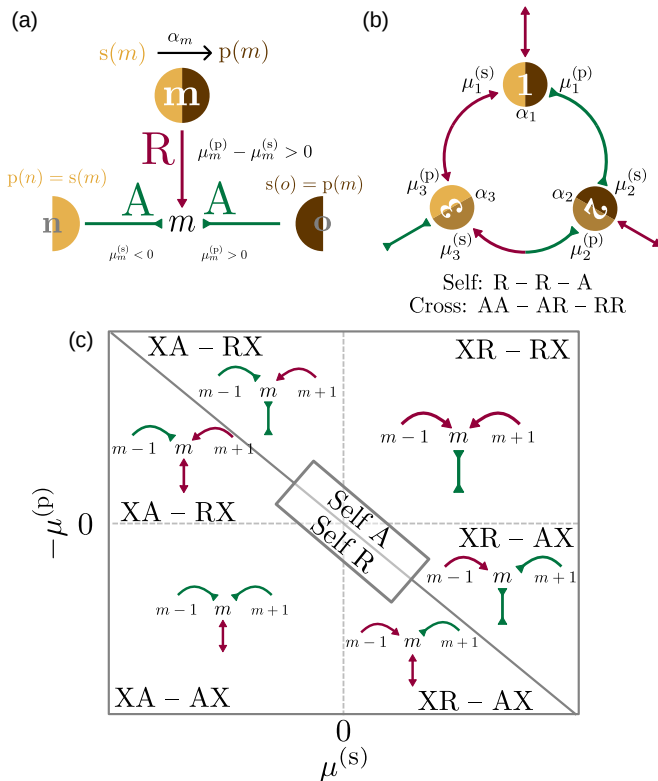
FIG. 1. (a) Specific interaction between catalytically active species. Particles of species m convert a substrate chemical into a product chemical at a rate α_m, and chemotax in concentration gradients of these two chemicals. These particles develop interactions with other catalytic species which modify the concentrations of their substrate (e.g. species n) and product (e.g. species o). (b) Metabolic cycle of three species, which interact with themselves and their neighbour in the cycle. Note the nonreciprocity of the 2-3 pair interaction. (c) All possible interaction motifs between a given species and its neighbors in the cycle, determined by its substrate mobility $\mu^{(\mathrm{s})}$ and its product mobility $\mu^{(\mathrm{p})}$. "A" denotes self-attracting species and "R" denotes self-repelling species. "X" can correspond to any sense of interaction.

self-organize, based on which interaction motifs they contain. The article is structured as follows. Section II describes the basic framework and summarizes the classification of the metabolic networks. Section III describes the model in detail, and our method for analyzing the stability of metabolic cycles. In Section IV, we classify the stability of cycles composed of species with a single chemotactic coefficient corresponding to the substrate of the reaction they catalyze, which can be done using a simple, parameter-free instability criterion. Finally, in Section V we generalize this classification to species that are chemotactic to both their substrate and their product, by deriving two instability criteria and determining which interaction motifs need to be present for these instability conditions to be satisfied. Section VI contains some discussions while some of the details of the calculations are relegated to the Appendices.

II. MODEL OVERVIEW AND SUMMARY OF RESULTS

We study self-organization of catalytically active particles belonging to M distinct species, and K chemical fields upon which these particles act. In particular, each particle of species m converts a substrate chemical, with index $k = \mathrm{s}(m)$, into a product chemical $k' = \mathrm{p}(m)$ at a rate α_m (Fig. 1(a)). The functions $\mathrm{s}(m)$ and $\mathrm{p}(m)$ therefore map each catalytic species index to the index of the substrate and product chemical, respectively, and define the topology of the *catalytic network*. Assuming that catalysts of species m have a concentration ρ_m, we can then write the evolution equations for the concentrations of the K chemical fields they produce and consume as:

$$\partial_t c_k(\mathbf{r}, t) = D^{(k)} \boldsymbol{\nabla}^2 c_k + \sum_m \left(\delta_{k, \mathrm{p}(m)} - \delta_{k, \mathrm{s}(m)} \right) \alpha_m \rho_m, \tag{1}$$

where $D^{(k)}$ is the diffusion coefficient of chemical species k, and $\delta_{m,n}$ is the Kronecker symbol, verifying $\delta_{m,n} = 1$ if $m = n$ and 0 else.

The active particles we consider are also taken to be chemotactic for both their substrate and their product. In a concentration gradient of its substrate $\nabla c_{\mathrm{s}(m)}$, a particle of species m develops a velocity going as $-\mu_m^{(\mathrm{s})} \nabla c_{\mathrm{s}(m)}$, which takes it towards the high (respectively low) concentrations of its substrate if $\mu_m^{(\mathrm{s})}$ is negative (respectively positive). The same is true for gradients of the product of species m, to which a product mobility $\mu_m^{(\mathrm{p})}$, also of arbitrary sign, and independent from $\mu_m^{(\mathrm{s})}$, is associated. We can then write the following continuity equation for the concentrations of the active species ρ_m:

$$\partial_t \rho_m(\mathbf{r}, t) = \boldsymbol{\nabla} \cdot \left[D_{\mathrm{p}} \boldsymbol{\nabla} \rho_m + \left(\mu_m^{(\mathrm{s})} \boldsymbol{\nabla} c_{\mathrm{s}(m)} + \mu_m^{(\mathrm{p})} \boldsymbol{\nabla} c_{\mathrm{p}(m)} \right) \rho_m \right], \tag{2}$$

where we take all catalysts to have the same diffusion coefficient D_{p}.

From Eqs. (1) and (2), it can be deduced that the catalytic species develop interactions mediated by the concentration fields of their respective substrates and products: through their chemotactic mobilities, the active particles we consider are able to develop induced velocities in response to chemical gradients created by the catalytic activity of other particles. Effective interactions relying on this mechanism have been previously shown to lead to self-organization of catalytic mixtures [16–18, 30]. Here, because we study species which act upon and react to a restricted subset of concentration fields, the emergent interactions are specific: a given species m only responds to concentration gradients of its substrates and products, and thus only species which act on these particular concentration fields will elicit a induced response in m (Fig. 1(a)). Moreover, these interactions are nonreciprocal: in general, the velocity response of species m to species n is different from the response of n to m

(Fig. 1(b)). Based on the choice of its mobilities, each catalyst species then develops a specific pattern of induced velocities to the other catalytic species, which determines the *interaction network* among species.

In this work, we seek to understand how different combinations of interaction patterns can lead to self-organization of catalytic mixtures whose components interact according to a network of specific, nonreciprocal interactions. We focus our study on the particular case of three species which are arranged into a model metabolic cycle (Fig. 1(b)), in which the substrate of species 1 is the product of species 3 and its product is the substrate of species 2, whose product is in turn the substrate of species 3. Catalytic species involved in such a cycle develop interactions with both other species and themselves, according to a set of six patterns shown in Fig. 1(c). In the later sections, we will systematically study the stability of all interaction pattern combinations, and find that any metabolic cycle of three species can be mapped onto nine "elementary" sets of networks, each of which belongs to one of five stability classes. The stability of all elementary network sets is listed in Table I, with the possible stability classes comprising the following cases:

- Always unstable: cycles of three self-attracting species which self-organize no matter the choice of parameters.

- Type-I unstable: cycles which involve self-attracting species, and which can self-organize if self-attraction overcomes self-repulsion.

- Type-IIa (or strongly) unstable: cycles of self-repelling species involving at least one instability-favouring pair.

- Type-IIb (or weakly) unstable: cycles of self-repelling species which include at least one pair which can be instability-favouring if some constraint on the mobilities of the active species is satisfied.

- Always stable: cycles of self-repelling species which do not include instability-favoring pair motifs, and cannot self-organize.

III. MODEL DESCRIPTION

We consider a set of $M = 3$ catalytic species involved in a metabolic cycle as described in the previous section. Due to this cycle structure, there are $K = 3$ chemical fields through which the catalysts interact, and we choose the convention that $s(m) = p(m-1) = m$. Note that, throughout this work, we will use periodic indices, so that species 0 is species 3 and species 4 corresponds to species 1, and so on.

In this setting, we perform a linear stability analysis on Eqs. (1) and (2) (see Appendix A) and find that the stability of the cycle is set by the eigenvalue equation

$$\lambda \delta \rho_m = -\sum_{n=1}^{3} \Lambda_{m,n} \delta \rho_n, \tag{3}$$

with $\delta \rho_n$ being the perturbation of the concentration of species n. The catalytic species involved in the metabolic cycle then undergo spatial self-organization through a system-wide instability if $\mathrm{Re}(\lambda) > 0$, the conditions for which we seek to uncover in the rest of this work. Eq. (3) involves $\mathbf{\Lambda}$, which is the matrix of effective interactions between the active species, and has coefficients

$$\Lambda_{m,n} = \begin{cases} \alpha_{m-1} \tilde{\mu}_m^{(s)} \rho_{0m} & \text{if } n = m - 1, \\ \alpha_m \left(\tilde{\mu}_m^{(p)} - \tilde{\mu}_m^{(s)} \right) \rho_{0m} & \text{if } n = m, \\ -\alpha_{m+1} \tilde{\mu}_m^{(p)} \rho_{0m} m & \text{if } n = m + 1. \end{cases} \tag{4}$$

Here, we have set $\tilde{\mu}_m^{(s)} = \mu_m^{(s)}/D^{(m)}$ and $\tilde{\mu}_m^{(p)} = \mu_m^{(p)}/D^{(m+1)}$, and ρ_{0m} is the density of species m in the homogeneous state. The response of species m to species n is attractive if $\Lambda_{m,n} < 0$, and repulsive if $\Lambda_{m,n} > 0$. We can then characterize the structure of the interactions of a metabolic cycle via the signs of the self- and pair-interactions of its constituent species, the encoding of which is shown in Fig. 1(b): a repulsive interaction is denoted by the letter "R", and an attractive interaction by the letter "A". In the example of Fig. 1(b), the self-interaction pattern is written as R–R–A, meaning that species 1 and 2 are self-attracting, and species 3 is self-repelling. The pair interactions, meanwhile, read AA–AR–RR, which denotes the fact that species 1 and 2 attract each other, species 2 chases species 3, and species 1 and 3 both repel each other.

According to Eq. (4), the self-interaction of a given species m can be expressed as a linear combination of its cross-interactions with other species. This constrains the signs of the triplet $(\Lambda_{m-1,m}, \Lambda_{m,m}, \Lambda_{m,m+1})$ to belong to one of the six, rather than the theoretically possible $2^3 = 8$, patterns shown in Fig. 1(c). Any possible interaction network for a metabolic cycle of three species can then be built by independently choosing one of these six patterns for each species. In the rest of this work, we classify the stability behaviour of all such possible $6^3 = 216$ networks.

IV. PHASE DIAGRAM FOR PRODUCT-INSENSITIVE SPECIES

The number of possible interaction combinations can be reduced by setting the product mobilities of all species to zero, i.e. $\mu_m^{(p)} = 0$, which sets $\Lambda_{m,m+1} = 0$ for all species. In this case, catalysts of a given species m can only interact with catalysts of the same species or the previous species $m - 1$. Additionally, the self-interaction now satisfies $\Lambda_{m,m} = -\frac{\alpha_m}{\alpha_{m+1}} \Lambda_{m,m-1}$, meaning that the self-interaction of a given species is of the opposite sign

Stability Class	Interaction Motifs		Elementary Cycle
	Self [11–22–33]	Mutual [12–23–31]	
Always UNSTABLE	**A** – **A** – **A**	XX – XX – XX	
Type-I UNSTABLE	R – **A** – X	XX – XX – XX	
Type-IIa (strongly) UNSTABLE	R – R – R	AR – **AA** – RR	
	R – R – R	AR – **AA** – RA	
	R – R – R	**AA** – **AA** – **RR**	
Type-IIb (weakly) UNSTABLE	R – R – R	**AA** – RA – RA	
	R – R – R	RA – AA – **AA**	
STABLE	R – R – R	AA – AA – AA	
	R – R – R	AR – AR – AR	

TABLE I. classification of the different emergent possibilities for a size-3 metabolic cycle. Left column: Instability class; see main text for the definitions. Middle-left column: single-species interaction motifs, with A denoting self-attracting species and R denoting self-repelling species. X can correspond to any sense of interaction. Middle-right column: pair interaction motifs. Right column: corresponding metabolic cycle.

as its response to the previous species. Only two interaction motifs are then possible in this case, one being self-attracting and repelled by the previous species, and the other, self-repelling and attracted by the previous species. This makes for a total number of possible interaction networks of $2^3 = 8$, which are easily enumerated.

We can determine the stability of each network of purely substrate-sensitive interactions by carrying out the linear stability analysis, which in this particular case yields parameter-independent instability conditions, and determining how these conditions intersect with regions of the parameter space corresponding to the different interaction patterns. The eigenvalues for strictly substrate-sensitive species are found as

$$\lambda_\pm = |\Lambda_{1,1}| \left[-\frac{1}{2}(\tilde{\Lambda}_1 + \tilde{\Lambda}_2 + \tilde{\Lambda}_3) \pm \frac{1}{2}\sqrt{\left(\tilde{\Lambda}_1 + \tilde{\Lambda}_2 + \tilde{\Lambda}_3\right)^2 - 4\left(\tilde{\Lambda}_1\tilde{\Lambda}_2 + \tilde{\Lambda}_2\tilde{\Lambda}_3 + \tilde{\Lambda}_1\tilde{\Lambda}_3\right)} \right]. \tag{5}$$

Here, we have normalized the self-interactions with $\Lambda_{1,1}$, such that $\tilde{\Lambda}_m = \frac{\Lambda_{m,m}}{|\Lambda_{1,1}|}$ is the ratio of the self-interaction of species m to the magnitude of the self-interaction of species 1. From Eq. (5), two instability conditions can be deduced, which we respectively name type-I and type-II:

$$\text{type-I:} \quad \tilde{\Lambda}_1 + \tilde{\Lambda}_2 + \tilde{\Lambda}_3 < 0, \tag{6}$$

and

$$\text{type-II:} \quad \begin{cases} \tilde{\Lambda}_1 + \tilde{\Lambda}_2 + \tilde{\Lambda}_3 > 0, \\ \tilde{\Lambda}_1\tilde{\Lambda}_2 + \tilde{\Lambda}_2\tilde{\Lambda}_3 + \tilde{\Lambda}_1\tilde{\Lambda}_3 < 0. \end{cases} \tag{7}$$

The type-I condition Eq. (6) only contains self-interaction terms, and corresponds to having a mixture that is self-attracting on average, as found in Refs. [16] and [30] for systems with a non-cyclic interaction topology. In contrast, the type-II condition Eq. (7) includes terms involving pairs of particle species. This condition allows for the mixture to be self-repelling on average, and instead requires pairs with opposite self-interaction signs to have stronger self-interaction than pairs with equal self-interaction signs.

We can then study separately the cases where species 1 is self-attracting ($\tilde{\Lambda}_1 = -1$) and self-repelling ($\tilde{\Lambda}_1 = 1$). In the case of a self-attracting species 1, $\tilde{\Lambda}_1 = -1$, we rewrite Eqs. (6) and (7) as inequalities of $\tilde{\Lambda}_3$ as a function of $\tilde{\Lambda}_2$. It can be shown that, if $\tilde{\Lambda}_2 < 1$, the first and second order conditions are complementary, so that at least one is always satisfied, and that the overall instability condition then writes:

$$\begin{cases} \tilde{\Lambda}_2 \geq 1, \\ \tilde{\Lambda}_3 < \frac{\tilde{\Lambda}_2}{\tilde{\Lambda}_2 - 1}, \end{cases} \text{ or } \tilde{\Lambda}_2 < 1. \tag{8}$$

Furthermore, we can also write an oscillation condition by determining which parameters make Eq. (5) complex with a positive real part. Parameters which make the term under the square root in Eq. (5) also satisfy the type-I instability condition, leading to the oscillation condition

$$\begin{cases} \tilde{\Lambda}_2 < 0, \\ \tilde{\Lambda}_3 \in \left[-(1 + \sqrt{-\tilde{\Lambda}_2})^2, -(1 - \sqrt{-\tilde{\Lambda}_2})^2 \right]. \end{cases} \tag{9}$$

We plot the corresponding stability phase diagram in $(\tilde{\Lambda}_2, \tilde{\Lambda}_3)$ coordinates in the left panel of Fig. 2, and find that cycles of purely substrate-sensitive species are always unstable if they contain two or three self-attracting species, while they can be either stable or unstable if they contain one self-attracting and one self-repelling species. The oscillation condition Eq. (9), meanwhile, is only compatible with cycles of three self-attracting species (Fig. 2, purple region). These predicted stability diagram was confirmed by particle-based Brownian dynamics simulations (see Appendix B). In Fig. 2, filled circles correspond to simulations that remained homogeneous, while empty circles correspond to simulations that displayed clustering. Oscillations were never observed in simulations, which we ascribe to the fact that the real part of the complex eigenvalue is always larger than its imaginary part, meaning that the system is out of the linear-perturbation regime by the time a full oscillation period is completed.

We now consider species 1 to be self-repelling, $\tilde{\Lambda}_1 = 1$. Using similar calculations as in the self-attracting case, we find the instability condition

$$\begin{cases} \tilde{\Lambda}_2 \geq -1, \\ \tilde{\Lambda}_3 < -\frac{\tilde{\Lambda}_2}{\tilde{\Lambda}_2 + 1}, \end{cases} \text{ or } \tilde{\Lambda}_2 < -1. \tag{10}$$

Plotting the corresponding phase diagram in the right panel of Fig. 2, we once again find that cycles of two self-attracting, product-insensitive species are always unstable and that cycles including only one self-attracting species can either be stable or unstable. Finally, we find that a cycle composed of three self-repelling species verifying $\mu^{(\mathrm{p})} = 0$ is always stable. The oscillation condition obtained with $\tilde{\Lambda}_1 = 1$ is incompatible with the set of inequalities Eq. (10), confirming that all three species need to be self-attracting for the eigenvalue to be complex. These predictions were again successfully verified by the results of our Brownian dynamics simulations.
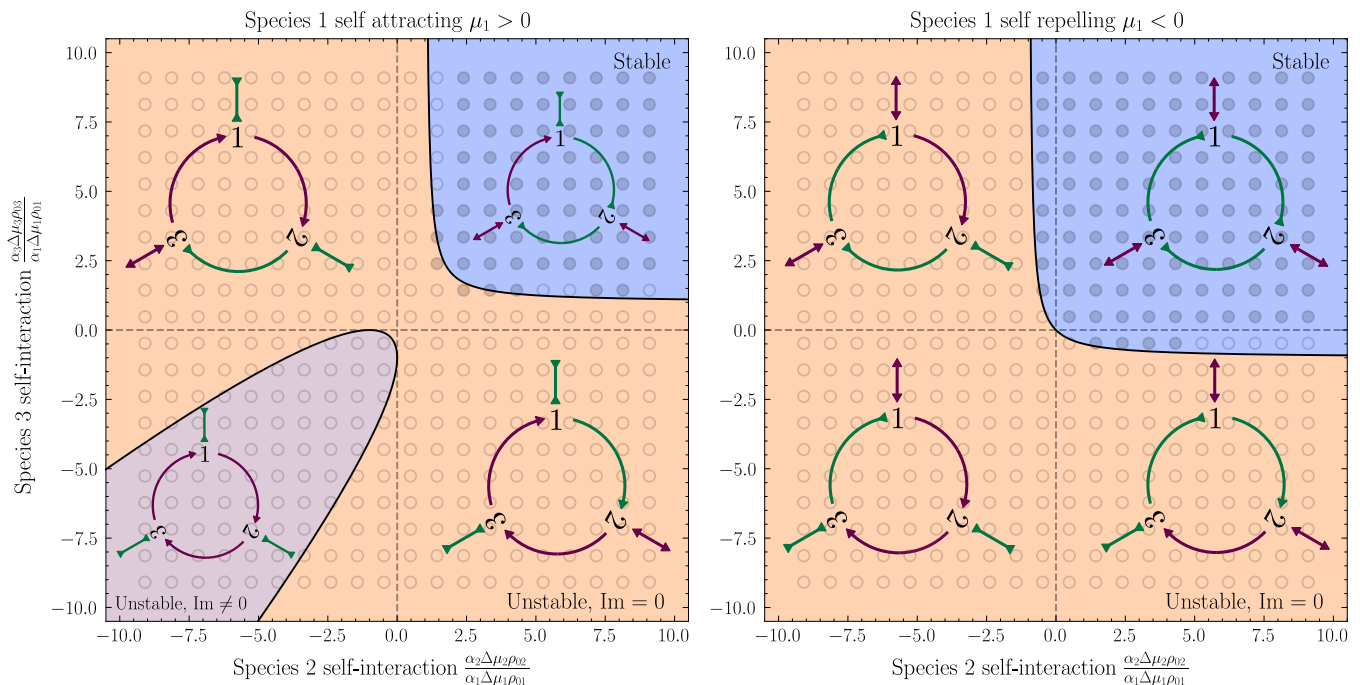
FIG. 2. Stability diagram for a cycle of three species chemotactic only to their substrate. Species 1 is self-attracting ($\mu_1 > 0$) in the left panel, and self-repelling ($\mu_1 < 0$) in the right panel. Complex eigenvalues occur in the purple region. Grey circles correspond to the results of Brownian dynamics simulations, with empty and filled circles corresponding to stable and unstable homogeneous states, respectively. For the simulation parameters and the expressions defining the stability lines, see Appendix B.

V. CLASSIFICATION OF GENERIC CYCLES

A. Type-I instabilities in generic cycles

We now consider the general case with both nonzero substrate and product mobilities. In this more general case, networks can be built by choosing three of any of the six interaction patterns from Fig. 1(c), and there are then $6^3 = 216$ possible interaction networks. We show here that the presence or absence of certain motifs in the interaction network can be used to infer the stability of the full system by using a semi-diagrammatic approach. Similarly to cycles of product-insensitive species, we first calculate the non-null eigenvalues, which are found as

$$\lambda_\pm = -\frac{1}{2}\sum_{m=1}^{3}\Lambda_{m,m} \pm \frac{1}{2}\sqrt{\left(\sum_{m=1}^{3}\Lambda_{m,m}\right)^2 - 4\sum_{m=1}^{3}(\Lambda_{m,m}\Lambda_{m+1,m+1} - \Lambda_{m+1,m}\Lambda_{m,m+1}.)}. \tag{11}$$

The homogeneous state is linearly unstable when the real part of the largest eigenvalue in Eq. (11) becomes positive, which leads to a type-I instability when

$$\sum_{m=1}^{3}\Lambda_{m,m} < 0, \tag{12}$$

effectively the same condition as Eq. (6), and corresponds to an overall self-attracting metabolic cycle.

Similarly to the case with substrate sensing only, any cycle of three self-attracting species is necessarily unstable according to Eq. (12). Cycles including at least one

self-attracting and one self-repelling species can be either stable or unstable according to the type-I condition (Table I, first two lines). The presence of at least one self-attracting species is then sufficient to conclude on the possible stability behavior of a given cycle, independent of the rest of the interactions, which allows us to classify the 189 networks with at least one self-attracting species.

Motif	Instability condition	Stability contribution
m — m+1 XA RA RX	$\dfrac{\mu_{m+1}^{(s)}}{\mu_{m+1}^{(p)}} + \dfrac{\mu_m^{(p)}}{\mu_m^{(s)}} < 1$	Stabilizing
m — m+1 XR AR AX	$\dfrac{\mu_{m+1}^{(s)}}{\mu_{m+1}^{(p)}} + \dfrac{\mu_m^{(p)}}{\mu_m^{(s)}} < 1$	Stabilizing
m — m+1 XA AA AX	Trivially stable	Stabilizing
m — m+1 XA RR XA	$\dfrac{\mu_{m+1}^{(s)}}{\mu_{m+1}^{(p)}} + \dfrac{\mu_m^{(p)}}{\mu_m^{(s)}} > 1$	Conditionally destabilizing
m — m+1 XR AA RX	$\dfrac{\mu_{m+1}^{(s)}}{\mu_{m+1}^{(p)}} + \dfrac{\mu_m^{(p)}}{\mu_m^{(s)}} > 1$	Destabilizing
m — m+1 XA AR AX	$\dfrac{\mu_{m+1}^{(p)}}{\mu_{m+1}^{(s)}}\left(1 - \dfrac{\mu_m^{(p)}}{\mu_m^{(s)}}\right) < 1$	Stabilizing
m — m+1 XA AA RX	$\dfrac{\mu_{m+1}^{(p)}}{\mu_{m+1}^{(s)}}\left(1 - \dfrac{\mu_m^{(p)}}{\mu_m^{(s)}}\right) > 1$	Conditionally destabilizing
m — m+1 XR AA AX	$\dfrac{\mu_m^{(s)}}{\mu_m^{(p)}}\left(1 - \dfrac{\mu_{m+1}^{(s)}}{\mu_{m+1}^{(p)}}\right) > 1$	Conditionally destabilizing
m — m+1 XA RA AX	$\dfrac{\mu_m^{(s)}}{\mu_m^{(p)}}\left(1 - \dfrac{\mu_{m+1}^{(s)}}{\mu_{m+1}^{(p)}}\right) < 1$	Stabilizing

TABLE II. Stability of all self-repelling pair motifs. Left column: exhaustive enumeration of pair interaction motifs composed of self-repelling species (labelled as "Self R" in Fig. 1(c)). "A" designates an attractive interaction, "R" corresponds to a repulsive interaction, and "X" can be any unspecified interaction. Middle column: condition on species mobilities for the corresponding term in Eq. (14) to be negative, i.e. instability-favouring. Right: contribution of the pair motif to the cycle stability, deduced from the corresponding middle-column condition (see Appendix C for details). A species pair is written as stabilizing if the associated condition cannot be satisfied, destabilizing if it is always satisfied, and conditionally destabilizing if it the outcome depends on the mobility values.

B. Stability of self-repelling species pairs

The 27 cycles that do not contain any self-attracting species can only exhibit a type-II instability, which corresponds to the following condition:

$$\sum_{m=1}^{3}\left(\Lambda_{m,m}\Lambda_{m+1,m+1} - \Lambda_{m,m+1}\Lambda_{m+1,m}\right) < 0. \quad (13)$$

This inequality involves the sum of three contributions, each of which corresponds to one of the three species pairs. We first determine which of the $3^2 = 9$ possible pairs of self-repelling species provide negative contributions to the sum written in Eq. (13) (see Appendix C). To do so, we expand the terms of the sum as

$$\sum_{m=1}^{3}\alpha_m\alpha_{m+1}\Delta_{m,m+1}\rho_{0m}\rho_{0m+1} < 0, \quad (14)$$

using the following definition

$$\Delta_{m,m+1} = \tilde{\mu}_m^{(s)}\tilde{\mu}_{m+1}^{(s)} + \tilde{\mu}_m^{(p)}\tilde{\mu}_{m+1}^{(p)} - \tilde{\mu}_m^{(s)}\tilde{\mu}_{m+1}^{(p)}, \quad (15)$$

and find the conditions on the mobilities of each of the self-repelling species which leads to $\Delta_{m,m+1} < 0$ (see Appendix C for the details of the derivation).

We compile the results in Table II. Out of the nine pairs of self-repelling species, five are always stabilizing, one is always destabilizing, and three are conditionally destabilizing, meaning that they favour instabilities if a certain inequality on the chemotactic mobilities of their constituent species is satisfied. Pairs that develop chasing interactions are all stability-favouring, which can be predicted from Eq. (13) with all self-interactions $\Lambda_{m,m}$ positive. On the other hand, species pairs which favor instability all interact reciprocally and involve some degree of repulsion, which tends to make the pair more destabilizing when its magnitude is increased. This is exemplified by the fact that the only pair which is always

instability-favouring, whose interactions can be described as XR–AA–RX, involves two species which reciprocally attract and are repelled by their other neighbour.

C. Stability of cycles of self-repelling species

Using the information gathered on the pairs of self-repelling species, we systematically classify the remaining 27 networks of only self-repelling species. We further reduce that number to seven "elementary" networks onto which any cycle of self-repelling species can be mapped through symmetry operations, using the invariance of the eigenvalue Eq. (11) under cyclic swap of the catalytic species, and the invariance of Eq. (13) under mirror symmetry around one pair (see Appendix D). We then classify the stability of each elementary network based on which species pair they contain.

We find that two networks contain the always destabilizing pair XR – AA – RX Table II, and are thus unstable if the magnitude of the activities, mobilities, or homogeneous concentrations associated to it are tuned so that the associated term in Eq. (13) overcomes the stabilizing term from the other pairs. As these cycles can be made unstable simply by adjusting the parameters in order to give enough weight to one-pair terms, we call them type-IIa, or strongly, unstable. Another cycle, whose pair interactions go as AA–AA–RR, contains three conditionally destabilizing pairs. However, the inequalities to be satisfied for all three pairs to be stable are incompatible, and at least one of the three is necessarily instability-favouring. This cycle can then also be classified as type-IIa-unstable, with the only difference with the two previous one being that the instability-favoring pair can be different based on the choice of mobilities.

Two more elementary cycles can be made unstable, but with stricter criteria than those of type-IIa. These cycles only contain species pairs which are either stabilizing, or conditionally destabilizing. In order for these to be unstable, two criteria then need to be fulfilled: the species mobilities must be chosen so that at least one conditionally destabilizing pair is unstable, and enough weight must be given in Eq. (13) to this pair, so that the whole cycle is unstable, a condition which we name type-IIb (or weakly) unstable networks. Finally, two elementary cycles are only composed of stabilizing pairs, and thus cannot be made unstable.

VI. DISCUSSION

In this work, we have studied the behavior of a metabolic cycle of three catalytic species which chemotax in response to gradients of their substrates and products, and interact nonreciprocally owing to these two properties. We have demonstrated that the interaction network between the species can be built by independently choosing one interaction pattern per species, and that the stability of the resulting network can be determined by independently considering single-species and species-pair motifs. For the particular case of cycles composed of species with no chemotaxis in response to product gradients (only in response to substrate gradients), we have calculated a parameter-free stability line and used it to classify all the possible interaction networks in such cycles. We found that, for this reduced model, at least one self-attracting interaction motif must be present in order to observe self-organization. For cycles of species chemotactic in response to both substrate and product gradients, we derived two instability criteria from which the stability behavior of any choice of interaction motifs can be determined. The first condition (type-I) concerns the single-species interaction motifs, and translates the fact that the presence of a self-attracting species is sufficient for a cycle to potentially be unstable. In the case in which a cycle is composed strictly of self-repelling species, a second condition (type-II) becomes relevant, which involves interaction motifs between pairs of species. The contribution to all possible pair interaction motifs to this condition can be classified as either stabilizing, destabilizing, or conditionally destabilizing. In turn, this classification of pairs can be used to classify the stability of self-repelling cycles according to the pair motifs that they contain, and distinguish type-II unstable cycles as type-IIa, or strongly, unstable if they contain at least a destabilizing species pair, and type-IIb, or weakly, unstable if they only contain conditionally destabilizing (and stabilizing) pairs.

We have restricted our investigation here to size-three metabolic cycles, which are structures of small size and complexity compared to many biologically-relevant metabolic pathways. An immediate extension would then be to use the methods we developed for small cycles and to apply them to larger chemical reaction networks, or to non-cycle geometries. The most straightforward generalization is the study of metabolic cycles of more than three species, which have already been shown to exhibit complex and cycle-size-dependent behaviour [18]. Intriguingly, our motif-based classification has shown that, in a size-three cycle, pair interactions can lead to self-organization with more relaxed conditions than non-cyclic topologies. In particular, self-organization may occur even for systems in which all species are self-repelling, as studied in more detail in [17]. Larger cycle sizes likely result in the emergence of higher-order terms in the linear stability analysis (for instance, triplets of species in a size-four cycle), which could further relax the instability condition and lead to new types of instability. In the context of larger, more complex biochemical reaction networks, one possible approach could be to identify and analyze small key motifs in the reaction pathway, akin to the network motifs which are studied in systems biology [31, 32] and other disciplines [33]. Finally, recent works have demonstrated that the spatial self-organization of enzymes can optimize the overall reaction rate of a pathway [34] or be used as a method for regulating the output

of a branch in a reaction network [35]. Such effects could be investigated in the context of our model metabolic cycle, for instance by particularizing one of the reaction products and studying the effect of self-organization on its production rate. Conversely, the spatial arrangement of catalysts can be designed to increase reaction yield [36], implying that reaction networks could be also be designed with a similar goal in mind by choosing catalysts which self-organize into a reaction-flux-optimizing structure.

ACKNOWLEDGMENTS

APPENDICES

Appendix A: Linear stability analysis

The stability of a size-three metabolic cycle can be determined by performing a linear stability analysis of Eqs. (1) and (2) as follows. We consider a homogeneous steady state of Eqs. (1) and (2), with time- and space-independent concentrations c_{0k} for chemical species k and ρ_{0m} for catalytic species m. We then perturb this steady state with perturbations $\delta\rho_n(\mathbf{r}, t)$ and $\delta c_k(\mathbf{r}, t)$, and develop Eqs. (1) and (2) to the first order in perturbation. With the quasi-steady-state assumption that $\partial_t \delta c_k = 0$, corresponding to the limit of fast-diffusing chemicals species, and using the Fourier mode decomposition $\delta\rho_n = \delta\rho_n(\mathbf{k})\mathrm{e}^{\lambda t}\mathrm{e}^{i\mathbf{k}\mathbf{r}}$ and $\delta c_k = \delta c_k(\mathbf{k})\mathrm{e}^{\lambda t}\mathrm{e}^{i\mathbf{k}\mathbf{r}}$, we obtain the following equation:

$$(\lambda + D_\mathrm{p}k^2)\delta\rho_m(\mathbf{k}) = -\sum_{n=1}^{3} \Lambda_{m,n}\delta\rho_n(\mathbf{k}). \qquad (A1)$$

It is easily seen that, if $\mathrm{Re}(\lambda) > 0$, then the $k = 0$ mode, which corresponds to a system-wide perturbation, is the most unstable one. We then focus our analysis on that mode, and to simplify notation use $\delta\rho_m \equiv \delta\rho_m(k = 0)$, which leads to Eq. (3).

Appendix B: Brownian dynamics simulation

In order to test the stability criteria for strictly substrate-chemotactic species given in Eqs. (8) and (10), we perform Brownian dynamics simulations of our system. We consider spherical catalysts of diameter σ, which we also take as the size scale for our simulations, and assume that they isotropically convert their substrate into their product on their surface at a rate α.

We first derive the expression for the velocity which a catalytically-active particle develops as a response to the presence of another particle. Using the same quasi-steady state approximation used in the linear stability analysis, we can write that the concentration field associated with species k follows at any time the Laplace equation

$$D^{(k)}\nabla^2 c_k = 0, \qquad (B1)$$

with boundary conditions obtained by balancing the reactive and diffusive fluxes at the surface of the catalysts. A particle with index i induces a velocity response for another particle j by creating perturbations of the latter's substrate and product concentrations, which we write as $\delta c^{\mathrm{s}(j)}$ and $\delta c^{\mathrm{p}(j)}$ respectively. The corresponding velocity of j in the presence of i is then $\mathbf{v}_{ji} = \mathbf{v}_{ji}^{\mathrm{s}} + \mathbf{v}_{ji}^{\mathrm{p}}$ with $\mathbf{v}_{ji}^{\mathrm{s}} = -\mu_j^{(\mathrm{s})}\nabla\delta c_i^{\mathrm{s}(j)}$ and $\mathbf{v}_{ji}^{\mathrm{p}} = -\mu_j^{(\mathrm{s})}\nabla\delta c_i^{\mathrm{p}(j)}$, which finally results in:

$$\mathbf{v}_{ji} = \frac{\Lambda_{j,i}}{4\pi}\frac{\mathbf{r}_{ji}}{r_{ji}^3} \qquad (B2)$$

where $\mathbf{r}_{ji} = \mathbf{r}_j - \mathbf{r}_i$, and Λ is defined as in (4) except without the density ρ_{0m}.

The location $\mathbf{r}_i$ of catalyst i then evolves according to the Langevin equation

$$\frac{\mathrm{d}}{\mathrm{d}t}\mathbf{r}_i(t) = \sum_{j\neq i} \mathbf{v}_{ij} + \sqrt{2D_\mathrm{p}}\boldsymbol{\eta}_i \qquad (B3)$$

where $\boldsymbol{\eta}_i$ is a centred Gaussian white noise with intensity one. We simulate a mixture of three species, each of which has a population N_m, yielding a set of $N_1 + N_2 + N_3$ Langevin equations which we integrate using the forward Euler method with time step $\mathrm{d}t$ for a duration t_{tot}. The three chemical species are assumed to have the same diffusion coefficient, $D^{(1)} = D^{(2)} = D^{(3)} = D$. The quantities α_0 and μ_0 are arbitrary activity and mobility scales, from which a time scale $\tau = \alpha_0\mu_0/(4\pi D\sigma^3)$ and a diffusion coefficient scale $D_0 = (4\pi\sigma)/\alpha_0\mu_0$ can be built. The particles are simulated in a cubic box of size chosen so that the particles occupy a volume fraction $\Phi = 0.005$, with the interactions implemented according to the minimum image convention. Finally, we simulate short-range repulsion between the catalytic particles by performing an overlap correction after each time step using the elastic collision method described in [37].

To generate the phase diagram shown in Fig. 2, we simulate a set of $N_1 = N_2 = N_3 = 500$ particles with the following parameters: activity $\alpha/\alpha_0 = 1$, time step $\mathrm{d}t/\tau = 0.001$, simulation duration $t_{\mathrm{tot}}/\tau = 600$, noise intensity $D_\mathrm{p}/D_0 = 0.01$. The mobility of species 1 is fixed at $\mu_1^{(\mathrm{s})}/\mu_0 = \pm 0.33$, and the mobilities of species 2 and 3 are taken on a 20 by 20 grid with range $\mu_{2,3}^{(\mathrm{s})}/\mu_0 \in [-3, 3]$.

Appendix C: Determination of pair instability conditions

We use the fact that the three possible interaction motifs for self-repelling species are each associated to certain constraints on the species mobilities (see Fig. 1(c) for the mobility signs corresponding to the interactions):

- XA–RX: As $\mu_m^{(s)} < 0, \mu_m^{(p)} < 0, \mu_m^{(p)} > \mu_m^{(s)}$, we can write:

$$0 < \frac{\mu_m^{(p)}}{\mu_m^{(s)}} < 1 \tag{C1}$$

- XR–AX: As $\mu_m^{(s)} > 0, \mu_m^{(p)} > 0, \mu_m^{(p)} > \mu_m^{(s)}$, we can write:

$$0 < \frac{\mu_m^{(s)}}{\mu_m^{(p)}} < 1 \tag{C2}$$

- XA–AX: As $\mu_m^{(s)} < 0, \mu_m^{(p)} > 0$, we can write:

$$\frac{\mu_m^{(p)}}{\mu_m^{(s)}} < 0 \tag{C3}$$

We then study the stability of all possible pairs of these motifs. To do so, we first write the pair stability factor as given by Eq. (13). We write the condition $\Delta_{m,m+1} < 0$, subtract the negative terms so that the inequality only involves positive quantities, and rewrite the resulting inequality into a condition involving the ratios $\frac{\mu_{m \text{ or } m+1}^{(s)}}{\mu_{m \text{ or } m+1}^{(p)}}$ and $\frac{\mu_{m \text{ or } m+1}^{(p)}}{\mu_{m \text{ or } m+1}^{(s)}}$. From the conditions in Eqs. (C1) to (C3), it can then be determined whether the motif is unstable. For instance, for the interaction motif XA–RA–RX, the condition can be rearranged to have positive left- and right-hand-side terms as $\mu_m^{(p)}\mu_{m+1}^{(p)} + \mu_m^{(s)}\mu_{m+1}^{(s)} < \mu_m^{(s)}\mu_{m+1}^{(p)}$. This inequality can be further rearranged in terms of mobility ratios under the previously enumerated constraints as $\frac{\mu_{m+1}^{(s)}}{\mu_{m+1}^{(p)}} + \frac{\mu_m^{(p)}}{\mu_m^{(s)}} < 1$. Because $\frac{\mu_{m+1}^{(s)}}{\mu_{m+1}^{(p)}} > 1$ and $\frac{\mu_m^{(p)}}{\mu_m^{(s)}} > 0$, this condition is impossible to realize: the motif is always stable. By systematically applying this recipe, we analyze the stability of all motifs, which is given in Table II.

Appendix D: Mirror symmetry operation

One key aspect making the classification of cyclic networks easier is that the stability conditions are invariant under reflection symmetry around a pair of species. The corresponding symmetry operation is to swap the interaction network around a reflection line. For instance, applying a reflection symmetry around pair (2,3) involves:

- Turning $\mu_1^{(s)}$ into $-\mu_1^{(p)}$ and vice versa

- Turning $\mu_2^{(p)}$ into $-\mu_3^{(s)}$ and vice versa

- Turning $\mu_2^{(s)}$ into $-\mu_3^{(p)}$ and vice versa

with the sign change of the mobilities coming from the fact that substrate and product interactions of the same signs have opposite associated mobility signs. See Fig. 3 for a graphical example. Additionally, the activities and homogeneous densities of the species whose mobilities are swapped also need to be exchanged.

The stability of all possible networks of self-repelling species can then be determined by enumerating them and, for a given network, applying the cyclic swap and reflection symmetry to determine all equivalent networks. We can group the interaction networks of self-repelling species into three classes, based on whether they contain one, two, or three unique motifs. We determine the stability of each of the retained elementary networks using the method described in Section V B, and compile the results in Table I.
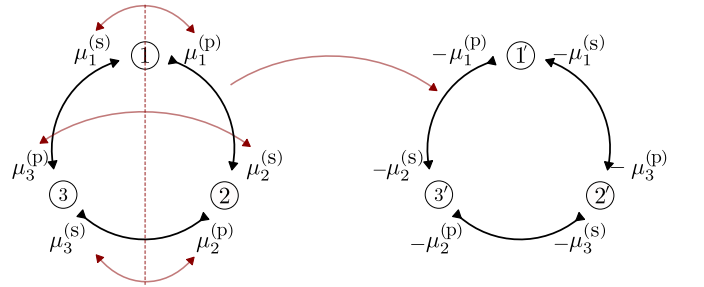
FIG. 3. Example of a reflection symmetry around pair $(2,3)$ applied to the network with pair interaction motifs AR–AA–RR, yielding the network RR–AA–RA, which is equivalent with respect to the second order instability condition.

[1] R. Golestanian, Phoretic Active Matter, in *Active Matter and Nonequilibrium Statistical Physics: Lecture Notes of the Les Houches Summer School: Volume 112, September 2018* (Oxford University Press, 2022).

[2] A. Varma, T. D. Montenegro-Johnson, and S. Michelin, Clustering-induced self-propulsion of isotropic au-

tophoretic particles, Soft Matter **14**, 7155 (2018).

[3] H. Stark, Artificial chemotaxis of self-phoretic active colloids: Collective behavior, Accounts of Chemical Research **51**, 2681 (2018).

[4] S. Saha, R. Golestanian, and S. Ramaswamy, Clusters, asters, and collective oscillations in chemotactic colloids,

Phys. Rev. E **89**, 062316 (2014).

[5] F. Schmidt, B. Liebchen, H. Löwen, and G. Volpe, Light-controlled assembly of active colloidal molecules, The Journal of Chemical Physics **150**, 094905 (2019).

[6] R. Golestanian, Collective Behavior of Thermally Active Colloids, Physical Review Letters **108**, 038303 (2012).

[7] J. A. Cohen and R. Golestanian, Emergent Cometlike Swarming of Optically Driven Thermally Active Colloids, Physical Review Letters **112**, 068302 (2014).

[8] E. F. Keller and L. A. Segel, Initiation of slime mold aggregation viewed as an instability, Journal of Theoretical Biology **26**, 399 (1970).

[9] A. Gelimson and R. Golestanian, Collective Dynamics of Dividing Chemotactic Cells, Physical Review Letters **114**, 028101 (2015).

[10] R. Soto and R. Golestanian, Self-Assembly of Catalytically Active Colloidal Molecules: Tailoring Activity Through Surface Chemistry, Physical Review Letters **112**, 068301 (2014).

[11] R. Soto and R. Golestanian, Self-assembly of active colloidal molecules with dynamic function, Physical Review E **91**, 052304 (2015).

[12] A. Sengupta, T. Kruppa, and H. Löwen, Chemotactic predator-prey dynamics, Physical Review E **83**, 031914 (2011).

[13] C. H. Meredith, P. G. Moerman, J. Groenewold, Y.-J. Chiu, W. K. Kegel, A. van Blaaderen, and L. D. Zarzar, Predator–prey interactions between droplets driven by non-reciprocal oil exchange, Nat. Chem. **12**, 1136 (2020).

[14] S. Saha, J. Agudo-Canalejo, and R. Golestanian, Scalar Active Mixtures: The Nonreciprocal Cahn-Hilliard Model, Physical Review X **10**, 041009 (2020).

[15] M. Fruchart, R. Hanai, P. B. Littlewood, and V. Vitelli, Non-reciprocal phase transitions, Nature **592**, 363 (2021).

[16] J. Agudo-Canalejo and R. Golestanian, Active Phase Separation in Mixtures of Chemically Interacting Particles, Phys. Rev. Lett. **123**, 018101 (2019).

[17] V. Ouazan-Reboul, J. Agudo-Canalejo, and R. Golestanian, Network effects lead to self-organization in metabolic cycles of self-repelling catalysts, arXiv:2303.09832 ().

[18] V. Ouazan-Reboul, J. Agudo-Canalejo, and R. Golestanian, Self-organization of primitive metabolic cycles due to non-reciprocal interactions, arXiv:2303.09832 ().

[19] K. A. Dill, S. B. Ozkan, M. S. Shell, and T. R. Weikl, The Protein Folding Problem, Annual Review of Biophysics **37**, 289 (2008).

[20] K. A. Dill, Theory for the folding and stability of globular proteins, Biochemistry **24**, 1501 (1985).

[21] R. Phillips, J. Kondev, J. Theriot, H. G. Garcia, and N. Orme, *Physical Biology of the Cell*, 2nd ed. (Garland Science, New York, 2012).

[22] T. Hoque, M. Chetty, and A. Sattar, Extended HP Model for Protein Structure Prediction, Journal of Computational Biology **16**, 85 (2009).

[23] H. S. Chan, Folding alphabets, Nature Structural Biology **6**, 994 (1999).

[24] D. S. Riddle, J. V. Santiago, S. T. Bray-Hall, N. Doshi, V. P. Grantcharova, Q. Yi, and D. Baker, Functional rapidly folding proteins from simplified amino acid sequences, Nature Structural Biology **4**, 805 (1997).

[25] J. Jumper, R. Evans, A. Pritzel, T. Green, M. Figurnov, O. Ronneberger, K. Tunyasuvunakool, R. Bates, A. Žídek, A. Potapenko, A. Bridgland, C. Meyer, S. A. A. Kohl, A. J. Ballard, A. Cowie, B. Romera-Paredes, S. Nikolov, R. Jain, J. Adler, T. Back, S. Petersen, D. Reiman, E. Clancy, M. Zielinski, M. Steinegger, M. Pacholska, T. Berghammer, S. Bodenstein, D. Silver, O. Vinyals, A. W. Senior, K. Kavukcuoglu, P. Kohli, and D. Hassabis, Highly accurate protein structure prediction with AlphaFold, Nature **596**, 583 (2021).

[26] H. Li, R. Helling, C. Tang, and N. Wingreen, Emergence of preferred structures in a simple model of protein folding, Science **273**, 666 (1996).

[27] H. Li, C. Tang, and N. S. Wingreen, Are protein folds atypical?, Proceedings of the National Academy of Sciences **95**, 4987 (1998).

[28] W. A. Lim and R. T. Sauer, Alternative packing arrangements in the hydrophobic core of λ repressor, Nature **339**, 31 (1989).

[29] S. Kamtekar, J. M. Schiffer, H. Xiong, J. M. Babik, and M. H. Hecht, Protein Design by Binary Patterning of Polar and Nonpolar Amino Acids, Science **262**, 1680 (1993).

[30] V. Ouazan-Reboul, J. Agudo-Canalejo, and R. Golestanian, Non-equilibrium phase separation in mixtures of catalytically active particles: Size dispersity and screening effects, Eur. Phys. J. E **44**, 113 (2021).

[31] U. Alon, Network motifs: Theory and experimental approaches, Nature Reviews Genetics **8**, 450 (2007).

[32] R. Milo, S. Shen-Orr, S. Itzkovitz, N. Kashtan, D. Chklovskii, and U. Alon, Network Motifs: Simple Building Blocks of Complex Networks, Science **298**, 824 (2002).

[33] L. Stone, D. Simberloff, and Y. Artzy-Randrup, Network motifs and their origins, PLOS Computational Biology **15**, e1006749 (2019).

[34] A. Buchner, F. Tostevin, and U. Gerland, Clustering and Optimal Arrangement of Enzymes in Reaction-Diffusion Systems, Physical Review Letters **110**, 208104 (2013).

[35] F. Hinzpeter, F. Tostevin, and U. Gerland, Regulation of reaction fluxes via enzyme sequestration and coclustering, J. R. Soc. Interface **16**, 20190444 (2019).

[36] C. Xie, C. Chen, Y. Yu, J. Su, Y. Li, G. A. Somorjai, and P. Yang, Tandem Catalysis for CO2 Hydrogenation to C2–C4 Hydrocarbons, Nano Letters **17**, 3798 (2017).

[37] P. Strating, Brownian dynamics simulation of a hard-sphere suspension, Phys. Rev. E **59**, 2175 (1999).

6
Conclusion and discussion

An exciting trend in current research is the increasing coupling between biology and physics, which can for instance be illustrated with the link between biomolecular condensates and the physics of liquid-liquid phase separation. The field of active matter is an integral part of this trend, encountering some success in the description of groups of organisms[185] and at the same time inspiring new physical theories[102]. A similar approach motivates the work undertaken in this thesis, in which we attempted to bridge observations made on catalytic enzymes and biomolecular condensates with the physics of non-reciprocally interacting active particles.

Here, we have contributed to this dynamic field of research by extending existing models to capture additional effects which are relevant to biological systems and introduce new

collective behaviors. Two main lines of investigation were followed: a more detailed description of the catalytic species, and the introduction of several chemical fields which the catalysts specifically interact with, with a focus on cyclic reaction networks.

In Chapter 2, we analytically studied the consequences at the collective level of a detailed description of self-organizing enzymes. We found that adding a linear concentration dependence of catalytic activity on substrate concentration couples the active species' activity and mobility terms in a manner which inhibits self-organization. This is manifested by an effective screening term, which leads to a stricter criterion for self-organization and a switch from system-wide to finite-size clustering. We then analyzed the effect of size differences between different enzymes, which limited our study to binary mixtures. We discovered that considering two catalytic species with different diffusion coefficients leads to the emergence of two new behaviors: local self-organization with a loosened instability criterion, and oscillatory global self-organization. Taking both effects into account was shown to result in a rich stability phase diagram, which can undergo local self-organization with different oscillatory behaviors based on the species' parameters.

In Chapter 3, motivated by the study of an origin-of-life scenario, we analytically and numerically characterized the behavior of an arbitrary number of catalytic species participating in a metabolic cycle. As a part of this structure, each species provides its product as the substrate of the next; this introduces a topology to the inter-species interactions, which qualitatively changes the self-organization process. Particle-based simulations showed that the metabolic cycles can aggregate with a faster-than-exponential time dependence, which constitutes a candidate mechanism through which early components of protocells could quickly come together. Strikingly, we demonstrated, both analytically and numerically, that the phe-

nomenology of the system is totally different based on whether the cycle contains an even or an odd number of species. A cycle composed of an even number of species can aggregate into two balanced clusters, which is not possible if the number of species is odd. The resulting frustration can lead to oscillatory steady states involving periodic cluster formation and dissolution.

The study of metabolic cycles was continued in Chapter 4 with a different approach. Instead of a cycle of arbitrary size where all species have the same parameters, we considered another limiting case for which analytical calculations are readily carried out: a metabolic cycle of three species with distinct parameters. This allowed for more general interaction patterns between the catalysts, leading to an unique feature which was the focus of this chapter: the ability of an overall self-repelling cycle to self-organize. The condition for this mode of self-organization was analytically calculated in the simplified case involving catalytic species which only chemotax in concentration gradients of their substrate. The resulting expression forbade the self-organization of cycles composed only of self-repelling species, a process which we instead found to be possible if the catalytic species chemotax in gradients of both their substrate and product. We derived a set of sufficient conditions for this all-repelling-self-organization to be possible, and drew a phase diagram for a specific choice of parameters which we validated and illustrated using particle-based numerical simulations.

Chapter 5 is also related to the three-species metabolic cycles described in Chapter 4. We performed a comprehensive survey of the possible self-organization behaviors such cycles can exhibit, based on the interaction patterns between their constitutive species. We once again started with the study of cycles of non-product-chemotactic catalysts, for which we derived a parameter-free stability phase diagram that we validated with numerical simulations. In the

case of species both substrate- and product-chemotactic species, we found two instability conditions, which allowed for the classification of all possible three-species interaction networks based on the single- and pair-interaction motifs they contain.

Following this overview of the results presented in this thesis, we would like to present some ideas for future research.

A natural extension of our existing work would be to continue the path initially laid out in Chapter 2, and to further refine our description of catalytically active particles. One possible addition would be a dependence of the chemotactic mobility μ of the active species on their substrate's concentration, for instance by multiplying it with a normalized sensing function with values between 0 and 1. Such a term would be relevant to the study of chemotactic bacteria, which can be described with similar equations as the ones involved in Chapter 2[116], in which case a natural choice would be logarithmic sensing[36]. A consequence of this would be an added dependence of the chemotactic flux on the magnitude of the concentration field, as opposed to only its gradient, adding further coupling between activity and mobility, which is already known to have an influence in a Keller-Segel description of bacterial chemotaxis[117].

A limitation of our approach which would be very informative to overcome is that the analytical and numerical methods we use are technically valid only at low densities. Linear stability analysis indeed only describes a system at the onset of instability, and the particle-based Brownian dynamics simulations we performed use a far-field approximation. Taking into account near-field effects can qualitatively change the behaviors of active particles at a small separation[98], which could influence the phase-separated state observed in simulations. To incorporate these effects in our work, we could attempt generalizing the exact solution for the phoretic velocity of a pair of catalytic particles to an arbitrary number of them. Another

option would be to perform hybrid particle-field simulations, such as the ones described in Ref. 186, which would also allow us to go beyond the quasi-static assumption made for the field dynamics.

Such simulations can also include the activity dependence on concentration which was studied at the linear level in Chapter 2, with the added benefit of considering the full Michaelis-Menten kinetics. This would allow us to test the analytical phase diagram derived in Chapter 2, and to observe the predicted modes of self-organization. Another question which could be tackled through the study of the phase-separated regime accessible in simulations is the effect of enzyme clustering on their reaction flux. Previous work (Ref. 187) has studied the effect of enzyme spatial structuring on the catalytic flux for several spatial patterns, but has done so by considering initially phase-separated enzymes. Meanwhile, Ref. 178 describes the phase separation of an enzyme-substrate-product mixture with a Flory-Huggins-based description, and predicts a reduction of the catalytic flux in the phase-separated state. Simulations would give us access to similar information for our model chemotactic catalysts, and allow us to determine the modification of catalytic reaction flux induced by chemotactic self-organization and its dependence upon the choice of parameters. The work undertaken in Chapters 3 to 5 also opens the door to the study of the effect of self-organization on the efficiency of actual metabolic pathways. This would necessitate the study of non-cyclic topologies, and the "opening" of the metabolic cycles to capture the input and output of reaction material.

The results obtained in Chapters 3 to 5 can be viewed as a first exploration of the behavior of the chemotactic interaction networks which can emerge from the combination of field-mediated interactions and metabolic reaction networks. Even in very simple metabolic cycle

geometries, the combinatorial number of possible interaction network leads to a wide variety of possible behaviors, in particular the overcoming of the overall-self-attracting instability condition previously derived for catalytically active systems (Refs. 139, Chapters 2 and 3). A natural extension of that work would be to consider metabolic cycles of arbitrary size with species-dependent parameters, in which higher orders of combinations of interspecies couplings would become relevant, which we predict could lead to more relaxed self-organization conditions as the cycle size grows. Such generalized results could be relevant to the study of chemically active biomolecular condensates: for instance the purinosome[171] concentrates at least ten enzymes, implying high-order coupling between the enzyme species involved in the relevant pathway. These results could then shine light on the relevance of enzyme chemotaxis to the formation of active condensates.

One limit of the work undertaken in this thesis is its purely theoretical nature, which would be well complemented by experimental studies. Our work relies on the assumption that catalytically active particles, and in particular enzymes, develop effective interactions through the chemical fields upon which they act. While such interactions have been experimentally observed in active colloids[118] and active droplets[106], we have found no direct evidence of interactions between active enzymes in the literature. Existing experimental results mostly cover the colocation of active enzymes involved in a reaction cascade[92,180], and so it would be an interesting undertaking to perform single-molecule experiments such as the ones used to observe enhanced diffusion in order to measure the effect the presence a single enzyme has on the motion of another. We think an ideal model system for testing our predictions are catalytically active colloids, for instance in order to test our results on the self-organization of metabolic cycles. This could in principle be achieved by using colloids coated with successive enzymes

involved in a relatively simple metabolic cycle, for instance the Calvin cycle[188]. Enzyme-coated colloids[189] and liposomes[190] have indeed been shown to chemotax, and their microscopic size makes the observation of their behavior much easier than individual enzymes'. Additionally, as the stability phase diagrams we established involve the homogeneous concentration of the active species, simply varying the amount of colloids may suffice to explore all the possible phase behaviors.

A common thread of our work has been to consider non-reciprocal interactions only for isotropic (i.e. non-polar) particles. As has been shown[80,82,140], generalizing field-mediated interactions to Janus colloids, which have some anisotropy, leads to a rich phenomenology compared to isotropic particles. We would like to adapt our models to such situations, for instance by generalizing the model of Ref. 99 to a multi-species mixture of active colloids.

We motivate a large portion of our work with the observed ability of enzymes to chemotax. However, due to their nanometric size, enzymes are very sensitive to thermal fluctuations, as has been previously explored in theoretical work modeling them as two hydrodynamically coupled subunits which experience fluctuations[191,192]. This stochasticity is not captured by the mean-field, Keller-Segel-like formalism which we used throughout our work. A complementary approach would then be to write a bottom-up model, starting from a Langevin description of catalytic enzymes, and to build a many-body theory for an enzyme mixture[122,125].

Finally, on a much more long-term note, the spatial self-organization of catalysts may even have some industrial applications. Enzymes are known to be staggeringly better at speeding up reactions than artificial catalysts[141], and an increasing body of research is dedicated to harnessing them for industrial processes, in particular biofuel cells[193,194]. As it now established that concentrating enzymes into droplet-like structures increases their catalytic activity[175], re-

search has now started on the possibility of spatially organizing enzymes in order to maximize their yield[195]. A better theoretical understanding of the processes of enzyme self-organization could ultimately lead to the development of more efficient catalysts for industrial processes.

References

[1] Andrea Cavagna and Irene Giardina. Bird Flocks as Condensed Matter. *Annual Review of Condensed Matter Physics*, 5(1):183–207, 2014. doi:10.1146/annurev-conmatphys-031113-133834.

[2] Brian L. Partridge, Tony Pitcher, J. Michael Cullen, and John Wilson. The three-dimensional structure of fish schools. *Behavioral Ecology and Sociobiology*, 6(4):277–288, March 1980. doi:10.1007/BF00292770.

[3] Eric Karsenti. Self-organization in cell biology: A brief history. *Nature Reviews Molecular Cell Biology*, 9(3):255–262, March 2008. doi:10.1038/nrm2357.

[4] Tamás Vicsek, András Czirók, Eshel Ben-Jacob, Inon Cohen, and Ofer Shochet. Novel Type of Phase Transition in a System of Self-Driven Particles. *Physical Review Letters*, 75(6):1226–1229, August 1995. doi:10.1103/PhysRevLett.75.1226.

[5] M. C. Marchetti, J. F. Joanny, S. Ramaswamy, T. B. Liverpool, J. Prost, Madan Rao, and R. Aditi Simha. Hydrodynamics of soft active matter. *Reviews of Modern Physics*, 85(3):1143–1189, July 2013. doi:10.1103/RevModPhys.85.1143.

[6] Sriram Ramaswamy. The Mechanics and Statistics of Active Matter. *Annual Review of Condensed Matter Physics*, 1(1):323–345, August 2010. doi:10.1146/annurev-conmatphys-070909-104101.

[7] Gerhard Gompper, Roland G Winkler, Thomas Speck, Alexandre Solon, Cesare Nardini, Fernando Peruani, Hartmut Löwen, Ramin Golestanian, U Benjamin Kaupp, Luis Alvarez, Thomas Kiørboe, Eric Lauga, Wilson C K Poon, Antonio DeSimone, Santiago Muiños-Landin, Alexander Fischer, Nicola A Söker, Frank Cichos, Raymond Kapral, Pierre Gaspard, Marisol Ripoll, Francesc Sagues, Amin Doostmohammadi, Julia M Yeomans, Igor S Aranson, Clemens Bechinger, Holger Stark, Charlotte K Hemelrijk, François J Nedelec, Trinish Sarkar, Thibault Aryaksama, Mathilde Lacroix, Guillaume Duclos, Victor Yashunsky, Pascal Silberzan, Marino Arroyo, and Sohan Kale. The 2020 motile active matter roadmap. *Journal of Physics: Condensed Matter*, 32(19):193001, May 2020. doi:10.1088/1361-648X/ab6348.

[8] Clemens Bechinger, Roberto Di Leonardo, Hartmut Löwen, Charles Reichhardt, Giorgio Volpe, and Giovanni Volpe. Active Particles in Complex and Crowded Environments. *Reviews of Modern Physics*, 88(4):045006, November 2016. doi:10.1103/RevModPhys.88.045006.

[9] John Toner, Yuhai Tu, and Sriram Ramaswamy. Hydrodynamics and phases of flocks. *Annals of Physics*, 318(1):170–244, July 2005. doi:10.1016/j.aop.2005.04.011.

[10] Eric Bertin, Michel Droz, and Guillaume Grégoire. Boltzmann and hydrodynamic description for self-propelled particles. *Physical Review E*, 74(2):022101, August 2006. doi:10.1103/PhysRevE.74.022101.

[11] Gašper Tkačik and William Bialek. Information Processing in Living Systems. *Annual Review of Condensed Matter Physics*, 7(1):89–117, 2016. doi:10.1146/annurev-conmatphys-031214-014803.

[12] George H. Wadhams and Judith P. Armitage. Making sense of it all: Bacterial chemotaxis. *Nature Reviews Molecular Cell Biology*, 5(12):1024–1037, December 2004. doi:10.1038/nrm1524.

[13] Gautam Reddy, Venkatesh N. Murthy, and Massimo Vergassola. Olfactory Sensing and Navigation in Turbulent Environments. *Annual Review of Condensed Matter Physics*, 13(1):191–213, 2022. doi:10.1146/annurev-conmatphys-031720-032754.

[14] Eric Lauga and Thomas R. Powers. The hydrodynamics of swimming microorganisms. *Reports on Progress in Physics*, 72(9):096601, August 2009. doi:10.1088/0034-4885/72/9/096601.

[15] E. M. Purcell. Life at low Reynolds number. *American Journal of Physics*, 45(1):3–11, January 1977. doi:10.1119/1.10903.

[16] Eric Lauga. Life around the scallop theorem. *Soft Matter*, 7(7):3060–3065, 2011. doi:10.1039/C0SM00953A.

[17] Howard C. Berg, editor. *E. Coli in Motion*. Biological and Medical Physics, Biomedical Engineering. Springer, New York, NY, 2004. doi:10.1007/b97370.

[18] Howard C. Berg. The Rotary Motor of Bacterial Flagella. *Annual Review of Biochemistry*, 72(1):19–54, 2003. doi:10.1146/annurev.biochem.72.121801.161737.

[19] Felix Thiel, Lutz Schimansky-Geier, and Igor M. Sokolov. Anomalous diffusion in run-and-tumble motion. *Physical Review E*, 86(2):021117, August 2012. doi:10.1103/PhysRevE.86.021117.

[20] F. Matthäus, M. Jagodič, and J. Dobnikar. E. coli Superdiffusion and Chemotaxis—Search Strategy, Precision, and Motility. *Biophysical Journal*, 97(4):946–957, August 2009. doi:10.1016/j.bpj.2009.04.065.

[21] Howard C. Berg and Douglas A. Brown. Chemotaxis in Escherichia coli analysed by Three-dimensional Tracking. *Nature*, 239(5374):500–504, October 1972. doi:10.1038/239500a0.

[22] Rachel R. Bennett and Ramin Golestanian. A steering mechanism for phototaxis in Chlamydomonas. *Journal of The Royal Society Interface*, 12(104):20141164, March 2015. doi:10.1098/rsif.2014.1164.

[23] Anja Paulick, Vladimir Jakovljevic, SiMing Zhang, Michael Erickstad, Alex Groisman, Yigal Meir, William S Ryu, Ned S Wingreen, and Victor Sourjik. Mechanism of bidirectional thermotaxis in Escherichia coli. *eLife*, 6:e26607, August 2017. doi:10.7554/eLife.26607.

[24] Jonas Cremer, Tomoya Honda, Ying Tang, Jerome Wong-Ng, Massimo Vergassola, and Terence Hwa. Chemotaxis as a navigation strategy to boost range expansion. *Nature*, 575(7784):658–663, November 2019. doi:10.1038/s41586-019-1733-y.

[25] Leanid Laganenka, Remy Colin, and Victor Sourjik. Chemotaxis towards autoinducer 2 mediates autoaggregation in Escherichia coli. *Nature Communications*, 7(1):12984, September 2016. doi:10.1038/ncomms12984.

[26] Remy Colin, Bin Ni, Leanid Laganenka, and Victor Sourjik. Multiple functions of flagellar motility and chemotaxis in bacterial physiology. *FEMS Microbiology Reviews*, 45(6):fuab038, November 2021. doi:10.1093/femsre/fuab038.

[27] Gudrun F. Debes, Carrie N. Arnold, Alan J. Young, Stefan Krautwald, Martin Lipp, John B. Hay, and Eugene C. Butcher. Chemokine receptor CCR7 required for T lymphocyte exit from peripheral tissues. *Nature Immunology*, 6(9):889–894, September 2005. doi:10.1038/ni1238.

[28] Francis Lin and Eugene C. Butcher. T cell chemotaxis in a simple microfluidic device. *Lab on a Chip*, 6(11):1462–1469, 2006. doi:10.1039/B607071J.

[29] C R Mackay. Chemokine receptors and T cell chemotaxis. *Journal of Experimental Medicine*, 184(3):799–802, September 1996. doi:10.1084/jem.184.3.799.

[30] Evanthia T. Roussos, John S. Condeelis, and Antonia Patsialou. Chemotaxis in cancer. *Nature Reviews Cancer*, 11(8):573–587, August 2011. doi:10.1038/nrc3078.

[31] G Gerisch. Chemotaxis in Dictyostelium. *Annual Review of Physiology*, 44(1):535–552, 1982. doi:10.1146/annurev.ph.44.030182.002535.

[32] Shuangyu Bi and Victor Sourjik. Stimulus sensing and signal processing in bacterial chemotaxis. *Current Opinion in Microbiology*, 45:22–29, October 2018. doi:10.1016/j.mib.2018.02.002.

[33] Victor Sourjik and Ned S Wingreen. Responding to chemical gradients: Bacterial chemotaxis. *Current Opinion in Cell Biology*, 24(2):262–268, April 2012. doi:10.1016/j.ceb.2011.11.008.

[34] A. Celani, T. S. Shimizu, and M. Vergassola. Molecular and Functional Aspects of Bacterial Chemotaxis. *Journal of Statistical Physics*, 144(2):219–240, July 2011. doi:10.1007/s10955-011-0251-6.

[35] Evelyn F. Keller and Lee A. Segel. Model for chemotaxis. *Journal of Theoretical Biology*, 30(2):225–234, February 1971. doi:10.1016/0022-5193(71)90050-6.

[36] Yevgeniy V. Kalinin, Lili Jiang, Yuhai Tu, and Mingming Wu. Logarithmic Sensing in Escherichia coli Bacterial Chemotaxis. *Biophysical Journal*, 96(6):2439–2448, March 2009. doi:10.1016/j.bpj.2008.10.027.

[37] Evelyn F. Keller and Lee A. Segel. Initiation of slime mold aggregation viewed as an instability. *J. Theor. Biol.*, 26(3):399–415, March 1970. doi:10.1016/0022-5193(70)90092-5.

[38] Holger Stark. Artificial Chemotaxis of Self-Phoretic Active Colloids: Collective Behavior. *Accounts of Chemical Research*, 51(11):2681–2688, November 2018. doi:10.1021/acs.accounts.8b00259.

[39] Jaime Agudo-Canalejo, Tunrayo Adeleke-Larodo, Pierre Illien, and Ramin Golestanian. Enhanced Diffusion and Chemotaxis at the Nanoscale. *Acc. Chem. Res.*, 51(10):2365–2372, October 2018. doi:10.1021/acs.accounts.8b00280.

[40] Jiang-Xing Chen, Yu-Guo Chen, and Yu-Qiang Ma. Chemotactic dynamics of catalytic dimer nanomotors. *Soft Matter*, 12(6):1876–1883, 2016. doi:10.1039/C5SM02647D.

[41] Theresa Jakuszeit, James Lindsey-Jones, François J. Peaudecerf, and Ottavio A. Croze. Migration and accumulation of bacteria with chemotaxis and chemokinesis. *The European Physical Journal E*, 44(3):32, March 2021. doi:10.1140/epje/s10189-021-00009-w.

[42] Dina Ralt, Mira Manor, Anat Cohen-Dayag, Ilan Tur-Kaspa, Izhar Ben-Shlomo, Amnon Makler, Izhak Yuli, Jehoshua Dor, Shmaryahu Blumberg, Shlomo Mashiach, and Michael Eisenbach. Chemotaxis and Chemokinesis of Human Spermatozoa to Follicular Factors1. *Biology of Reproduction*, 50(4):774–785, April 1994. doi:10.1095/biolreprod50.4.774.

[43] Linlin Wang, Andrea Kaeppler, Dieter Fischer, and Juliane Simmchen. Photocatalytic TiO2 Micromotors for Removal of Microplastics and Suspended Matter. *ACS Applied Materials & Interfaces*, 11(36):32937–32944, September 2019. doi:10.1021/acsami.9b06128.

[44] Jemish Parmar, Diana Vilela, Katherine Villa, Joseph Wang, and Samuel Sánchez. Micro- and Nanomotors as Active Environmental Microcleaners and Sensors. *Journal of the American Chemical Society*, 140(30):9317–9331, August 2018. doi:10.1021/jacs.8b05762.

[45] Wei Gao and Joseph Wang. Synthetic micro/nanomotors in drug delivery. *Nanoscale*, 6(18):10486–10494, 2014. doi:10.1039/C4NR03124E.

[46] Xiaoping Yu, Yana Li, Jie Wu, and Huangxian Ju. Motor-Based Autonomous Microsensor for Motion and Counting Immunoassay of Cancer Biomarker. *Analytical Chemistry*, 86(9):4501–4507, May 2014. doi:10.1021/ac500912c.

[47] Rémi Dreyfus, Jean Baudry, Marcus L. Roper, Marc Fermigier, Howard A. Stone, and Jérôme Bibette. Microscopic artificial swimmers. *Nature*, 437(7060):862–865, October 2005. doi:10.1038/nature04090.

[48] Wei Gao, Sirilak Sattayasamitsathit, Kalayil Manian Manesh, Daniel Weihs, and Joseph Wang. Magnetically Powered Flexible Metal Nanowire Motors. *Journal of the American Chemical Society*, 132(41):14403–14405, October 2010. doi:10.1021/ja1072349.

[49] Ramin Golestanian. Phoretic Active Matter. In Julien Tailleur, Gerhard Gompper, M Cristina Marchetti, Julia M Yeomans, and Christophe Salomon, editors, *Active matter and nonequilibrium statistical physics*, Lecture Notes of the 2018 Les Houches Summer School. Oxford University Press, London, England, November 2022.

[50] B. V. Derjaguin, N. V. Churaev, and V. M. Muller. *Surface Forces*. Springer US, Boston, MA, 1987. doi:10.1007/978-1-4757-6639-4.

[51] J Anderson. Colloid Transport by Interfacial Forces. *Annu. Rev. Fluid Mech.*, 21:61–99, November 1989. doi:10.1146/annurev.fl.21.010189.000425.

[52] Shawn A. Putnam and David G. Cahill. Transport of Nanoscale Latex Spheres in a Temperature Gradient. *Langmuir*, 21(12):5317–5323, June 2005. doi:10.1021/la047056h.

[53] R. Piazza and A. Parola. Thermophoresis in colloidal suspensions. *Journal of Physics: Condensed Matter*, 20(15):153102, March 2008. doi:10.1088/0953-8984/20/15/153102.

[54] John L Anderson. Effect of nonuniform zeta potential on particle movement in electric fields. *Journal of Colloid and Interface Science*, 105(1):45–54, May 1985. doi:10.1016/0021-9797(85)90345-5.

[55] F. A Morrison. Electrophoresis of a particle of arbitrary shape. *Journal of Colloid and Interface Science*, 34(2):210–214, October 1970. doi:10.1016/0021-9797(70)90171-2.

[56] R. W O'Brien and D. N Ward. The electrophoresis of a spheroid with a thin double layer. *Journal of Colloid and Interface Science*, 121(2):402–413, February 1988. doi:10.1016/0021-9797(88)90443-2.

[57] J. P. Ebel, John L. Anderson, and D. C. Prieve. Diffusiophoresis of latex particles in electrolyte gradients. *Langmuir*, 4(2):396–406, March 1988. doi:10.1021/la00080a024.

[58] B. V. Derjaguin, S. S. Dukhin, and A. A. Korotkova. Diffusiophoresis in electrolyte solutions and its role in the Mechanism of the formation of films from caoutchouc latexes by the ionic deposition method. *Progress in Surface Science*, 43(1):153–158, May 1993. doi:10.1016/0079-6816(93)90024-P.

[59] B. V. Derjaguin, G. Sidorenkov, E. Zubashchenko, and E. Kiseleva. Kinetic Phenomena in the boundary layers of liquids 1. the capillary osmosis. *Progress in Surface Science*, 43(1):138–152, May 1993. doi:10.1016/0079-6816(93)90023-O.

[60] J. L. Anderson, M. E. Lowell, and D. C. Prieve. Motion of a particle generated by chemical gradients Part 1. Non-electrolytes. *Journal of Fluid Mechanics*, 117:107–121, April 1982. doi:10.1017/S0022112082001542.

[61] John L. Anderson. Movement of a semipermeable vesicle through an osmotic gradient. *The Physics of Fluids*, 26(10):2871–2879, October 1983. doi:10.1063/1.864051.

[62] Jaime Agudo-Canalejo, Pierre Illien, and Ramin Golestanian. Phoresis and Enhanced Diffusion Compete in Enzyme Chemotaxis. *Nano. Lett.*, 18(4):2711–2717, April 2018. doi:10.1021/acs.nanolett.8b00717.

[63] Howard A. Stone and Aravinthan D. T. Samuel. Propulsion of Microorganisms by Surface Distortions. *Physical Review Letters*, 77(19):4102–4104, November 1996. doi:10.1103/PhysRevLett.77.4102.

[64] B. Abécassis, C. Cottin-Bizonne, C. Ybert, A. Ajdari, and L. Bocquet. Boosting migration of large particles by solute contrasts. *Nature Materials*, 7(10):785–789, October 2008. doi:10.1038/nmat2254.

[65] Frank Jülicher and Jacques Prost. Generic theory of colloidal transport. *Eur. Phys. J. E*, 29:27–36, 2009. doi:10.1140/epje/i2008-10446-8.

[66] Jeffrey L. Moran and Jonathan D. Posner. Phoretic Self-Propulsion. *Annual Review of Fluid Mechanics*, 49(1):511–540, 2017. doi:10.1146/annurev-fluid-122414-034456.

[67] R. Golestanian, T. B. Liverpool, and A. Ajdari. Designing phoretic micro- and nano-swimmers. *New J. Phys.*, 9(5):126–126, May 2007. doi:10.1088/1367-2630/9/5/126.

95

[68] Pierre Illien, Ramin Golestanian, and Ayusman Sen. 'Fuelled' motion: Phoretic motility and collective behaviour of active colloids. *Chemical Society Reviews*, 46(18):5508–5518, 2017. doi:10.1039/C7CS00087A.

[69] Ramin Golestanian, Tanniemola B. Liverpool, and Armand Ajdari. Propulsion of a Molecular Machine by Asymmetric Distribution of Reaction Products. *Physical Review Letters*, 94(22):220801, June 2005. doi:10.1103/PhysRevLett.94.220801.

[70] Walter F. Paxton, Kevin C. Kistler, Christine C. Olmeda, Ayusman Sen, Sarah K. St. Angelo, Yanyan Cao, Thomas E. Mallouk, Paul E. Lammert, and Vincent H. Crespi. Catalytic Nanomotors: Autonomous Movement of Striped Nanorods. *Journal of the American Chemical Society*, 126(41):13424–13431, October 2004. doi:10.1021/ja047697z.

[71] Sébastien Michelin, Eric Lauga, and Denis Bartolo. Spontaneous autophoretic motion of isotropic particles. *Physics of Fluids*, 25(6):061701, June 2013. doi:10.1063/1.4810749.

[72] Rodrigo Soto and Ramin Golestanian. Self-Assembly of Catalytically Active Colloidal Molecules: Tailoring Activity Through Surface Chemistry. *Physical Review Letters*, 112(6):068301, February 2014. doi:10.1103/PhysRevLett.112.068301.

[73] Rodrigo Soto and Ramin Golestanian. Self-assembly of active colloidal molecules with dynamic function. *Phys. Rev. E*, 91(5):052304, May 2015. doi:10.1103/PhysRevE.91.052304.

[74] Akhil Varma, Thomas D. Montenegro-Johnson, and Sébastien Michelin. Clustering-induced self-propulsion of isotropic autophoretic particles. *Soft Matter*, 14(35):7155–7173, 2018. doi:10.1039/C8SM00690C.

[75] Falko Schmidt, Benno Liebchen, Hartmut Löwen, and Giovanni Volpe. Light-controlled assembly of active colloidal molecules. *The Journal of Chemical Physics*, 150(9):094905, March 2019. ISSN 0021-9606. doi:10.1063/1.5079861.

[76] Ran Niu, Denis Botin, Julian Weber, Alexander Reinmüller, and Thomas Palberg. Assembly and Speed in Ion-Exchange-Based Modular Phoretic Microswimmers. *Langmuir*, 33(14):3450–3457, April 2017. doi:10.1021/acs.langmuir.7b00288.

[77] Yang Wang, Rose M. Hernandez, David J. Bartlett, Julia M. Bingham, Timothy R. Kline, Ayusman Sen, and Thomas E. Mallouk. Bipolar Electrochemical Mechanism for the Propulsion of Catalytic Nanomotors in Hydrogen Peroxide Solutions. *Langmuir*, 22(25):10451–10456, December 2006. doi:10.1021/la0615950.

[78] J. L. Moran, P. M. Wheat, and J. D. Posner. Locomotion of electrocatalytic nanomotors due to reaction induced charge autoelectrophoresis. *Physical Review E*, 81(6):065302, June 2010. doi:10.1103/PhysRevE.81.065302.

[79] Jonathan R. Howse, Richard A. L. Jones, Anthony J. Ryan, Tim Gough, Reza Vafabakhsh, and Ramin Golestanian. Self-Motile Colloidal Particles: From Directed Propulsion to Random Walk. *Physical Review Letters*, 99(4):048102, July 2007. doi:10.1103/PhysRevLett.99.048102.

[80] Suropriya Saha, Ramin Golestanian, and Sriram Ramaswamy. Clusters, asters, and collective oscillations in chemotactic colloids. *Physical Review E*, 89(6):062316, June 2014. doi:10.1103/PhysRevE.89.062316.

[81] Mihail N. Popescu, William E. Uspal, Clemens Bechinger, and Peer Fischer. Chemotaxis of Active Janus Nanoparticles. *Nano Letters*, 18(9):5345–5349, September 2018. doi:10.1021/acs.nanolett.8b02572.

[82] Benno Liebchen and Hartmut Löwen. Synthetic Chemotaxis and Collective Behavior in Active Matter. *Accounts of Chemical Research*, 51(12):2982–2990, December 2018. doi:10.1021/acs.accounts.8b00215.

[83] Yiying Hong, Nicole M. K. Blackman, Nathaniel D. Kopp, Ayusman Sen, and Darrell Velegol. Chemotaxis of Nonbiological Colloidal Rods. *Physical Review Letters*, 99(17): 178103, October 2007. doi:10.1103/PhysRevLett.99.178103.

[84] Hong-Ren Jiang, Natsuhiko Yoshinaga, and Masaki Sano. Active Motion of a Janus Particle by Self-Thermophoresis in a Defocused Laser Beam. *Physical Review Letters*, 105(26):268302, December 2010. doi:10.1103/PhysRevLett.105.268302.

[85] Rob Phillips, Jane Kondev, Julie Theriot, Hernan G. Garcia, and Nigel Orme. *Physical Biology of the Cell*. Garland Science, New York, second edition, November 2012. doi:10.1201/9781134111589.

[86] Samudra Sengupta, Krishna K. Dey, Hari S. Muddana, Tristan Tabouillot, Michael E. Ibele, Peter J. Butler, and Ayusman Sen. Enzyme Molecules as Nanomotors. *J. Am. Chem. Soc.*, 135(4):1406–1414, January 2013. doi:10.1021/ja3091615.

[87] Ah-Young Jee, Yoon-Kyoung Cho, Steve Granick, and Tsvi Tlusty. Catalytic enzymes are active matter. *Proc. Natl. Acad. Sci. U.S.A.*, 115(46):E10812–E10821, November 2018. doi:10.1073/pnas.1814180115.

[88] Subhadip Ghosh, Ambika Somasundar, and Ayusman Sen. Enzymes as Active Matter. *Annual Review of Condensed Matter Physics*, 12(1):177–200, 2021. doi:10.1146/annurev-conmatphys-061020-053036.

[89] Samudra Sengupta, Krishna K. Dey, Hari S. Muddana, Tristan Tabouillot, Michael E. Ibele, Peter J. Butler, and Ayusman Sen. Enzyme molecules as nanomotors. *Journal of the American Chemical Society*, 135(4):1406–1414, 2013. doi:10.1021/ja3091615.

[90] Samudra Sengupta, Michelle M. Spiering, Krishna K. Dey, Wentao Duan, Debabrata Patra, Peter J. Butler, R. Dean Astumian, Stephen J. Benkovic, and Ayusman Sen. DNA Polymerase as a Molecular Motor and Pump. *ACS Nano*, 8(3):2410–2418, March 2014. doi:10.1021/nn405963x.

[91] Krishna Kanti Dey, Sambeeta Das, Matthew F. Poyton, Samudra Sengupta, Peter J. Butler, Paul S. Cremer, and Ayusman Sen. Chemotactic Separation of Enzymes. *ACS Nano*, 8(12):11941–11949, December 2014. doi:10.1021/nn504418u.

[92] Xi Zhao, Henri Palacci, Vinita Yadav, Michelle M. Spiering, Michael K. Gilson, Peter J. Butler, Henry Hess, Stephen J. Benkovic, and Ayusman Sen. Substrate-driven chemotactic assembly in an enzyme cascade. *Nat. Chem.*, 10(3):311–317, March 2018. doi:10.1038/nchem.2905.

[93] Ah-Young Jee, Sandipan Dutta, Yoon-Kyoung Cho, Tsvi Tlusty, and Steve Granick. Enzyme leaps fuel antichemotaxis. *Proceedings of the National Academy of Sciences*, 115(1):14–18, January 2018. doi:10.1073/pnas.1717844115.

[94] Mudong Feng and Michael K. Gilson. Enhanced Diffusion and Chemotaxis of Enzymes. *Annu. Rev. Biophys.*, 49:87–105, May 2020. doi:10.1146/annurev-biophys-121219-081535.

[95] Mengqi Xu, Jennifer L. Ross, Lyanne Valdez, and Aysuman Sen. Direct Single Molecule Imaging of Enhanced Enzyme Diffusion. *Physical Review Letters*, 123(12):128101, September 2019. doi:10.1103/PhysRevLett.123.128101.

[96] Zhijie Chen, Alan Shaw, Hugh Wilson, Maxime Woringer, Xavier Darzacq, Susan Marqusee, Quan Wang, and Carlos Bustamante. Single-molecule diffusometry reveals no catalysis-induced diffusion enhancement of alkaline phosphatase as proposed by FCS experiments. *Proceedings of the National Academy of Sciences*, 117(35):21328–21335, September 2020. doi:10.1073/pnas.2006900117.

[97] Ramin Golestanian. Collective Behavior of Thermally Active Colloids. *Physical Review Letters*, 108(3):038303, January 2012. doi:10.1103/PhysRevLett.108.038303.

[98] Babak Nasouri and Ramin Golestanian. Exact Phoretic Interaction of Two Chemically Active Particles. *Physical Review Letters*, 124(16):168003, April 2020. doi:10.1103/PhysRevLett.124.168003.

[99] Suropriya Saha, Sriram Ramaswamy, and Ramin Golestanian. Pairing, waltzing and scattering of chemotactic active colloids. *New Journal of Physics*, 21(6):063006, June 2019. doi:10.1088/1367-2630/ab20fd.

[100] Anatolij Gelimson, Kun Zhao, Calvin K. Lee, W. Till Kranz, Gerard C. L. Wong, and Ramin Golestanian. Multicellular Self-Organization of P. aeruginosa due to Interactions with Secreted Trails. *Physical Review Letters*, 117(17):178102, October 2016. doi:10.1103/PhysRevLett.117.178102.

[101] Ankush Sengupta, Tobias Kruppa, and Hartmut Löwen. Chemotactic predator-prey dynamics. *Physical Review E*, 83(3):031914, March 2011. doi:10.1103/PhysRevE.83.031914.

[102] Mark J. Bowick, Nikta Fakhri, M. Cristina Marchetti, and Sriram Ramaswamy. Symmetry, Thermodynamics, and Topology in Active Matter. *Physical Review X*, 12(1):010501, February 2022. doi:10.1103/PhysRevX.12.010501.

[103] Sarah A. M. Loos and Sabine H. L. Klapp. Irreversibility, heat and information flows induced by non-reciprocal interactions. *New Journal of Physics*, 22(12):123051, December 2020. doi:10.1088/1367-2630/abcc1e.

[104] Michel Fruchart, Ryo Hanai, Peter B. Littlewood, and Vincenzo Vitelli. Non-reciprocal phase transitions. *Nature*, 592(7854):363–369, April 2021. doi:10.1038/s41586-021-03375-9.

[105] Tingting Yu, Prabha Chuphal, Snigdha Thakur, Shang Yik Reigh, Dhruv P. Singh, and Peer Fischer. Chemical micromotors self-assemble and self-propel by spon-

taneous symmetry breaking. *Chem. Commun.*, 54(84):11933–11936, October 2018. doi:10.1039/C8CC06467A.

[106] Caleb H. Meredith, Pepijn G. Moerman, Jan Groenewold, Yu-Jen Chiu, Willem K. Kegel, Alfons van Blaaderen, and Lauren D. Zarzar. Predator–prey interactions between droplets driven by non-reciprocal oil exchange. *Nature Chemistry*, 12(12):1136–1142, December 2020. doi:10.1038/s41557-020-00575-0.

[107] Suropriya Saha, Jaime Agudo-Canalejo, and Ramin Golestanian. Scalar Active Mixtures: The Nonreciprocal Cahn-Hilliard Model. *Phys. Rev. X*, 10(4):041009, October 2020. doi:10.1103/PhysRevX.10.041009.

[108] Zhihong You, Aparna Baskaran, and M. Cristina Marchetti. Nonreciprocity as a generic route to traveling states. *Proceedings of the National Academy of Sciences*, 117(33):19767–19772, August 2020. doi:10.1073/pnas.2010318117.

[109] Suropriya Saha and Ramin Golestanian. Effervescent waves in a binary mixture with non-reciprocal couplings. *arXiv:2208.14985*, August 2022. doi:10.48550/arXiv.2208.14985.

[110] Lucas Barberis and Fernando Peruani. Large-Scale Patterns in a Minimal Cognitive Flocking Model: Incidental Leaders, Nematic Patterns, and Aggregates. *Physical Review Letters*, 117(24):248001, December 2016. doi:10.1103/PhysRevLett.117.248001.

[111] Mihir Durve, Arnab Saha, and Ahmed Sayeed. Active particle condensation by non-reciprocal and time-delayed interactions. *The European Physical Journal E*, 41(4):49, April 2018. doi:10.1140/epje/i2018-11653-4.

[112] Sarah A. M. Loos, Sabine H. L. Klapp, and Thomas Martynec. Long-range Order and Directional Defect Propagation in the Nonreciprocal XY Model with Vision Cone Interactions. *arXiv:2206.10519*, December 2022. doi:10.48550/arXiv.2206.10519.

[113] Mehdi Moussaïd, Dirk Helbing, and Guy Theraulaz. How simple rules determine pedestrian behavior and crowd disasters. *Proceedings of the National Academy of Sciences*, 108(17):6884–6888, April 2011. doi:10.1073/pnas.1016507108.

[114] François A. Lavergne, Hugo Wendehenne, Tobias Bäuerle, and Clemens Bechinger. Group formation and cohesion of active particles with visual perception–dependent motility. *Science*, 364(6435):70–74, April 2019. doi:10.1126/science.aau5347.

[115] Johannes Taktikos, Vasily Zaburdaev, and Holger Stark. Collective dynamics of model microorganisms with chemotactic signaling. *Physical Review E*, 85(5):051901, May 2012. doi:10.1103/PhysRevE.85.051901.

[116] Evelyn F. Keller and Lee A. Segel. Traveling bands of chemotactic bacteria: A theoretical analysis. *Journal of Theoretical Biology*, 30(2):235–248, February 1971. doi:10.1016/0022-5193(71)90051-8.

[117] Ricard Alert, Alejandro Martínez-Calvo, and Sujit S. Datta. Cellular Sensing Governs the Stability of Chemotactic Fronts. *Physical Review Letters*, 128(14):148101, April 2022. doi:10.1103/PhysRevLett.128.148101.

[118] I. Theurkauff, C. Cottin-Bizonne, J. Palacci, C. Ybert, and L. Bocquet. Dynamic Clustering in Active Colloidal Suspensions with Chemical Signaling. *Physical Review Letters*, 108(26):268303, June 2012. doi:10.1103/PhysRevLett.108.268303.

[119] T. Hillen and K. J. Painter. A user's guide to PDE models for chemotaxis. *Journal of Mathematical Biology*, 58(1):183, July 2008. doi:10.1007/s00285-008-0201-3.

[120] Kevin Painter and Thomas Hillen. Volume-filling and quorum-sensing in models for chemosensitive movement. *Can. Appl. Math. Q.*, 10:501–543, January 2002.

[121] T. J. Newman and R. Grima. Many-body theory of chemotactic cell-cell interactions. *Physical Review E*, 70(5):051916, November 2004. doi:10.1103/PhysRevE.70.051916.

[122] R. Grima. Strong-Coupling Dynamics of a Multicellular Chemotactic System. *Physical Review Letters*, 95(12):128103, September 2005. doi:10.1103/PhysRevLett.95.128103.

[123] Anatolij Gelimson and Ramin Golestanian. Collective Dynamics of Dividing Chemotactic Cells. *Physical Review Letters*, 114(2):028101, January 2015. doi:10.1103/PhysRevLett.114.028101.

[124] Riccardo Ben Alì Zinati, Charlie Duclut, Saeed Mahdisoltani, Andrea Gambassi, and Ramin Golestanian. Stochastic dynamics of chemotactic colonies with logistic growth. *Europhysics Letters*, 136(5):50003, March 2022. doi:10.1209/0295-5075/ac48c9.

[125] Saeed Mahdisoltani, Riccardo Ben Alì Zinati, Charlie Duclut, Andrea Gambassi, and Ramin Golestanian. Nonequilibrium polarity-induced chemotaxis: Emergent Galilean symmetry and exact scaling exponents. *Physical Review Research*, 3(1):013100, January 2021. ISSN 2643-1564. doi:10.1103/PhysRevResearch.3.013100.

[126] Kun Zhao, Boo Shan Tseng, Bernard Beckerman, Fan Jin, Maxsim L. Gibiansky, Joe J. Harrison, Erik Luijten, Matthew R. Parsek, and Gerard C. L. Wong. Psl trails guide

exploration and microcolony formation in Pseudomonas aeruginosa biofilms. *Nature*, 497(7449):388–391, May 2013. doi:10.1038/nature12155.

[127] W. Till Kranz, Anatolij Gelimson, Kun Zhao, Gerard C. L. Wong, and Ramin Golestanian. Effective Dynamics of Microorganisms That Interact with Their Own Trail. *Physical Review Letters*, 117(3):038101, July 2016. doi:10.1103/PhysRevLett.117.038101.

[128] Babak Vajdi Hokmabad, Jaime Agudo-Canalejo, Suropriya Saha, Ramin Golestanian, and Corinna C. Maass. Chemotactic self-caging in active emulsions. *Proceedings of the National Academy of Sciences*, 119(24):e2122269119, June 2022. doi:10.1073/pnas.2122269119.

[129] Melissa B. Miller and Bonnie L. Bassler. Quorum Sensing in Bacteria. *Annual Review of Microbiology*, 55(1):165–199, 2001. doi:10.1146/annurev.micro.55.1.165.

[130] S. P. Brown and R. A. Johnstone. Cooperation in the dark: Signalling and collective action in quorum-sensing bacteria. *Proceedings of the Royal Society of London. Series B: Biological Sciences*, 268(1470):961–965, May 2001. doi:10.1098/rspb.2001.1609.

[131] Vanessa Sperandio, Alfredo G. Torres, and James B. Kaper. Quorum sensing Escherichia coli regulators B and C (QseBC): A novel two-component regulatory system involved in the regulation of flagella and motility by quorum sensing in E. coli. *Molecular Microbiology*, 43(3):809–821, 2002. doi:10.1046/j.1365-2958.2002.02803.x.

[132] Hanh H. Hoang, Nataliya Gurich, and Juan E. González. Regulation of Motility by the ExpR/Sin Quorum-Sensing System in Sinorhizobium meliloti. *Journal of Bacteriology*, 190(3):861–871, February 2008. doi:10.1128/JB.01310-07.

[133] Claudia Lupp and Edward G. Ruby. Vibrio fischeri Uses Two Quorum-Sensing Systems for the Regulation of Early and Late Colonization Factors. *Journal of Bacteriology*, 187(11):3620–3629, June 2005. doi:10.1128/JB.187.11.3620-3629.2005.

[134] Tobias Bäuerle, Andreas Fischer, Thomas Speck, and Clemens Bechinger. Self-organization of active particles by quorum sensing rules. *Nature Communications*, 9(1):3232, August 2018. doi:10.1038/s41467-018-05675-7.

[135] Jeremie Palacci, Stefano Sacanna, Asher Preska Steinberg, David J. Pine, and Paul M. Chaikin. Living Crystals of Light-Activated Colloidal Surfers. *Science*, 339(6122):936–940, February 2013. doi:10.1126/science.1230020.

[136] Ivo Buttinoni, Julian Bialké, Felix Kümmel, Hartmut Löwen, Clemens Bechinger, and Thomas Speck. Dynamical Clustering and Phase Separation in Suspensions of Self-Propelled Colloidal Particles. *Physical Review Letters*, 110(23):238301, June 2013. doi:10.1103/PhysRevLett.110.238301.

[137] F. Ginot, I. Theurkauff, F. Detcheverry, C. Ybert, and C. Cottin-Bizonne. Aggregation-fragmentation and individual dynamics of active clusters. *Nature Communications*, 9(1):696, February 2018. doi:10.1038/s41467-017-02625-7.

[138] Jack A. Cohen and Ramin Golestanian. Emergent Cometlike Swarming of Optically Driven Thermally Active Colloids. *Physical Review Letters*, 112(6):068302, February 2014. doi:10.1103/PhysRevLett.112.068302.

[139] Jaime Agudo-Canalejo and Ramin Golestanian. Active Phase Separation in Mixtures of Chemically Interacting Particles. *Phys. Rev. Lett.*, 123(1):018101, July 2019. doi:10.1103/PhysRevLett.123.018101.

[140] Jie Zhang, Ricard Alert, Jing Yan, Ned S. Wingreen, and Steve Granick. Active phase separation by turning towards regions of higher density. *Nature Physics*, 17(8):961–967, August 2021. doi:10.1038/s41567-021-01238-8.

[141] Bruce Alberts. *Molecular Biology of the Cell*. W.W. Norton & Company, New York, sixth edition, August 2017. doi:10.1201/9781315735368.

[142] Tâm Mignot and Joshua W Shaevitz. Active and passive mechanisms of intracellular transport and localization in bacteria. *Current Opinion in Microbiology*, 11(6):580–585, December 2008. doi:10.1016/j.mib.2008.10.005.

[143] Steven B. Zimmerman and Stefan O. Trach. Estimation of macromolecule concentrations and excluded volume effects for the cytoplasm of Escherichia coli. *Journal of Molecular Biology*, 222(3):599–620, December 1991. doi:10.1016/0022-2836(91)90499-V.

[144] Bradley R. Parry, Ivan V. Surovtsev, Matthew T. Cabeen, Corey S. O'Hern, Eric R. Dufresne, and Christine Jacobs-Wagner. The Bacterial Cytoplasm Has Glass-like Properties and Is Fluidized by Metabolic Activity. *Cell*, 156(1):183–194, January 2014. doi:10.1016/j.cell.2013.11.028.

[145] Y. Koyano, H. Kitahata, and A. S. Mikhailov. Diffusion in crowded colloids of particles cyclically changing their shapes. *Europhysics Letters*, 128(4):40003, January 2020. doi:10.1209/0295-5075/128/40003.

[146] Norihiro Oyama, Takeshi Kawasaki, Hideyuki Mizuno, and Atsushi Ikeda. Glassy dynamics of a model of bacterial cytoplasm with metabolic activities. *Physical Review Research*, 1(3):032038, December 2019. doi:10.1103/PhysRevResearch.1.032038.

[147] Yongdae Shin and Clifford P. Brangwynne. Liquid phase condensation in cell physiology and disease. *Science*, 357(6357):eaaf4382, September 2017. doi:10.1126/science.aaf4382.

[148] Salman F. Banani, Hyun O. Lee, Anthony A. Hyman, and Michael K. Rosen. Biomolecular condensates: Organizers of cellular biochemistry. *Nat Rev Mol Cell Biol*, 18(5):285–298, May 2017. doi:10.1038/nrm.2017.7.

[149] Clifford P. Brangwynne, Christian R. Eckmann, David S. Courson, Agata Rybarska, Carsten Hoege, Jöbin Gharakhani, Frank Jülicher, and Anthony A. Hyman. Germline P Granules Are Liquid Droplets That Localize by Controlled Dissolution/Condensation. *Science*, 324(5935):1729–1732, June 2009. doi:10.1126/science.1172046.

[150] Anthony A. Hyman, Christoph A. Weber, and Frank Jülicher. Liquid-Liquid Phase Separation in Biology. *Annual Review of Cell and Developmental Biology*, 30(1):39–58, 2014. doi:10.1146/annurev-cellbio-100913-013325.

[151] Joel Berry, Clifford P. Brangwynne, and Mikko Haataja. Physical principles of intracellular organization via active and passive phase transitions. *Reports on Progress in Physics*, 81(4):046601, February 2018. doi:10.1088/1361-6633/aaa61e.

[152] Wilton T. Snead and Amy S. Gladfelter. The Control Centers of Biomolecular Phase Separation: How Membrane Surfaces, PTMs, and Active Processes Regulate Condensation. *Molecular Cell*, 76(2):295–305, October 2019. doi:10.1016/j.molcel.2019.09.016.

[153] Yuntao S. Mao, Hongjae Sunwoo, Bin Zhang, and David L. Spector. Direct visualization of the co-transcriptional assembly of a nuclear body by noncoding RNAs. *Nature Cell Biology*, 13(1):95–101, January 2011. doi:10.1038/ncb2140.

[154] Sergey P. Shevtsov and Miroslav Dundr. Nucleation of nuclear bodies by RNA. *Nature Cell Biology*, 13(2):167–173, February 2011. doi:10.1038/ncb2157.

[155] Mario Hofweber and Dorothee Dormann. Friend or foe—Post-translational modifications as regulators of phase separation and RNP granule dynamics. *Journal of Biological Chemistry*, 294(18):7137–7150, May 2019. doi:10.1074/jbc.TM118.001189.

[156] David Zwicker, Anthony A. Hyman, and Frank Jülicher. Suppression of Ostwald ripening in active emulsions. *Physical Review E*, 92(1):012317, July 2015. doi:10.1103/PhysRevE.92.012317.

[157] Christoph A. Weber, David Zwicker, Frank Jülicher, and Chiu Fan Lee. Physics of active emulsions. *Reports on Progress in Physics*, 82(6):064601, April 2019. doi:10.1088/1361-6633/ab052b.

[158] David Zwicker, Rabea Seyboldt, Christoph A. Weber, Anthony A. Hyman, and Frank Jülicher. Growth and division of active droplets provides a model for protocells. *Nat. Phys.*, 13(4):408–413, April 2017. doi:10.1038/nphys3984.

[159] Ramin Golestanian. Division for multiplication. *Nature Physics*, 13(4):323–324, April 2017. doi:10.1038/nphys3998.

[160] Dustin Updike and Susan Strome. P Granule Assembly and Function in Caenorhabditis elegans Germ Cells. *Journal of Andrology*, 31(1):53–60, 2010. doi:10.2164/jandrol.109.008292.

[161] Jens S. Andersen, Yun W. Lam, Anthony K. L. Leung, Shao-En Ong, Carol E. Lyon, Angus I. Lamond, and Matthias Mann. Nucleolar proteome dynamics. *Nature*, 433 (7021):77–83, January 2005. doi:10.1038/nature03207.

[162] Sheng Mao, Derek Kuldinow, Mikko P. Haataja, and Andrej Košmrlj. Phase behavior and morphology of multicomponent liquid mixtures. *Soft Matter*, 15(6):1297–1311, 2019. doi:10.1039/C8SM02045K.

[163] Tyler S. Harmon and Frank Jülicher. Molecular Assembly Lines in Active Droplets. *Physical Review Letters*, 128(10):108102, March 2022. doi:10.1103/PhysRevLett.128.108102.

[164] Paul A. Srere. The metabolon. *Trends in Biochemical Sciences*, 10(3):109–110, March 1985. doi:10.1016/0968-0004(85)90266-X.

[165] Lee J. Sweetlove and Alisdair R. Fernie. The role of dynamic enzyme assemblies and substrate channelling in metabolic regulation. *Nat. Commun.*, 9(1):2136, May 2018. doi:10.1038/s41467-018-04543-8.

[166] Ian Wheeldon, Shelley D. Minteer, Scott Banta, Scott Calabrese Barton, Plamen Atanassov, and Matthew Sigman. Substrate channelling as an approach to cascade reactions. *Nature Chemistry*, 8(4):299–309, April 2016. doi:10.1038/nchem.2459.

[167] Vidhi Pareek, Zhou Sha, Jingxuan He, Ned S. Wingreen, and Stephen J. Benkovic. Metabolic channeling: Predictions, deductions, and evidence. *Molecular Cell*, 81(18): 3775–3785, September 2021. ISSN 1097-2765. doi:10.1016/j.molcel.2021.08.030.

[168] Liubov Poshyvailo, Eric von Lieres, and Svyatoslav Kondrat. Does metabolite channeling accelerate enzyme-catalyzed cascade reactions? *PLOS ONE*, 12(2):e0172673, February 2017. doi:10.1371/journal.pone.0172673.

[169] Michele Castellana, Maxwell Z. Wilson, Yifan Xu, Preeti Joshi, Ileana M. Cristea, Joshua D. Rabinowitz, Zemer Gitai, and Ned S. Wingreen. Enzyme clustering accelerates processing of intermediates through metabolic channeling. *Nature Biotechnology*, 32(10):1011–1018, October 2014. doi:10.1038/nbt.3018.

[170] Florian Hinzpeter, Filipe Tostevin, and Ulrich Gerland. Regulation of reaction fluxes via enzyme sequestration and co-clustering. *J. R. Soc. Interface*, 16(156):20190444, July 2019. doi:10.1098/rsif.2019.0444.

[171] Anthony M. Pedley, Vidhi Pareek, and Stephen J. Benkovic. The Purinosome: A Case Study for a Mammalian Metabolon. *Annual Review of Biochemistry*, 91(1):89–106, 2022. doi:10.1146/annurev-biochem-032620-105728.

[172] Anthony M. Pedley and Stephen J. Benkovic. A New View into the Regulation of Purine Metabolism: The Purinosome. *Trends in Biochemical Sciences*, 42(2):141–154, February 2017. doi:10.1016/j.tibs.2016.09.009.

[173] Danielle L. Schmitt, Anand Sundaram, Miji Jeon, Bao Tran Luu, and Songon An. Spatial alterations of De Novo purine biosynthetic enzymes by Akt-independent PDK1 signaling pathways. *PLOS ONE*, 13(4):e0195989, April 2018. doi:10.1371/journal.pone.0195989.

[174] Anthony M. Pedley, Jack P. Boylan, Chung Yu Chan, Erin L. Kennedy, Minjoung Kyoung, and Stephen J. Benkovic. Purine biosynthetic enzymes assemble into liquid-like condensates dependent on the activity of chaperone protein HSP90. *Journal of Biological Chemistry*, 298(5), May 2022. doi:10.1016/j.jbc.2022.101845.

[175] Andrea Testa, Mirco Dindo, Aleksander A. Rebane, Babak Nasouri, Robert W. Style, Ramin Golestanian, Eric R. Dufresne, and Paola Laurino. Sustained enzymatic activity and flow in crowded protein droplets. *Nat. Commun.*, 12(1):6293, November 2021. doi:10.1038/s41467-021-26532-0.

[176] Leonardo Demarchi, Andriy Goychuk, Ivan Maryshev, and Erwin Frey. Enzyme-Enriched Condensates Show Self-Propulsion, Positioning, and Coexistence. *Physical Review Letters*, 130(12):128401, March 2023. doi:10.1103/PhysRevLett.130.128401.

[177] Jan Kirschbaum and David Zwicker. Controlling biomolecular condensates via chemical reactions. *Journal of The Royal Society Interface*, 18(179):20210255, June 2021. doi:10.1098/rsif.2021.0255.

[178] Matthew W. Cotton, Ramin Golestanian, and Jaime Agudo-Canalejo. Catalysis-induced phase separation and autoregulation of enzymatic activity. *Phys. Rev. Lett.*, 129:158101, Oct 2022. doi:10.1103/PhysRevLett.129.158101.

[179] Giovanni Giunta, Hamid Seyed-Allaei, and Ulrich Gerland. Cross-diffusion induced patterns for a single-step enzymatic reaction. *Communications Physics*, 3(1):1–9, 2020.

[180] Fei Wu, Lindsey N. Pelster, and Shelley D. Minteer. Krebs cycle metabolon formation: Metabolite concentration gradient enhanced compartmentation of sequential enzymes. *Chemical Communications*, 51(7):1244–1247, 2015. doi:10.1039/C4CC08702J.

[181] Vincent Ouazan-Reboul, Jaime Agudo-Canalejo, and Ramin Golestanian. Non-equilibrium phase separation in mixtures of catalytically active particles: Size dispersity and screening effects. *Eur. Phys. J. E*, 44(9):113, September 2021. doi:10.1140/epje/s10189-021-00118-6.

[182] Vincent Ouazan-Reboul, Jaime Agudo-Canalejo, and Ramin Golestanian. Self-organization of primitive metabolic cycles due to non-reciprocal interactions. *arXiv:2303.09832*, March 2023. doi:10.48550/arXiv.2303.09832.

[183] Vincent Ouazan-Reboul, Jaime Agudo-Canalejo, and Ramin Golestanian. Network effects lead to self-organization in metabolic cycles of self-repelling catalysts. *arXiv:2303.09832*, April 2023. doi:10.48550/arXiv.2304.09925.

[184] Vincent Ouazan-Reboul, Ramin Golestanian, and Jaime Agudo-Canalejo. Interaction-motif-based classification of self-organizing metabolic cycles. *arXiv:2305.05472*, May 2023. doi:10.48550/arXiv.2305.05472.

[185] Andrea Cavagna, Luca Di Carlo, Irene Giardina, Tomás S. Grigera, Stefania Melillo, Leonardo Parisi, Giulia Pisegna, and Mattia Scandolo. Natural swarms in 3.99 dimensions. *Nature Physics*, pages 1–7, April 2023. doi:10.1038/s41567-023-02028-0.

[186] Marcel Meyer, Lutz Schimansky-Geier, and Pawel Romanczuk. Active Brownian agents with concentration-dependent chemotactic sensitivity. *Physical Review E*, 89 (2):022711, February 2014. doi:10.1103/PhysRevE.89.022711.

[187] Florian Hinzpeter, Filipe Tostevin, Alexander Buchner, and Ulrich Gerland. Trade-offs and design principles in the spatial organization of catalytic particles. *Nature Physics*, 18(2):203–211, February 2022. ISSN 1745-2481. doi:10.1038/s41567-021-01444-4.

[188] Christine A. Raines. The Calvin cycle revisited. *Photosynthesis Research*, 75(1):1–10, January 2003. doi:10.1023/A:1022421515027.

[189] Krishna K. Dey, Xi Zhao, Benjamin M. Tansi, Wilfredo J. Méndez-Ortiz, Ubaldo M. Córdova-Figueroa, Ramin Golestanian, and Ayusman Sen. Micromotors Powered by Enzyme Catalysis. *Nano Letters*, 15(12):8311–8315, December 2015. doi:10.1021/acs.nanolett.5b03935.

[190] Ambika Somasundar, Subhadip Ghosh, Farzad Mohajerani, Lynnicia N. Massenburg, Tinglu Yang, Paul S. Cremer, Darrell Velegol, and Ayusman Sen. Positive and negative

chemotaxis of enzyme-coated liposome motors. *Nature Nanotechnology*, 14(12):1129–1134, December 2019. doi:10.1038/s41565-019-0578-8.

[191] Tunrayo Adeleke-Larodo, Pierre Illien, and Ramin Golestanian. Fluctuation-induced hydrodynamic coupling in an asymmetric, anisotropic dumbbell. *The European Physical Journal E*, 42(3):39, March 2019. doi:10.1140/epje/i2019-11799-5.

[192] P. Illien, T. Adeleke-Larodo, and R. Golestanian. Diffusion of an enzyme: The role of fluctuation-induced hydrodynamic coupling. *Europhysics Letters*, 119(4):40002, November 2017. doi:10.1209/0295-5075/119/40002.

[193] Matthew T. Meredith and Shelley D. Minteer. Biofuel Cells: Enhanced Enzymatic Bioelectrocatalysis. *Annual Review of Analytical Chemistry*, 5(1):157–179, 2012. doi:10.1146/annurev-anchem-062011-143049.

[194] Michael J. Moehlenbrock, Timothy K. Toby, Abdul Waheed, and Shelley D. Minteer. Metabolon Catalyzed Pyruvate/Air Biofuel Cell. *Journal of the American Chemical Society*, 132(18):6288–6289, May 2010. doi:10.1021/ja101326b.

[195] Sanne Schoffelen and Jan C. M. van Hest. Multi-enzyme systems: Bringing enzymes together in vitro. *Soft Matter*, 8(6):1736–1746, 2012. doi:10.1039/C1SM06452E.